AEROPREDICTION, INC.
9449 GROVER DRIVE
KING GEORGE, VA 22485

THE 2009 VERSION OF THE AEROPREDICTION CODE: THE AP09

BY: FRANK G. MOORE
LINDA Y. MOORE

API REPORT NO.3
JANUARY 2008

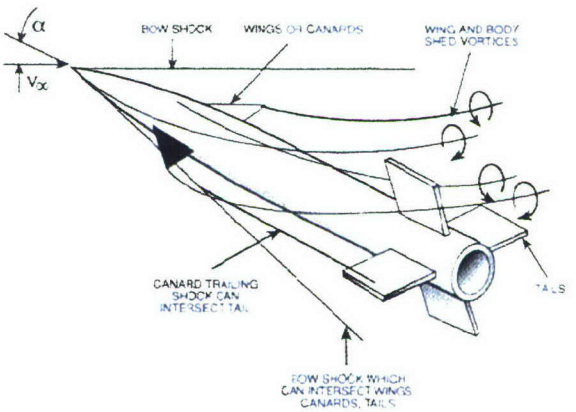

ABSTRACT

The AP05 code was evaluated when applied to configurations with boattails. Results of the evaluation indicated the AP05 predictions for normal force, center of pressure, pitch and roll damping moments needed improvement. As a result new and improved methods were developed and incorporated into the AP05 to be released as the AP09. Improvements include body alone lift characteristics for Mach numbers less than 2, low angle of attack improvements for roll and pitch damping for configurations with long boattails, incorporation of an improved boundary layer displacement model and refinement of several other existing methods. In addition, new methods were developed to predict nonlinear roll and pitch damping. Comparing the new and improved methods to existing experimental data indicated significant improvements in roll and pitch damping, normal force and center of pressure predictions compared to the AP05. However, validation of the AP09 code was not as complete as desired due to limited generic nonlinear roll and pitch damping data. Also, most of the available nonlinear dynamic derivative data has larger than desired accuracy boundaries due to model sting and wind tunnel wall interference issues. Weapons affected most by the new AP09 methodology are mortars, low drag bombs and projectiles in that order. However, the nonlinear dynamic derivative predictions affect all weapons. The AP09 is thus the most accurate and robust of the Aeroprediction Codes to date.

CONTENTS

CONTENTS (Continued)

ILLUSTRATIONS

ILLUSTRATIONS (Continued)

ILLUSTRATIONS (Continued)

ILLUSTRATIONS (Continued)

ILLUSTRATIONS (Continued)

ILLUSTRATIONS (Continued)

1.0 INTRODUCTION

A few years ago, Aeroprediction, Inc (API) was providing aerodynamic support to the Naval Surface Warfare Center, Dahlgren Division (NSWCDD) on a mortar round. API calculated normal force, axial force, pitching moment, center of pressure, roll and pitch damping moments for a wide variety of Mach numbers and angles of attack (AOAs) for several different mortar configurations. After the aerodynamic computations were complete, a set of experimental data on one of the configurations was made available to API. In comparing the AP05 predictions to experimental data, it was obvious that a large boundary layer was present on the long boattail of the mortar, negating some of the fin effectiveness in providing static stability along with reducing roll and pitch damping.

During the last three years, API undertook an evaluation of the weak areas of the AP05 when used on weapons with boattails, as well as developing new or improved ways to address the weak areas. This report serves to document the weak areas and methods developed to overcome or improve upon the weak areas. A User Guide example of a mortar and of a low drag bomb configuration is given. Otherwise the User Guide (Reference 1) for the AP05 is still relevant. Finally, several examples are given to show the improvement of the AP09 over the AP05 for configurations with and without boattails. The weapons affected (see Figure 1) are primarily mortars, low drag bombs, spin stabilized projectiles and some missiles.

In addition to boattailed configuration aerodynamic prediction weaknesses, the AP05 and all prior versions of the Aeroprediction Code have only linear values of roll and pitch damping. Many weapons can oscillate or rotate at AOA which can cause the dynamic derivatives to become nonlinear. No generic wind tunnel data base is available to allow accurate estimation of pitch and roll damping nonlinearities. However, there are limited dynamic derivative data bases available for specific configurations. As a result, the AP09 will provide a nonlinear prediction capability for roll and pitch damping. Unfortunately, since there is no "truth" model to validate the nonlinear dynamic stability predictions, refinements to the new methods at a later time are probable. On the other hand, the AP09 will be the first semiempirical code to provide nonlinear predictions of roll and pitch damping moments.

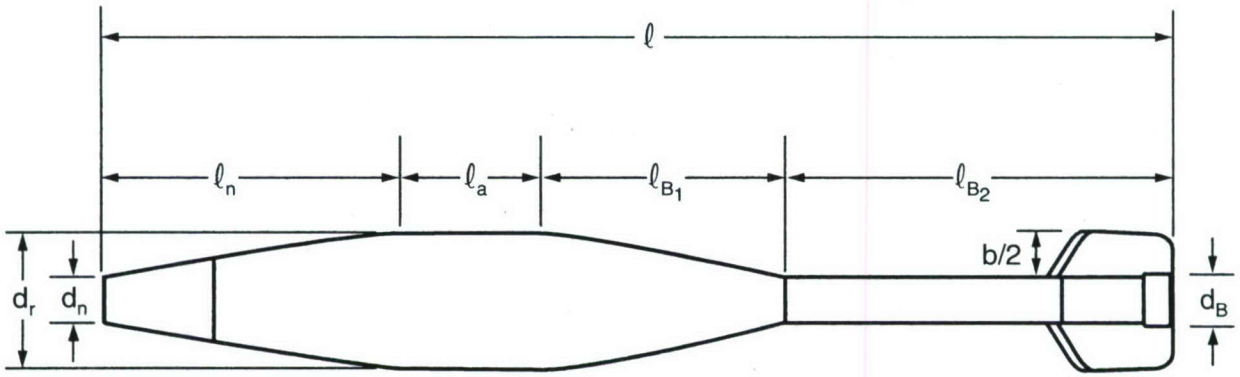

a. Typical Mortar Configuration

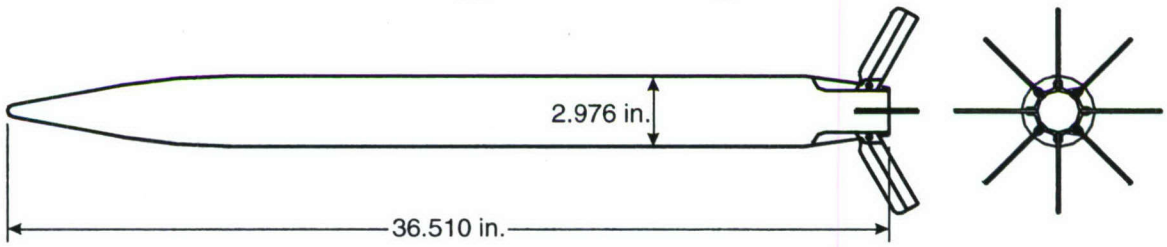

b. Schematic of Eight-Fin Guided Projectile Concept

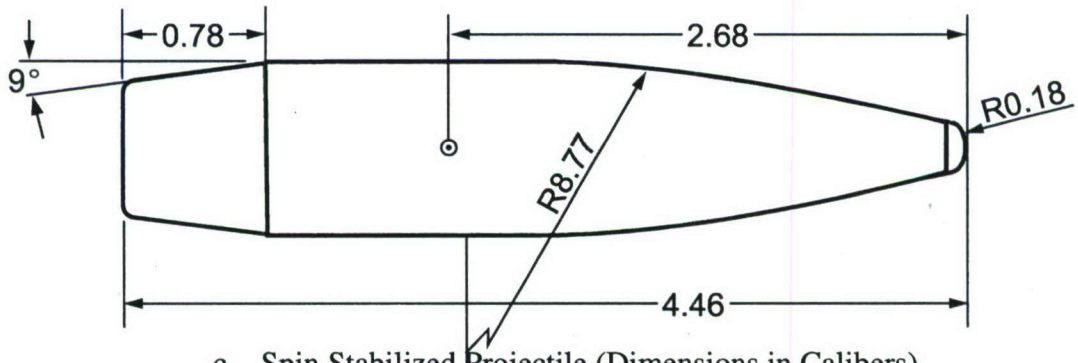

c. Spin Stabilized Projectile (Dimensions in Calibers)

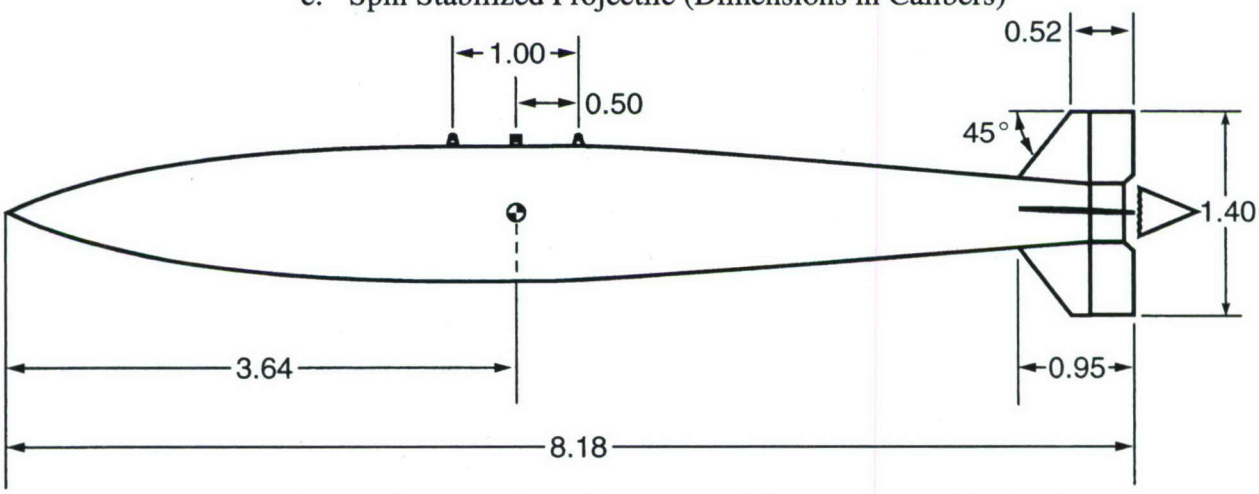

d. General Purpose Low Drag Bomb (Dimensions in Calibers)

FIGURE 1. SOME TYPICAL WEAPONS WITH BOATTAILS

1.1 WEAK AREAS OF AP05

The API review of the AP05 as applied to configurations with boattails was very thorough and, unfortunately, found several areas where improvements were needed. The first area examined was the body alone lift characteristics at subsonic and transonic speeds. The present methodology is mostly empirical and is defined in Reference 2, pages 154–157 (note Figure 4.23 of the original text was the incorrect figure and was corrected by the Errata sheet from AIAA). The body alone lift methodology is the original methodology incorporated into the first version of the Aeroprediction Code in 1972 (AP72)[3] and has not been modified since. The AP72 body alone lift methodology for subsonic and transonic speeds will be modified and improved for the AP09.

The body alone lift characteristics for low supersonic flow is predicted by the Hybrid Theory of Van Dyke[4] (HTVD). The HTVD uses a second order accurate method to predict axial force and a first order accurate method to predict normal force. In comparing HTVD predictions to data, it is clear that for configurations with boattails of short to moderate length the HTVD overpredicts the effect of the boattail on normal force. This overprediction of normal force on the boattail in turn causes the body alone normal force to be too low (since the boattail term is negative), which in turn shifts the center of pressure too far forward. Thus the body alone lift properties at low supersonic speeds will also be improved upon. Boundary layer displacement thickness effects are incorporated in the AP05 to modify the boattail angle and thus give good axial force predictions. However, the boundary layer displacement thickness (BLDT) effects are not large enough or accurate enough to give accurate normal force characteristics for a variety of configurations.

A third weak area of the body alone aerodynamics of the AP05 is pitch damping for bodies with long boattails. The current body alone dynamic derivative methodology is based on the all empirical GE Spinner Program of the early 70s[5]. The spinner empirical predictions were improved upon several years ago for long bodies and higher Mach numbers[6] and were made a part of the AP02[7]. However, the improvements in Reference 5 did not address configurations with long boattails, which fall well outside of the empirical data base upon which the Spinner code was based. Therefore, body alone pitch damping for configurations with long boattails also needs improvement.

The next four areas of the AP05 needing improvement involve fins when the fins are located on the boattail. The multi-fin factors computed by the full Navier Stokes equations at supersonic speeds and by the unsteady Euler Equations at subsonic speeds[8] was never checked out against multi-fin low aspect ratio configurations at subsonic speeds due to lack of data. The Reference 8 methodology was validated at supersonic speeds and at subsonic speeds for higher aspect ratios. The unsteady Euler calculations[8] for the low aspect ratio multi-fin factors appeared to be too high and out of line with the viscous Navier Stokes calculations at supersonic speeds. However, without experimental data, there was no rationale to modify the inviscid subsonic Euler computations of Reference 8. Wind tunnel data from multi-fin mortar configurations of low aspect ratio confirm the need to lower the values of the multi-fin factors for subsonic Mach numbers and aspect ratio one and lower.

The roll and pitch damping contributions of the fins are computed from linearized theory (Reference 2, pp 80-95) where the fins are assumed to go to the centerline of the body and as a result no wing-body and body-wing carryover effects are included for dynamic derivatives of the fins, unlike the static aerodynamic computations. Inherent in the dynamic derivative computations for the fins is the assumption that the dynamic pressure in the vicinity of the fins is close to freestream values. This assumption is not valid near the fin root and body juncture and thus for fins located on a boattail the fin span needs to be adjusted to account for viscous effects.

Another problem area for dynamic derivatives of body-tail or body-canard-tail cases is the fact that the body length at the root chord is included twice in the roll and pitch damping calculations. The double counting occurs because the fins go all the way to the body centerline for roll and pitch damping computations, yet the AP05 and all prior versions of the aeroprediction code do not subtract the root chord length from the overall body length when performing the body alone pitch and roll damping computations. This double counting has little effect on roll damping, since body alone roll damping is very small. However, the double counting of body length has a larger effect on pitch damping, since pitch damping is proportional to $(X_{fin}/d)^2$ and the fin is, in most cases, towards the rear of the body. The double counting of body length for roll and pitch damping is a problem for all configurations, not just configurations with boattails.

The third area of the AP05 needing improvement for body-tail configurations is to account for the BLDT effects on the fin if the fin is on the boattail. The BLDT has the effect of reducing the effective fin span and area which provides lift and static margin, thereby lowering both. The current AP05 accounts for BLDT on boattails as far as body alone configurations are concerned. However, the fin effectiveness is not reduced in terms of lift computations. Thus BLDT effects need to be considered when the fins lie on the boattail.

Another area needing improvement for body tail configurations is the nonlinear axial force at AOA for subsonic Mach numbers. The original methodology[9] had very little body tail data at subsonic Mach numbers. Hence, some refinement in the Reference 9 nonlinear AOA axial force predictions is also needed.

Many users of the Aeroprediction Code have noticed a sharp decrease and then a sharp increase in all normal force, pitching moments, center of pressure, roll and pitch damping around Mach one. This abrupt behavior in aerodynamics is caused by the use of Equations (65) and (67) of Reference 2, pps. 158-159. The methodology of Reference 2 attempts to account for the sharp drop off and then increase in normal force properties of a wing as the shock wave moves over and past the wing in transonic flow. Experimental data in general has never shown this large drop off on weapon wings. As a result, the transonic lift methodology of wings will be re-examined.

The final area needing improvement for all weapon configurations is to develop a nonlinear pitch and roll damping methodology that is a function of AOA and Mach number. To the author's knowledge, no semiempirical code exists with such a capability so the AP09 will be the first such code to have nonlinear pitch and roll damping predictions. However, since the amount of nonlinear dynamic derivative data is limited, and since some of the data is not totally

consistent, it is expected the new nonlinear roll and pitch damping will need to be improved upon as more data becomes available. Also, the dynamic derivative stability data has more issues of wind tunnel and model interference than static aerodynamics. Hence, even the data that is available has more accuracy issues than static aerodynamic data.

1.2 PHYSICAL CHARACTERISTICS OF CONFIGURATIONS WHERE AP05 AERODYNAMICS NEED IMPROVEMENT

Many weapons have boattails. Spin stabilized projectiles, missiles and low drag bombs use the boattails primarily, as drag reduction mechanisms. The base drag is reduced by

$$C_{A_B} = C_{P_B}\left(\frac{d_B}{d_{ref}}\right)^3 \tag{1}$$

where C_{P_B} is the base pressure coefficient of a circular cylinder with no boattail. For transonic and supersonic speeds, the drag reduction from Equation (1) is partially offset by the increase in wave drag due to the expansion of the flow from the cylinder onto the boattail. Other weapons use the boattail as a means to allow the fins to be placed on a weapon in an unfolded means and provide adequate static margin. Mortars and, to some extent, low drag bombs, are examples of this class of weapon. Mortars typically are launched from an unrifled gun barrel, are low cost, and have enough fins and fin area to provide static stability. Figure 1 shows typical weapons with boattails.

The spin stabilized projectile and tactical missile (or guided projectile) shown in Figure 1 typically have small boattails of a caliber or less and the AP05 does a reasonably good job in computing the aerodynamics of these cases. However, as already pointed out, the lift characteristics need improvement for the body alone for $M_\infty \leq 2.0$. The body alone lift inaccuracy is not as apparent on the guided missile as on the spin stabilized projectile, since the fin lift dominates the total lift of the missile configuration.

The AP05 accuracy is the worst for the mortar configuration of Figure 1. Mortars are lower cost weapons, tend to have fins that are thick with blunt leading and trailing edges, long boattails, and a boom with fins mounted on the boom with a maximum span no more than the body maximum diameter. Low drag bombs also present accuracy problems for the AP05 due to the long boattail. However, the fins are thinner and lower drag since they are not in a region where a blast from gun powder is located, as is the case for mortars.

1.3 FLOW PHYSICS OF CONFIGURATIONS WITH BOATTAILS

Assessing the AP05 problems alluded to in Section 1.1, it is clear that many of the Section 1.1 problems arise as a result of trying to model the highly viscous flow region in the boattail area. In developing a semiempirical code, it is important to understand the physics of the flow before one can develop an approximate model of the physics. Figure 2 illustrates this

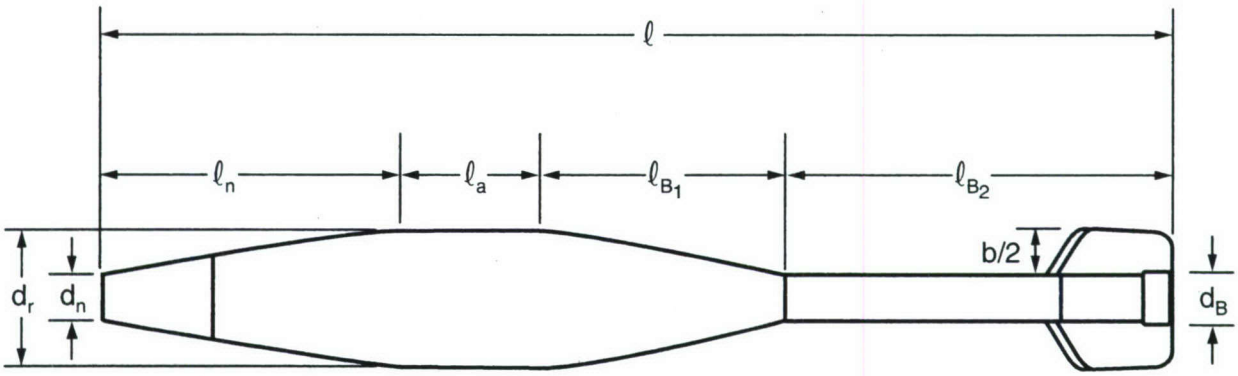

a. Typical Mortar Configuration

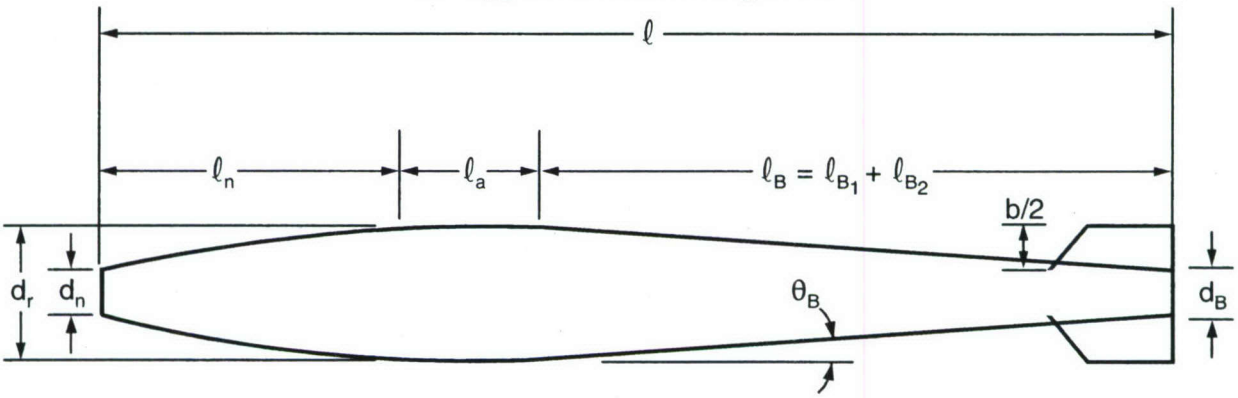

b. AP05 Representation of Mortar Configuration

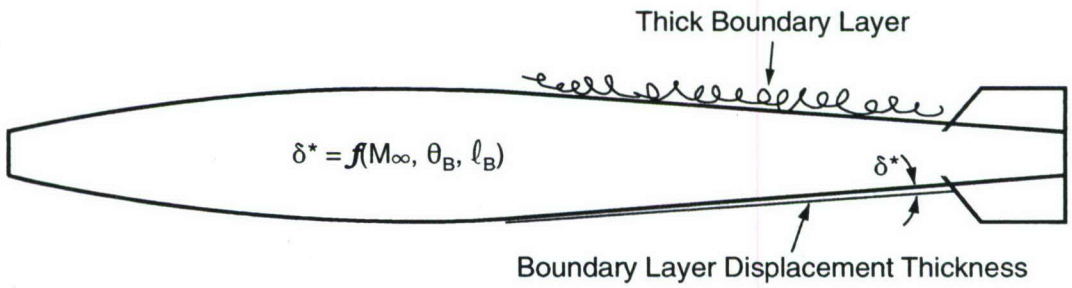

c. Illustration of Viscous Effects on Mortar

FIGURE 2. ILLUSTRATION OF AP05 REPRESENTATION OF A MORTAR AND THE VISCOUS FLOW REGION ON BOATTAIL

flow region on a mortar configuration. In examining Figure 2, Figure 2A illustrates a typical mortar configuration showing a nose of length ℓ_n with a nose tip diameter d_n, an afterbody of length ℓ_a, a boattail of length ℓ_{B_1}, and a boom of length ℓ_{B_2}. The boom or base diameter is d_B and the reference diameter is d_r. The fins have a semispan of b/2 and the fin semispan plus the boom diameter is approximately equal to the reference diameter, d_r.

Figure 2B is the AP05 representation of the mortar configuration in Figure 2A. Note that all dimensions are basically the same except the AP05 requires the boattail and boom length of

Figure 1A be combined into a single boattail. The Figure 1B geometry requirement of the AP05 is driven by the fact the AP05 requires a nose, afterbody, and boattail or flare for Mach numbers less than 1.6, which is the Mach number of interest for mortars. The boom must therefore be combined with the boattail.

Figure 2C illustrates the thick boundary layer on the boattail of the mortar at the top of the boattail. The bottom of the boattail illustrates the BLDT on the boattail. The BLDT is typically only a fraction of the boundary layer total thickness. The displacement thickness indicates the distance by which the external streamlines are shifted away from the body due to the boundary layer. For example, to include viscous effects into an inviscid code, it is common practice to add the BLDT to the body. As seen in Figure 2C, the BLDT has the effect of reducing the fin semispan, thus reducing static stability, roll and pitch damping.

If the mortar boattail angle of Figure 2 is fairly small (say 8 deg or less) and not too long (say one caliber or less), the boundary layer remains attached to the body and can be reasonably well predicted in thickness and thus accounted for. The AP05 currently accounts for BLDT on smaller boattails. However, for longer boattails such as exhibited on low drag bombs and mortars, the boundary layer thickens considerably, producing a low dynamic pressure region in the root chord region of the fins, and needs to be accounted for in both static and dynamic aerodynamic computations for the fins. The BLDT is not adequately accounted for in the AP05 and is a source of error for configurations that have long boattails with fins on the boattail.

2.0 IMPROVEMENTS IN AP09

This section of the report will discuss improvements made to the AP05 to form the AP09. The weak areas of Section 1.1 will be dealt with individually in terms of modifications to existing methods or new technology developed and added to the AP09.

2.1 BODY ALONE LIFT CHARACTERISTICS FOR $M_\infty < 1.2$

The body alone normal force characteristics were all empirical. The center of pressure of the nose and boattail normal force were defined based on slender body theory (SBT) and the afterbody normal force center of pressure was predicted empirically (see Reference 2). Each component of normal force and center of pressure will be re-examined. In investigating the nose component of normal force, the method of Reference 2 was compared to the data of Reference 10. Reference 10 had data for short ogives as well as truncated ogives. It was found that even though the nose shape was anything but slender, the SBT value of 2.0 was actually more accurate than the method of Reference 2, which was based primarily on experimental data for cones (see Figure 4.21 of Reference 2). Hence, the method of Reference 2 will be replaced by the SBT value of 2 for the nose component of normal force coefficient slope near $\alpha = 0$. SBT will continue to be used for center of pressure prediction for the nose normal force at low AOA. The additional normal force due to the presence of an afterbody and the normal force center of pressure is predicted by the method of Wu and Aoyoma[11] transonically and empirically by the data of Spring[12] and Given and Spring[13] in the AP05 (again see Reference 2, page 156). The only change in the AP09 will be to make the curve of Figure 4.22, page 156 of Reference 2 for $M_\infty = 1.1$ and 1.2 for $M_\infty = 1.2$ only. The value for $M_\infty = 1.1$ is interpolated between the value at $M_\infty = 1.0$ and that for $M_\infty = 1.2$. The revised Figure 4.22 of Reference 2 and Figure 4.24 of Reference 2 are repeated here as Figures 3 and 4 respectively.

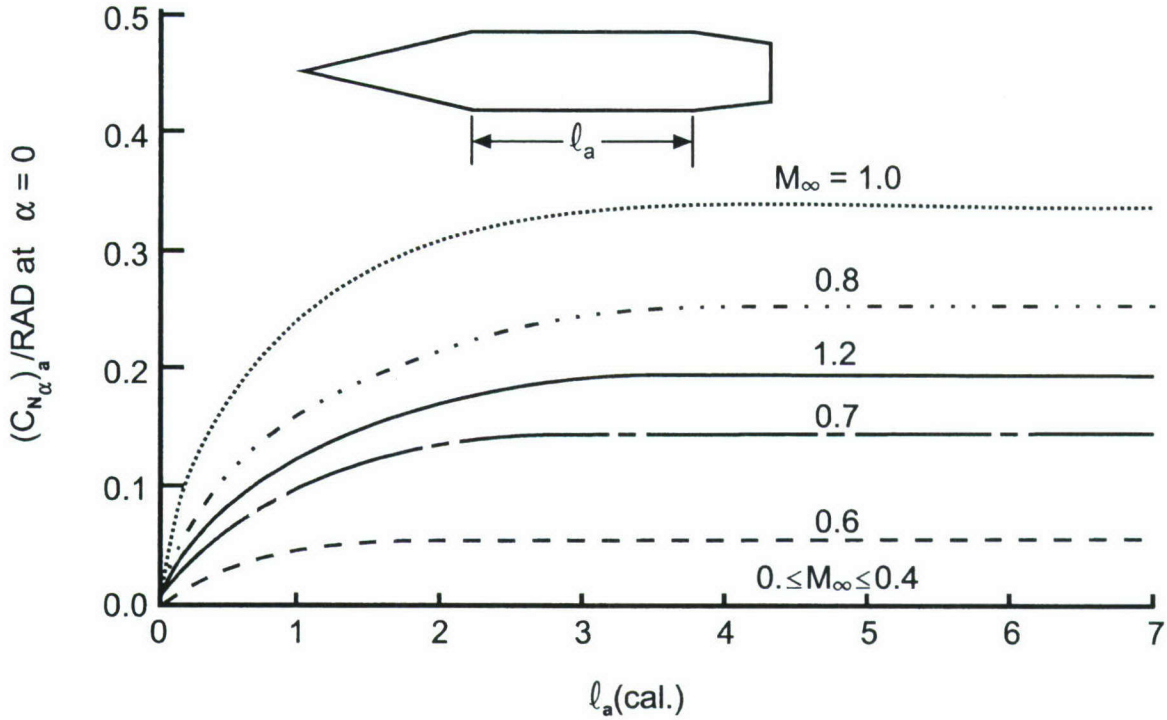

FIGURE 3. INCREASE IN (C_{N_α}) AT SUBSONIC AND TRANSONIC MACH NUMBERS DUE TO AFTERBODY

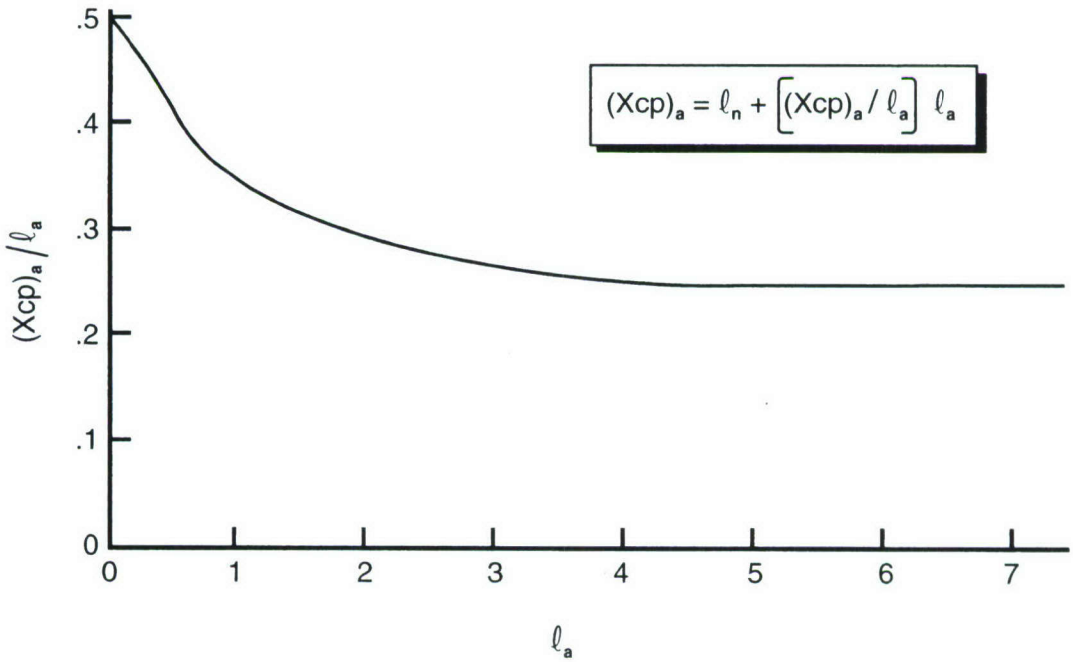

FIGURE 4. CENTER OF PRESSURE OF AFTERBODY LIFT FOR M_∞<1.2

The normal force coefficient on the boattail was changed from the value used in the AP05 and prior versions of the aeroprediction code to that used in the AP09. Figure 5 gives the new values of the boattail normal force coefficient slope for low AOA and compares it to the older data[5,14]. The new curve of Figure 5 is based on data from several more recent data bases[15-18] than the data bases used for the AP72 of Figure 5. Note the new curve of Figure 5 does not have quite as large a negative value of C_{N_α} for the boattail as did the older curve. The AP05 used SBT for the center of pressure of the boattail. For most short boattails, SBT was adequate. However, for longer boattails SBT values of center of pressure were found to be too far aft. As a result, a value closer to the intersection of the afterbody and boattail was chosen. This value is defined by Equation (2A).

$$(X_{CP}) = \ell - C\ell_B \tag{2A}$$

where: $\ell_B \leq 1.0$ cal, $C = 0.75$

$$\left.\begin{array}{l} 1.0 < \ell_B \leq 2.0 \\ 0.5 < M_\infty < 1.2 \end{array}\right\} C = (.243 - .286\, M_\infty)\ell_B + .507 + .286\, M_\infty$$

$$\left.\begin{array}{l} 1.0 < \ell_B \leq 2.0 \\ M_\infty \leq 0.5 \end{array}\right\} C = 0.65 + .1\,\ell_B$$

$$\left.\begin{array}{l} \ell_B > 2.0 \\ 0.5 < M_\infty < 1.2 \end{array}\right\} C = .993 - .286\, M_\infty$$

$$\left.\begin{array}{l} \ell_B > 2.0 \\ M_\infty \leq 0.5 \end{array}\right\} C = 0.85$$

In addition to the Equation (2A) center of pressure change for boattails, it was found that an upper bound on magnitude of boattail normal force computed from Figure 5 was needed. This upper value was:

$$\left.\begin{array}{l} \left|(C_{N_\alpha})_b\right|_{max} = -1.5 + 0.2\, M_\infty, \\ \qquad\qquad 0.5 < M_\infty < 1.2 \\ = -1.5,\ M_\infty \leq 0.5 \end{array}\right\} \tag{2B}$$

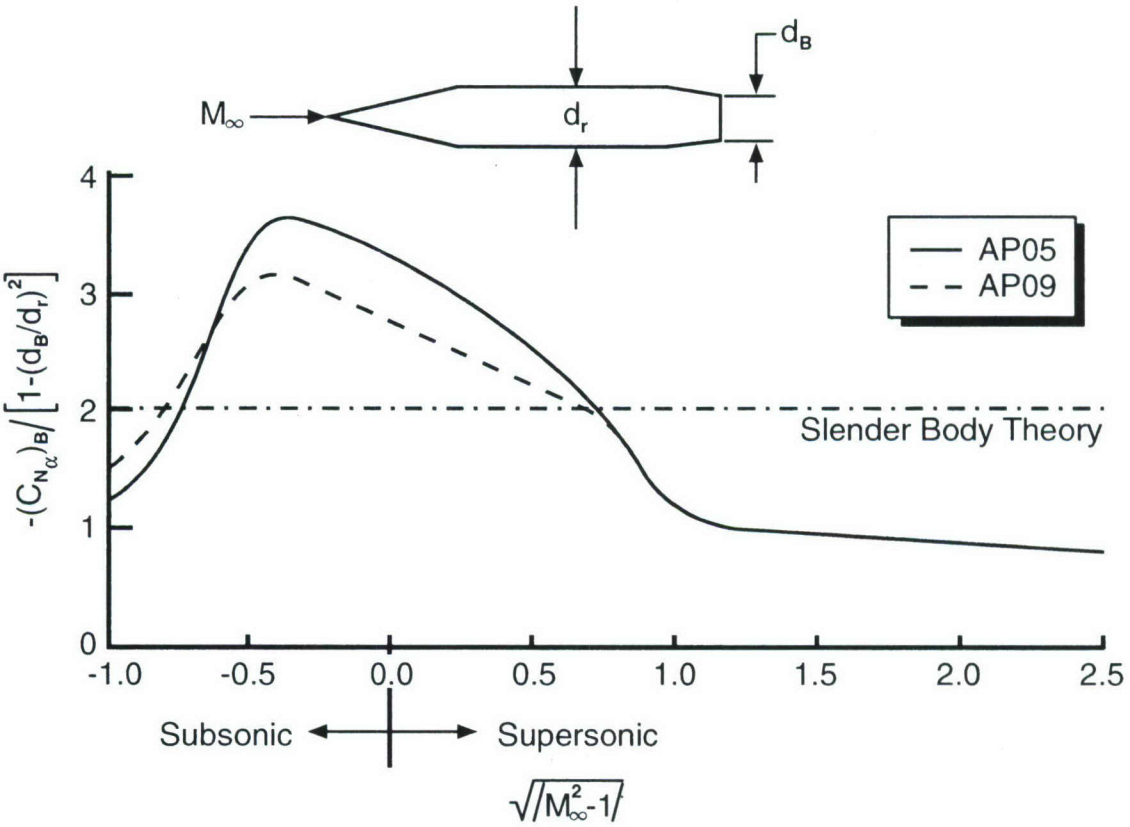

FIGURE 5. DECREASE IN $C_{N\alpha}$ DUE TO BOATTAIL

To summarize the new body alone lift characteristics for Mach numbers less than 1.2, we have the following:

$$\left.\begin{aligned} &(C_{N_\alpha})_n = 2.0 \quad ; \quad (X_{CP})_n = \ell_n - \frac{(vol)_n}{\pi R_r^2} \\ &(C_{N_\alpha})_a = \text{Figure 3} \quad ; \quad (X_{CP})_a = \text{Figure 4} \\ &(C_{N_\alpha})_b = \text{Figure 5} \quad ; \quad (X_{CP})_b = \text{Equation (2A)} \\ &\qquad\qquad + \\ &\qquad \text{Equation (2B)} \end{aligned}\right\} \tag{2C}$$

The pitching moment coefficient derivative is then:

$$C_{M_\alpha} = -\left[(C_{N_\alpha})_n (X_{CP})_n + (C_{N_\alpha})_a (X_{CP})_a + (C_{N_\alpha})_b (X_{CP})_b\right] \tag{3}$$

The total normal force coefficient derivative and center of pressure for the body is then:

$$C_{N_\alpha} = (C_{N_\alpha})_n + (C_{N_\alpha})_a + (C_{N_\alpha})_b \tag{4}$$

$$X_{CP} = -\frac{C_{M_\alpha}}{C_{N_\alpha}} \tag{5}$$

2.2 BODY ALONE LIFT CHARACTERISTICS FOR $M_\infty \geq 1.2$

The best way to illustrate the problem the HTVD has in predicting the normal force coefficient derivative at low AOA correctly for a boattailed configuration is to compare the pressure coefficients to experimental data or a more accurate Navier Stokes model. Figure 6 (taken from Reference 2 as Figure 3.6) compares the pressure coefficients predicted by the second order Van Dyke (SOVD) method on a sharp ten degree cone-cylinder at 0 deg AOA at a Mach number of 2.0. Note the excellent agreement of pressure prediction to experimental data. This excellent agreement of theory and experiment is the reason the SOVD method gives good axial force prediction.

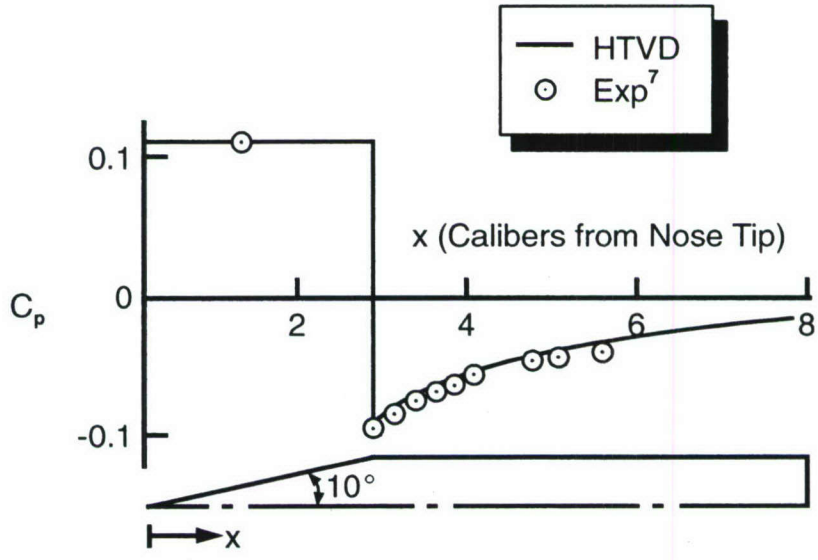

FIGURE 6. PRESSURE COEFFICIENT ON CONE CYLINDER (M_∞=2.07, α=0°)

Figure 7 (taken from Reference 2 as Figure 3.7) shows the comparison of the HTVD (which combines a second order accurate axial force predictor with a first order accurate normal force predictor) to experimental data on the same cone cylinder of Figure 6, except the Mach number is 2.07 and AOA is 12 deg. Note the prediction of pressure by the Hybrid Theory is still quite good on the cone, but starts to deviate on the afterbody, particularly in the leeward plane (Φ = 0 deg). Unfortunately, I was unable to find pressure coefficient data for a nose-cylinder-boattail configuration. However, suffice it to say, that if the afterbody pressure coefficients deviate from experimental data, as in Figure 7, then the pressure prediction on the boattail will also deviate.

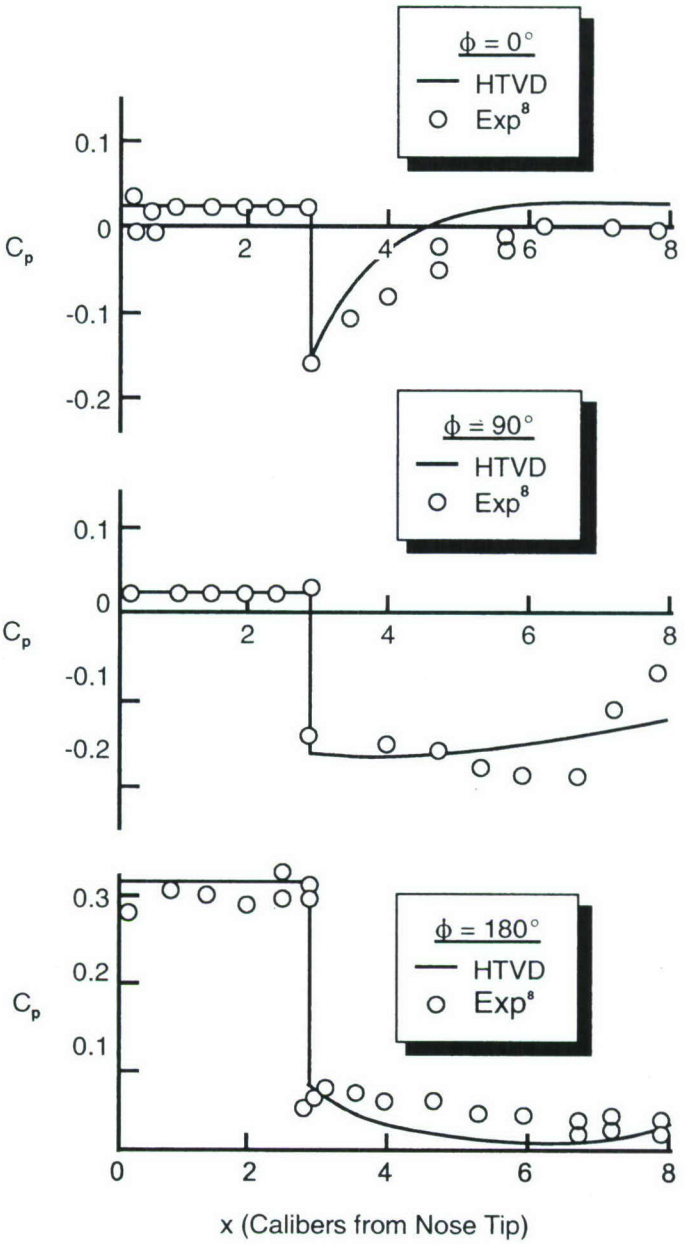

FIGURE 7. PRESSURE COEFFICIENT ON CONE CYLINDER (M_∞=2.0, α=12°) OF FIGURE 6

The Aeroprediction Code allows a nose-cylinder-boattail/flare for Mach numbers where the SOVD theory is used. The nose allows two sections. If subscripts 1, 2 denote the two nose sections, subscripts 3 and 4 denote the cylinder and boattail/flare sections respectively, then a method to correct the prediction of the forces and moments of the SOVD was found to be:

$$C_{N_B} = C_{N_{BN}} + C_{N_1} + C_{N_2} + C_{N_3} + (BF)C_{N_4} \tag{6A}$$

$$C_{M_B} = C_{M_{BN}} + C_{M_1} + C_{M_2} + C_{M_3} + (BF)C_{M_4} \tag{6B}$$

The first term of Equation (6) is the normal force and pitching moment on the blunt nose if the configuration has a blunt nose. The next two terms of Equation (6) are the normal force and pitching moment of the two nose segments, the fourth term is the afterbody normal force and pitching moment and the last term is the normal force and pitching moment of the boattail or flare. The boattail factor (BF) was defined by trial and error on configurations that have boattails as:

$$\left.\begin{aligned} BF &= \left(1-\frac{M_\infty}{2}\right)\frac{\ell_B}{2}+\frac{3M_\infty}{4}-\frac{1}{2} \\ &\quad ;\ 1.0 \le \ell_B \le 3.0 \\ BF &= \frac{M_\infty}{2} \quad ;\ \ell_B < 1.0 \\ BF &= 1.0 \quad ;\ M_\infty \ge 2.0 \\ BF &= 1.0 \quad ;\ \ell_B > 3.0 \\ BF &= 1.0 \quad ;\ r_B \ge r_r \end{aligned}\right\} \qquad (6C)$$

In examining Equation (6C), it is seen that the boattail factor is one (i.e. no change from the AP05) if either Mach number is greater than 2.0, boattail length (ℓ_B) is greater than 3.0 cal or the configuration has a flare ($r_B \ge r_r$) versus a boattail. One may naturally ask if the pressure prediction of the boattail leads to consistent errors in normal force and pitching moment, won't there be errors in axial force coefficient prediction as well. The answer is yes, but the normal force and pitching moment coefficient errors are larger and easier to predict whereas the axial force errors are small enough that good axial force prediction accuracy is still obtained on boattailed configurations. Hence, no attempt was made to develop a correction for axial force coefficient predictions of the SOVD theory.

2.3 BODY ALONE PITCH DAMPING CHARACTERISTICS FOR CONFIGURATIONS WITH LONG BOATTAILS

As discussed earlier, the body alone pitch damping is empirical and based on the SPINNER code of the early 70's[5]. The body alone pitch damping was improved upon[6] for the AP02. The improvements were aimed at longer bodies, higher Mach numbers and configurations with flares. However, when a body has a long boattail, the pitch damping is decreased drastically and the improved methodology of Reference 6 does not account for the long boattail. When a configuration has a long boattail the pitch damping is decreased for two reasons. First, the body pitch damping is based on body planform area, which is decreased when a boattail is present. Secondly, the rotational portion of the pitch damping is decreased even more due to the fact the pitch damping is proportional to the normal force component of a segment of the body times the distance of that segment from the center of moments squared. The boattail area decreases as the distance from the center of moments increases. The combination of the above mentioned two phenomena means the body alone pitching damping methodology of the AP05 needs to be modified for configurations with long boattails.

The method chosen to address the AP05 weakness on body alone pitch damping prediction for long boattails was to define a factor to multiply the AP05 prediction that was a function of base diameter, center of moment location, and Mach number. It was found in comparing the AP05 C_{M_q} predictions to data that these were the most important variables. Thus:

$$\left(C_{M_q}\right)_{09} = \left(C_{M_q}\right)_{05} \left(\frac{r_B}{r_r}\right)^x \tag{7}$$

where $\left(C_{M_q}\right)_{09}$ and $\left(C_{M_q}\right)_{05}$ represent the AP09 and AP05 predictions for pitch damping respectively. The factor $\left(r_B/r_r\right)^x$ of Equation (7) was derived based on comparisons to data.

We also know that when $\left(r_B/r_r\right) > 0.85$, we have good agreement of AP05 pitch damping to data. Hence, the exponent "x" of Equation (7) should go to zero when r_B/r_r increased above about 0.85. We also know that as the center of moment moves toward the nose, the AP05 C_{M_q} predictions get worse since the loss of planform area from the long boattail gets farther from the center of moments. Thus, the exponent "x" of Equation (7) will get larger as the center of moments moves forward.

Figure 8 gives the final methodology derived for the exponent "x" of Equation (7). Note that in Figure 8, three cases are considered for center of mass location:

$$\frac{X_{CG}}{l} \le 0.44$$

$$\frac{X_{CG}}{l} \ge 0.55$$

$$0.44 < \frac{X_{CG}}{l} < 0.55$$

A forward location of X_{CG}/l of 0.44 and an aft location of X_{CG}/l of 0.55 are fairly practical values of center of gravity extremes for weapons. Most configurations with long boattails fall in the X_{CG}/l of 0.44 category. As seen in Figure 8, the exponent "x" of Equation (7) tends to zero as r_B/r_r approaches one and also gets larger with more forward values of X_{CG}/l. It should also be kept in mind that Figure 8 was derived for long boattails where the boattail angle is much less than 8 deg. When the boattail angle is greater than 8 deg, the AP05 constraint of a maximum of 8 deg still applies.

I. $\underline{X_{CG}/l \leq 0.44}$

$\underline{M_\infty \leq 1.0}$

$X_2 = 2.3$

IF $(r_B/r_r) > 0.5$, $X_2 = 4.16 - 3.71\ (r_B/r_r)$

IF $(r_B/r_r) > 0.85$, $X_2 = 1.0$

$\underline{M_\infty \geq 2.0}$

$X_2 = 1.8$

IF $(r_B/r_r) > 0.5$, $X_2 = 2.94 - 2.29\ (r_B/r_r)$

IF $(r_B/r_r) > 0.85$, $X_2 = 1.0$

$\underline{1.0 < M\infty < 2.0}$

$X_2 = 2.8 - 0.5\ M_\infty$

IF $(r_B/r_r) > 0.5$, $X_2 = [4.16 - 3.71\ (r_B/r_r)]\ [2.0 - M_\infty] + [2.94 - 2.29\ (r_B/r_r)]\ [M_\infty - 1]$

IF $(r_B/r_r) > 0.85$, $X_2 = 1.0$

II. $\underline{X_{CG}/l \geq 0.55}$

$X_2 = 1.7$

IF $(r_B/r_r) > 0.5$, $X_2 = 2.7 - 2.0\ (r_B/r_r)$

IF $(r_B/r_r) > 0.85$, $X_2 = 1.0$

III. $\underline{0.44 < X_{CG}/l < 0.55}$

Linear interpolate between methodology for $X_{CG}/l \leq 0.44$ and $X_{CG}/l \geq 0.55$ based on value of X_{CG}/l

IV. Blend Large Boattail to Small Boattail

IF $(r_B/r_r) \leq 0.65$, $P_3 = 1.0$

IF $(r_B/r_r) > 0.65$, $P3 = -50.2 + 173.0\ (r_B/r_r) - 189.6 \left(\frac{r_B}{r_r}\right)^2 + 68.8 \left(\frac{r_B}{r_r}\right)^3$

IF $P_3 > 2.0$, $P_3 = 2.0$

$X_3 = 2.0 - P_3$

V. Final Equation

$x = (X_2)(X_3)$

$$\left(C_{M_Q}\right)_{09} = \left(C_{M_Q}\right)_{05} \left(\frac{r_B}{r_r}\right)^X$$

FIGURE 8. METHODOLOGY FOR BODY ALONE PITCH DAMPING FOR CONFIGURATIONS WITH LONG BOATTAILS

2.4 MULTI-FIN FACTORS FOR LOW ASPECT RATIO WINGS AT SUBSONIC SPEEDS

The new multi-fin factors for configurations with 6 and 8 fins are given in Figure 9. The only change in these factors from the AP05[19] is for the $M_\infty \leq 0.6$ column for the aspect ratio of 2.0 and less. Note the new values are now more in line with the Navier Stokes computations for $M \geq 1.5$, as opposed to much higher values previously used that were based on unsteady Euler computations.

It is speculated that the reason the inviscid values for aspect ratio 4, which have been previously validated, are much higher than the multi-fin factors for the lower aspect ratio is viscous effects. The Navier Stokes code automatically includes boundary-layer displacement effects, which are much more important on fins that have a small span than on fins with a larger span. Thus the low aspect ratio values of the multi-fin factors, which had not been previously validated for $M_\infty < 1.0$, were modified in accordance with data and are now more in line with the supersonic multi-fin factors computed from a full Navier Stokes code.

2.5 LINEAR ROLL AND PITCH DAMPING IMPROVEMENTS FOR FINNED CONFIGURATIONS WITH LONG BOATTAILS

Both pitch and roll damping of fins at zero AOA is computed by linearized theory and assumes the fins go all the way to the body centerline. This approach of computing pitch and roll damping of fins when the fins are on a cylindrical body works well. However, when the fins lie on a long boattail, the fin span needs to be reduced to an effective span to account for the low dynamic pressure and viscous effects in the vicinity of the body. Including BLDT effects had little effect on either the roll or pitch damping since any reduction in fin span was compensated for by the equivalent increase in body radius. That is if the span of the wings for roll and pitch damping computations is:

$$b_1 = b + 2R \tag{8}$$

and we decrease b by twice the BLDT and increase R by the BLDT, the net result is no change in dynamic derivatives.

The approach used in the AP09 is therefore to define effective values of the radius where the tail on the boattail is located. For pitch damping calculations this effective radius is:

$$R_{eff} = [1 + C_1(M)]r_w - C_1(M)r_r \tag{9A}$$

$$C_1(M) = 0.33 \quad ; \quad M_\infty \leq 0.6$$

where $= 0.33 - 0.55(M_\infty - 0.6); \; 0.6 < M < 1.2$

$= 0 \quad ; \quad M_\infty \geq 1.2$

AR	α	F_6 MACH NUMBER					F_8 MACH NUMBER				
		0.6	1.5	2.0	3.0	4.5	0.6	1.5	2.0	3.0	4.5
.25	0	1.26	1.37	1.27	1.19	1.22	1.42	1.42	1.40	1.27	1.20
	15	1.00	1.00	1.10	1.19	1.35	1.21	1.03	1.17	1.27	1.35
	30	1.00	1.00	1.00	1.19	1.22	1.00	1.00	1.01	1.27	1.22
	45	1.00	1.00	1.00	1.00	1.00	1.00	1.00	1.00	1.00	1.00
	60	1.00	1.00	1.00	1.00	1.00	1.00	1.00	1.00	1.00	1.00
	75	1.00	1.00	1.00	1.00	1.00	1.00	1.00	1.00	1.00	1.00
	90	1.00	1.00	1.00	1.00	1.00	1.00	1.00	1.00	1.00	1.00
.50	0	1.26	1.25	1.20	1.30	1.47	1.44	1.36	1.28	1.35	1.72
	15	1.05	1.10	1.15	1.29	1.50	1.22	1.18	1.24	1.40	1.83
	30	1.00	1.00	1.07	1.29	1.36	1.00	1.08	1.16	1.41	1.60
	45	1.00	1.00	1.00	1.00	1.00	1.00	1.00	1.04	1.06	1.20
	60	1.00	1.00	1.00	1.00	1.00	1.00	1.00	1.00	1.00	1.00
	75	1.00	1.00	1.00	1.00	1.00	1.00	1.00	1.00	1.00	1.00
	90	1.00	1.00	1.00	1.00	1.00	1.00	1.00	1.00	1.00	1.00
1.0	0	1.28	1.22	1.35	1.42	1.50	1.50	1.38	1.58	1.96	2.00
	15	1.15	1.13	1.23	1.32	1.50	1.34	1.38	1.38	1.80	2.00
	30	1.06	1.00	1.00	1.21	1.38	1.10	1.28	1.15	1.64	2.00
	45	1.02	1.00	1.00	1.10	1.13	1.00	1.05	1.00	1.48	1.61
	60	1.00	1.00	1.00	1.00	1.00	1.00	1.00	1.00	1.32	1.25
	75	1.00	1.00	1.00	1.00	1.00	1.00	1.00	1.00	1.16	1.00
	90	1.00	1.00	1.00	1.00	1.00	1.00	1.00	1.00	1.00	1.00
2.0	0	1.42	1.50	1.50	1.50	1.50	1.68	1.77	1.97	1.92	1.90
	15	1.31	1.41	1.27	1.39	1.50	1.52	1.95	1.75	1.77	2.00
	30	1.17	1.00	1.03	1.27	1.45	1.35	1.65	1.57	1.62	2.10
	45	1.03	1.00	1.00	1.14	1.23	1.18	1.32	1.27	1.47	1.95
	60	1.00	1.00	1.00	1.00	1.00	1.02	1.00	1.02	1.32	1.62
	75	1.00	1.00	1.00	1.00	1.00	1.00	1.00	1.00	1.17	1.32
	90	1.00	1.00	1.00	1.00	1.00	1.00	1.00	1.00	1.00	1.00
4.0	0	1.50	1.50	1.50	1.50	1.50	2.00	1.90	2.00	2.00	2.00
	15	1.33	1.41	1.27	1.39	1.50	1.70	1.95	1.75	1.77	2.00
	30	1.17	1.00	1.03	1.27	1.45	1.47	1.65	1.57	1.62	2.00
	45	1.03	1.00	1.00	1.14	1.23	1.25	1.32	1.27	1.47	1.95
	60	1.00	1.00	1.00	1.00	1.00	1.02	1.00	1.02	1.32	1.62
	75	1.00	1.00	1.00	1.00	1.00	1.00	1.00	1.00	1.17	1.32
	90	1.00	1.00	1.00	1.00	1.00	1.00	1.00	1.00	1.00	1.00

FIGURE 9. APPROXIMATED VALUES OF THE FACTORS F_6 AND F_8 OBTAINED FROM SMOOTHED VALUES OF THE ZEUS AND GASP CODE COMPUTATIONS AND ENGINEERING JUDGEMENT

In examining Equation (9A), it is seen that for $M_\infty > 1.2$. the effective radius becomes r_W, the body radius at the wing mid chord, which is the current value of r in the AP05.

For roll damping, the effective radius is

$$R_{eff} = 1.20\, r_B - 0.20\, r_r \tag{9B}$$

Equation (8) now becomes:

$$b_1 = b + 2\, R_{eff} \tag{10}$$

and Equation (9A) and Equation (9B) define R_{eff} for pitch and roll damping calculations respectively, at all Mach numbers. Both Equations (9A) and (9B) were derived based on numerical experiments applying the AP05 code and comparing the resulting computations to experiment.

It was mentioned earlier that the body length under the wing was used in computing roll damping and pitch damping, even though for the dynamic derivatives the wing was assumed to go all the way to the body centerline. To avoid the double counting of body length and area for dynamic derivatives, the root chord length was subtracted from the overall body length. That is:

$$\ell_1 = \ell - c_{r_w} \tag{11}$$

Equation (11) will effect dynamic derivatives of all configurations with lifting surfaces present.

It was also found that for transonic flow, the methodology of Reference 2 (pp 158-159) gave undesirable results past the force break Mach number. To overcome the sudden decrease and subsequent increase in wing lift, roll and pitch damping, the wing lift was computed as at present up to the force break Mach number. From the force break Mach number to Mach 1.2, the values of wing normal force (and hence roll and pitch damping) were linearly interpolated between the values at the force break Mach number and the value at $M_\infty = 1.2$.

2.6 INCORPORATION OF BOUNDARY LAYER DISPLACEMENT EFFECTS ON BODY-TAIL CONFIGURATIONS WITH LONG BOATTAILS

The AP05 and prior versions of the Aeroprediction Code has a boundary layer displacement model included for boattails. This model has two elements. The first element reduces the boattail to a maximum of 8 deg if the boattail angle is greater than 8 deg. The second part of the model reduces the boattail angle by 10 percent. That is

$$(\theta_b)_{eff} = 0.9\, \theta_b \tag{12}$$

where θ_b is the actual boattail angle and $(\theta_b)_{eff}$ is the reduced angle due to BLDE. In applying the model represented by Equation (12) to configurations with long boattails, it was found that only

one additional criteria was needed. The additional criteria was to put an upper bound on the maximum allowable negative value of normal force coefficient derivative for the boattail for $M_\infty < 1.0$. The maximum value for $(C_{N_\alpha})_b$ is approximated by

$$(C_{N_\alpha})_b = -1.5 + 0.2\, M_\infty \tag{13}$$

for $M_\infty < 1.2$. For $M_\infty \geq 1.2$, the Hybrid Theory of Van Dyke computes the value of $(C_{N_\alpha})_b$ for Mach numbers up to about 2.0 and the Second Order Shock Expansion Theory calculates $(C_{N_\alpha})_b$ for Mach numbers of about 2 and higher. All theoretical methods and empirical methods utilize Equation (12) with the upper values of θ_b reduced to 8 deg before Equation (12) is applied. In other words, the body boattail shape is changed before pressure coefficients are computed. The Equation (12) approach for accounting for BLDE has been shown to give reasonable results over a wide range of boattail shapes.

The main problem with the AP05 and all prior versions of the Aeroprediction Code is that the BLDE is not accounted for in wing span reduction. Section 2.5 discussed how the fin span reduction effects were included in the roll and pitch damping computations. However, for lift computations, the wing span does not include the body radius and instead wing-body and body-wing interference effects are included to get the complete lift computations. To include the BLDT in wing lift calculations, we need to decrease the wing semispan by the BLDT, decrease the wing root chord slightly, increase the distance from the nose to the wing leading edge slightly and increase the radius at the wing by the BLDT. Figure 10 illustrates physically what is changed for the wing-body geometry when BLDT is included. "X" in Figure 10 is the distance to the midpoint of the root chord (or centroid of wing area if available) from the nose tip and X_{AFT} is the distance from the nose tip to the start of the boattail.

The geometry of Figure 10 is "hard wired" into the AP09. Thus the code user will simply put in the configuration geometry as in the AP05. However, the AP09 has logic based on whether the configuration has a boattail or not. If the configuration has a boattail with a fin on it, the geometry of Figure 10 is automatically used for wing lift calculations. The effect of including BLDT into the aerodynamic calculations is to reduce wing normal force, axial force, pitching moment and configuration static stability. The amount of the decrease is dependent on the boattail angle and length.

2.7 NONLINEAR AXIAL FORCE MODIFICATIONS FOR BODY-TAIL CONFIGURATIONS

The nonlinear axial force coefficient at AOA was given in Reference 9 and summarized in Reference 2 pages 258-265. The approach used in the AP05 for the nonlinear axial force term is to define the term empirically based on data bases. That is

$$C_A = C_{A_0} + f(M_\infty, \alpha) \tag{14}$$

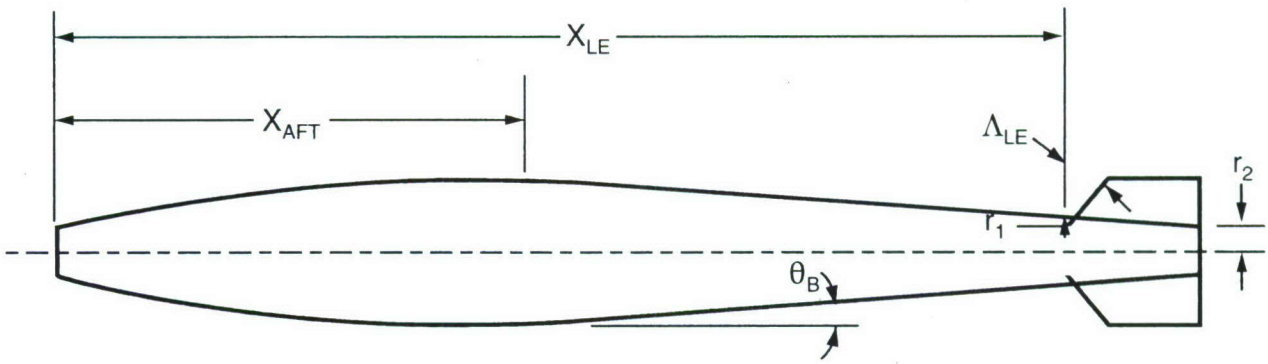

Mortar Configuration

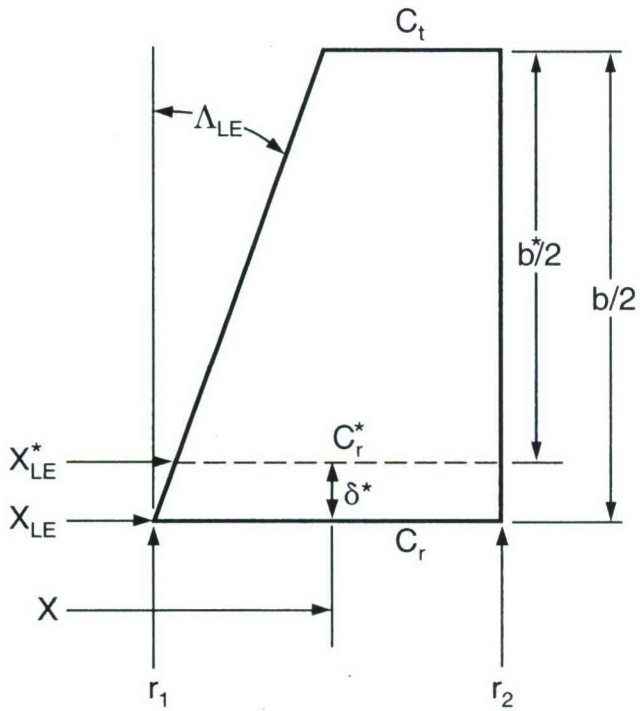

$$\text{Tan } \Lambda_{LE} = \frac{C_r - C_t}{b/2} = \frac{C_r^* - C_t}{b/2}$$

$$C_r^* = \left(\frac{C_r - C_t}{b/2} \right) b^*/2 + C_t$$

$$b^*/2 = b/2 - \delta^*$$

$$\delta^* = 0.10\theta_b \, (X - X_{AFT})$$

$$X = X_{LE} + \frac{C_r}{2}$$

$$X_{LE}^* = X_{LE} + C_r - C_r^*$$

$$r_W = \frac{r_1 + r_2}{2} + \delta^*$$

Enlarged View of Wing and Mathematics of Implementing BLDT

FIGURE 10. GEOMETRY INVOLVED IN INCORPORATING BOUNDARY LAYER DISPLACEMENT THICKNESS EFFECTS INTO WING LIFT CALCULATIONS

where C_{A_o} is the value calculated for axial force at zero AOA and $f(M_\infty,\alpha)$ is the nonlinear term given by

$$f(M_\infty \alpha) = A\alpha + B\alpha^2 + C\alpha^3 + D\alpha^4 \qquad (15)$$

The constants A, B, C and D are defined based on the conditions $f'(M_\infty,0)$, $f(M_\infty,30)$, $f(M_\infty,60)$ and $f(M_\infty,90)$. The values of the parameters $f'(M_\infty,0)$ and $f(M_\infty,30)$ are modified slightly for the

body tail case at low Mach numbers and are now closer to the values for the body alone configuration. No changes were made to the body alone and wing-body-tail case. The new values of $f(M_\infty,\alpha)$ for body tail cases are given in Figure 11.

M	f'(M,0)	F(M,30)	F(M,60)	F(M,90)
0	0.20	-0.16	-0.79	-0.060
0.6	0.20	-.016	-0.66	-0.060
0.8	0.15	-0.160	-0.46	-0.060
0.9	0.12	-0.135	-0.38	-0.060
1.0	0.120	-0.110	-0.26	-0.060
1.15	0.160	-0.020	-0.18	-0.140
1.2	0.186	0	-0.12	-0.160
1.3	0.200	0.040	-0.06	-0.220
1.5	0.258	0.100	0.06	-0.240
2.0	0.330	0.150	0.20	-0.130
2.5	0.350	0.180	0.28	-0.060
3.0	0.346	0.190	0.30	0
3.5	0.325	0.200	0.32	0.030
4.5	0.230	0.220	0.33	0.065
≥6.0	0.180	0.230	0.34	0.070

FIGURE 11. VALUES OF THE AXIAL FORCE AOA PARAMETERS FOR A BODY-TAIL CONFIGURATION

2.8 NEW METHODS TO PREDICT NONLINEAR PITCH DAMPING MOMENTS

One area that has basically remained the same since the 1977 version of the Aeroprediction Code (AP77) is the linearity of the dynamic derivatives in the code. Nonlinear static aerodynamics were first incorporated into the code in 1993 up to AOA 30 deg. The nonlinear static aerodynamics were extended to 90 deg AOA in 1995 and to the roll position of 45 deg in 1998. The nonlinear static aerodynamics were then improved upon with the AP02 based on a new wind tunnel data base that varied r/s. The static aerodynamic nonlinearities are well documented in References 2 and 7.

Unfortunately, no such generic wind tunnel data bases exist for dynamic derivatives as exist for static aerodynamics. In researching the literature, several pieces of dynamic derivative wind tunnel data was available for various configurations. These wind tunnel and ballistic range data (References 20-35) are all for a specific configuration at a limited number of Mach numbers and AOAs. References 20-29 are all open literature whereas References 30-35 are unclassified, but limited distribution.

The wind tunnel data was generally taken by one of three methods. The first approach (pioneered in the late 50's and early 60's) at the then Naval Ordnance Lab, White Oak, Maryland, was to place a steel rod through the center of gravity of the model and attach it to the wind tunnel walls. The model was then deflected to a certain AOA and the damping motion was recorded in both time and AOA. This type of testing was referred to as "free oscillation" and required the model to be statically stable. For large AOA, the damping derivatives were measured in increments of AOA decay (see Reference 20 for example), and the pitch damping moment was determined from the linearized equation:

$$I_y \ddot{\alpha} + \mu\dot{\alpha} + M_\alpha \alpha = 0 \tag{16}$$

where I_y = moment of inertia about the pitch plane
μ = damping constant
M_α = pitch moment slope

Equation (16), while linear, was assumed to apply over increments in AOA, even though the C_{M_α} and μ may be different from increment to increment. That is, for the increment of interest, C_{M_α} and μ were assumed constant.

A second type of pitch damping test for small to moderate AOAs was performed at AEDC[34] where a sting was attached to the model and the model was forced to oscillate about 3 deg AOA range. This type of mechanism could determine pitch damping for stable or unstable configurations. The sting and model were moved to a certain AOA and a forced oscillation of ±3 deg in AOA was performed by the sting on the model and the decay of the model measured. This type of testing is referred to as "forced oscillation testing".

A third type of pitch damping test for high AOA was also performed at AEDC where a strut was mounted to the leeward plane of the model[21]. A similar forced oscillation system was used to record the damping derivatives as in Method 2 discussed above. However, here due to the strut mounting technique, AOAs to 90 deg can be achieved.

Fundamentally, the first and third types of testing have issues of wind tunnel wall or model installation interference issues or both. The pitch damping tests performed in the late 50's and early 60's at NSWC/WO was in a small test section with a model that had a rod going through the center of gravity. Thus wall interference and rod interference on the damping characteristics are both issues. The strut used in the high AOA testing is quite thick and definitely will influence aerodynamics behind the strut. The second type of pitch damping testing is similar to static aerodynamic testing and should have minimal wind tunnel interference. Unfortunately, most of the data bases at AOA in the open literature have used either test technique one or three. As a result, development of a nonlinear semiempirical pitch damping model will be based on a meager amount of data that unfortunately has more wind tunnel interference issues associated with the data than is desired. Ballistic range data helps to validate wind tunnel data at low AOA but is of no help at moderate to high AOA.

Three methods will be investigated for predicting nonlinear pitch damping moments. Two of the methods are either new or improved upon state of the art methods. Also, two of the methods are based strictly on the static aerodynamics whereas the third method is based on the improved zero AOA pitch damping method of the AP09 discussed in Sections 2.1 – 2.6. Each of the three different methods will now be discussed individually.

The first two methods are based on more generalized methods of Reference 36, Chapter 9. The total normal force for a wing-body-tail configuration can be defined by:

$$C_N = C_{N_B} + C_{N_{W(B)}} + \Delta C_{N_{B(W)}} + C_{N_{T(B)}} + \Delta C_{N_{B(T)}} + C_{N_{T(V)}} \tag{17}$$

Using the Reference 36 analogy, the pitch damping moment is thus:

$$\begin{aligned} C_{M_q} + C_{M_{\dot\alpha}} = {} & \left(C_{N_\alpha}\right)_B \left(\frac{X_{CP} - X_{CG}}{d}\right)^2_B + \left(C_{N_\alpha}\right)_{W(B)} \left(\frac{X_{CP} - X_{CG}}{d}\right)^2_{W(B)} \\ & + \left(\Delta C_{N_\alpha}\right)_{B(W)} \left(\frac{X_{CP} - X_{CG}}{d}\right)^2_{B(W)} + \left(C_{N_\alpha}\right)_{T(B)} \left(\frac{X_{CP} - X_{CG}}{d}\right)^2_{T(B)} \\ & + \left(\Delta C_{N_\alpha}\right)_{B(T)} \left(\frac{X_{CP} - X_{CG}}{d}\right)^2_{B(T)} + \left(C_{N_\alpha}\right)_{T(V)} \left(\frac{X_{CP} - X_{CG}}{d}\right)^2_{T(V)} \end{aligned} \tag{18}$$

Before proceeding to utilize Equation (18), discussion of the nonlinearities in the aeroprediction code to predict each of the static aerodynamic terms of Equation (18) is appropriate. As an example consider the term $C_{N_{W(B)}}$ of Equation (17) which can be expanded as follows:

$$C_{N_{W(B)}} = \left[K_{W(B)} \sin\alpha + k_{W(B)} \sin\delta\right] \left(C_{N_\alpha}\right)_W \tag{19}$$

Each of the terms in Equation (19), $K_{W(B)}$, $k_{W(B)}$ and $\left(C_{N_\alpha}\right)_W$ are nonlinear in AOA or control deflection and Mach number. The nonlinearities were based on several large wind tunnel data bases in addition to other missile data. As an example of the nonlinearities, consider the wing-body interference term $K_{W(B)}$. $K_{W(B)}$ is typically close to the slender body theory value at zero AOA and at all Mach numbers. However, at low Mach number, as α increases, $K_{W(B)}$ will typically decrease to a value of 1.0 at high AOA. On the other hand, as Mach number increases $K_{W(B)}$ will approach one at fairly low AOAs.

Not only are the normal force coefficient terms of Equation (17) all nonlinear, but the center of pressure terms of Equation (18) as well. For a complete description of the static aerodynamic nonlinearities in the Aeroprediction Code, References 2 and 7 should be consulted.

The first approach taken to predict nonlinear pitch damping moments was to utilize Equation (18) directly where all the terms in Equation (18) are the nonlinear aerodynamic terms computed in the AP09. Figure 12 compares the results of Method 1 to experimental data for the Army Navy Finner (ANF) of References 20, 21, and 29. Note that the Method 1 compares quite

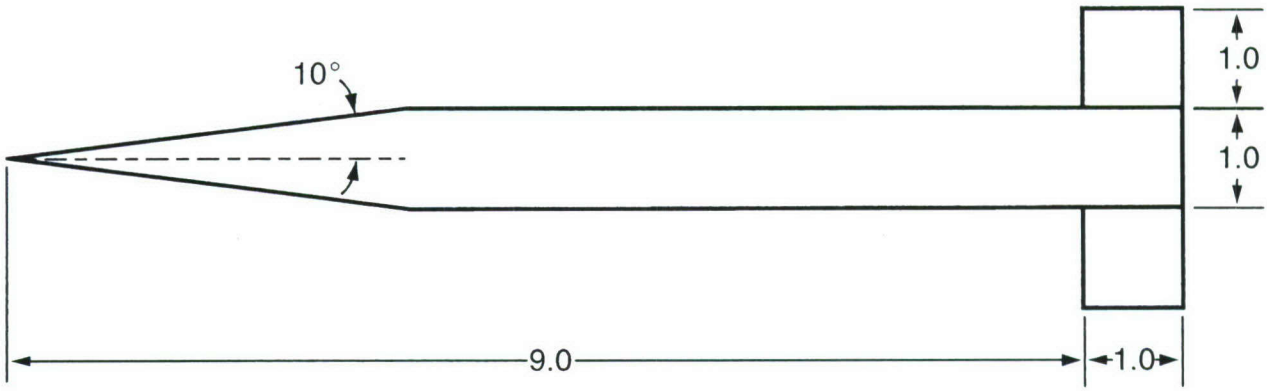

ANF Configuration (Dimensions in Calibers)

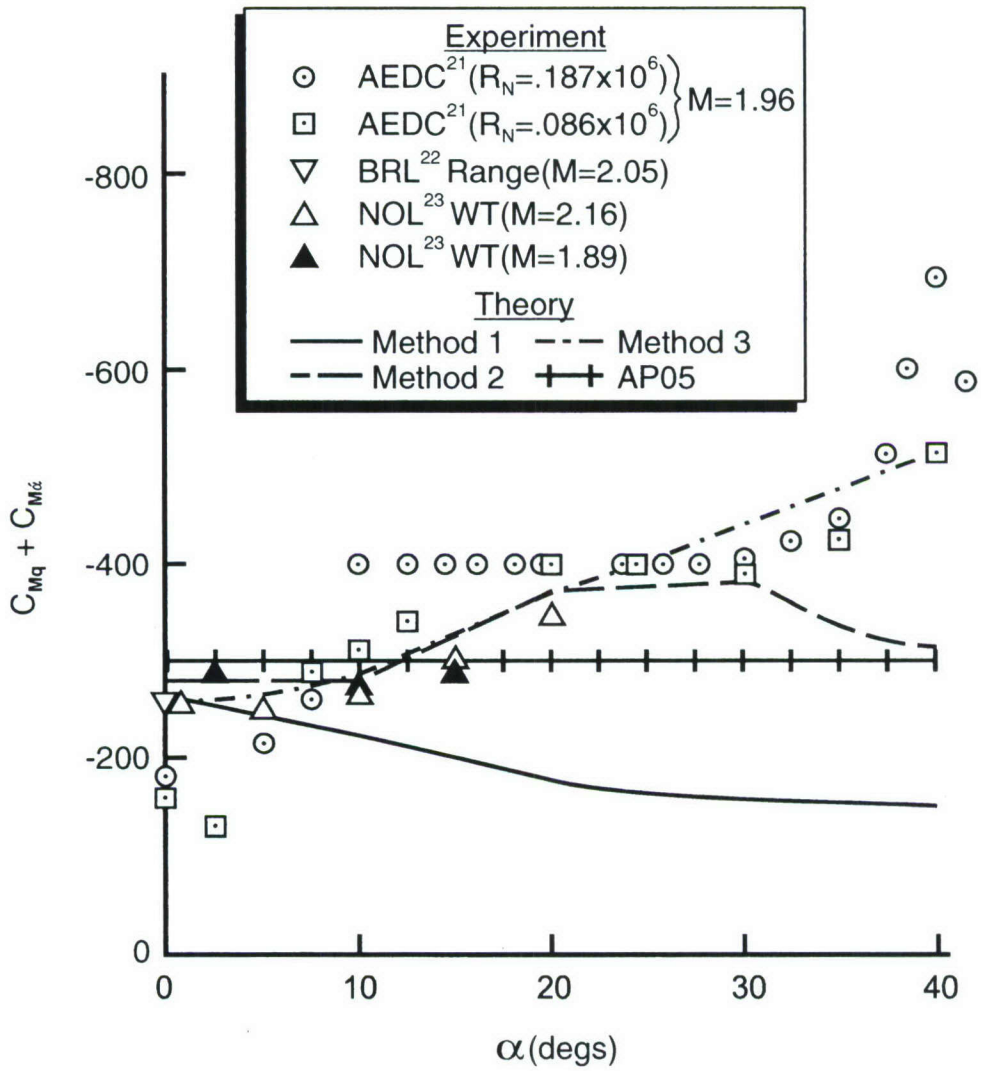

FIGURE 12. COMPARISON OF VARIOUS THEORETICAL APPROACHES TO PREDICT NONLINEAR PITCH DAMPING MOMENT TO EXPERIMENTAL DATA FOR THE ANF

well to data at low AOA but actually decreases with AOA versus increases as the data suggests. In investigating why Method 1 decreases with increasing AOA, it was found that the body-wing and wing-body interference terms decreased with AOA, which tended to somewhat compensate for the increase in wing alone normal force. Secondly, it was found that when treating the body as a point source, the body center of pressure moved towards the center of gravity as AOA increased, thus causing the term $\left(\frac{X_{CP} - X_{CG}}{d}\right)^2_B$ to decrease. As a result of the disappointing results of Method 1 in Figure 12, it will not be considered any further and other approaches will be attempted.

A logical extension of Method 1 is to distribute the load along the body, as opposed to treating the body as a point source. The Structural Load Methodology[37] of the AP09 code will be utilized to perform this task. To illustrate the structural load methodology of the AP09, Figure 13 shows the AP09 loads at $M_\infty = 2.87$, $\Phi = 45$ deg and $\alpha = 10$ deg compared to Navier Stokes Computations for a wing-body-tail configuration. There are two aeroprediction results in Figure 13, original and adjusted. The adjusted curve takes part of the nose overprediction on load and redistributes it while still maintaining accuracy of normal force and pitching moments. The increase in load on the mid and aft body areas of Figure 13 is the wing-body carry over normal force distribution. The major point of Figure 13 is to illustrate the accuracy of the Aeroprediction Code in calculating loads on a body, which can be important in predicting pitch damping moments.

Figure 14 now illustrates the local loads on two more relevant configurations that nonlinear pitch damping moment data is available, the ANF and the MK 82 General Purpose Low Drag Bomb (GPLDB)[25,26]. The ANF is shown on the left of Figure 14 along with local loads at $\Phi = 0$, $M = 2.16$ and $\alpha = 5$ and 35 deg and the GPLDB is on the right of Figure 14 along with local loads at $\Phi = 0$, $M = 1.5$, and α of 5 and 35 deg. Note that load distribution of the ANF is similar at 5 deg and 35 deg as is the loads on the GPLDB at 5 and 35 deg. Of course the loads at 35 deg are much higher than those at 5 deg. It is also worthy to note the negative load on the boattail area of the GPLDB. Returning to Equation (18), it is seen that as the center of pressure of the overall normal force load of Figures 13 and 14 move towards the center of gravity, the moment arm gets smaller and thus according to Equation (18), the pitch damping term of the body goes down substantially. This is a prime reason for the Method 1 of Figure 12 decreasing as α increases as opposed to increasing as the experimental data suggests.

Reference 32, on the other hand, obtains body alone pitch damping through a summation of local normal force on a body component where the body is divided into 20 parts. In viewing Figures 13 and 14, it is clearly seen that using an average of center of pressure is not acceptable because the average is a linear average, whereas Equation (18) has a square of the distance to each of the body parts, whether the body is 20 or more parts. It is also seen in viewing the GPLDB of Figure 14 that the boattail will decrease the pitch damping moment since the C_{N_α} of the local body normal force component in the boattail region is negative. In other words, one can not use the overall nonlinear body center of pressure to compute body pitch damping as AOA increases, as was done in Method 1 of Figure 12.

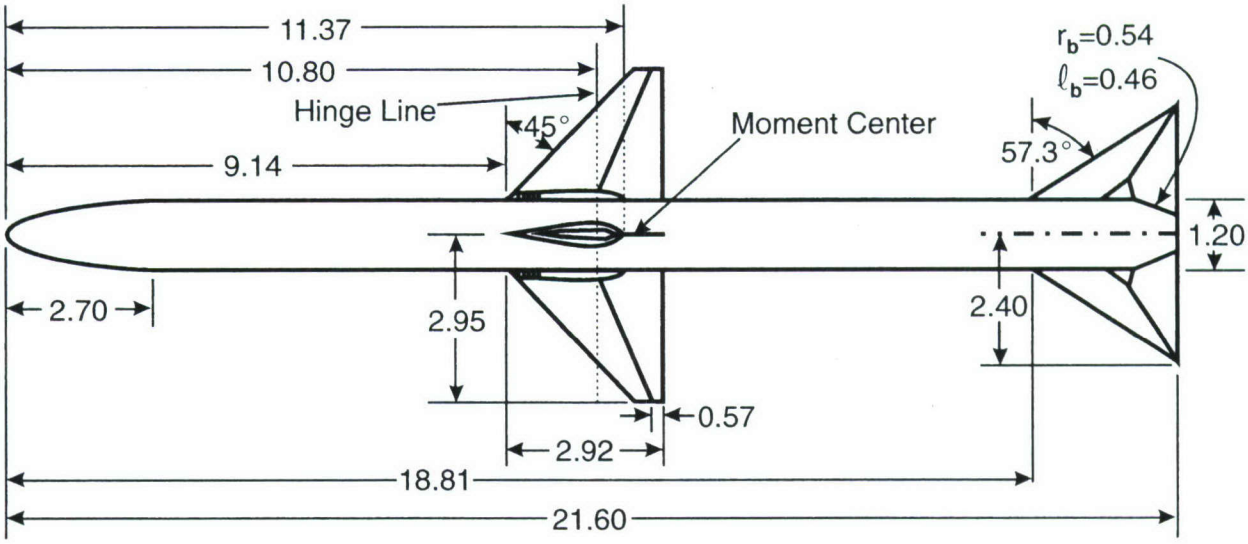

Wing-Body-Tail Configuration Used in Structural Loads Methodology (All Dimensions in Inches)

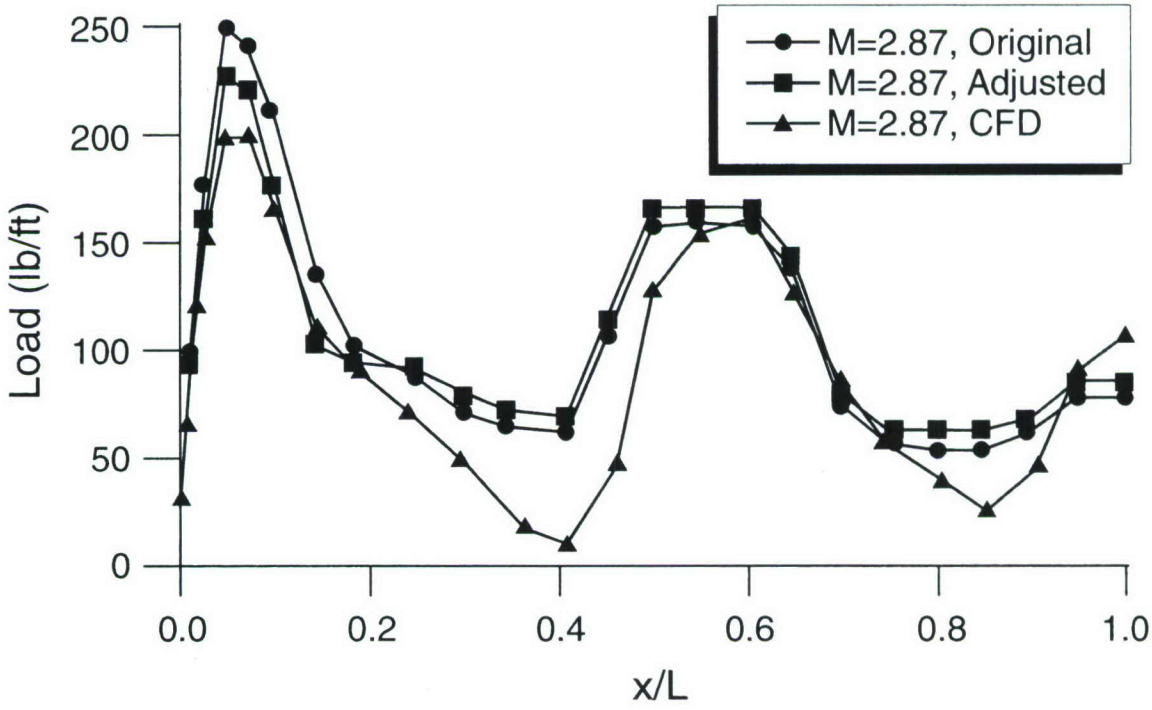

Effect of Adjustment of Nonlinear Component of Nose Load Φ=45°, α=10°

FIGURE 13. ILLUSTRATION OF LOCAL LOAD ON A WING-BODY-TAIL CONFIGURATION

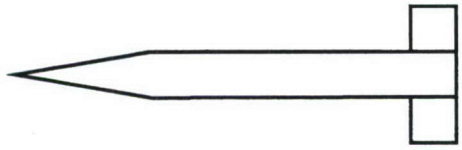

Army-Navy Finner Sketch

MK 82 GPLDB Sketch

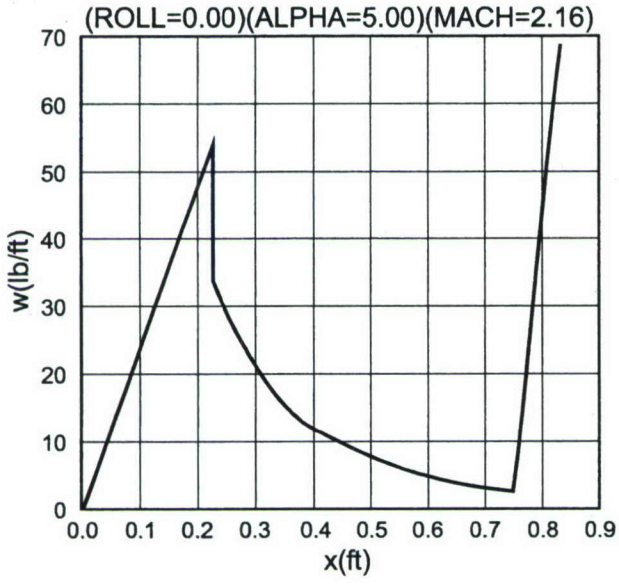

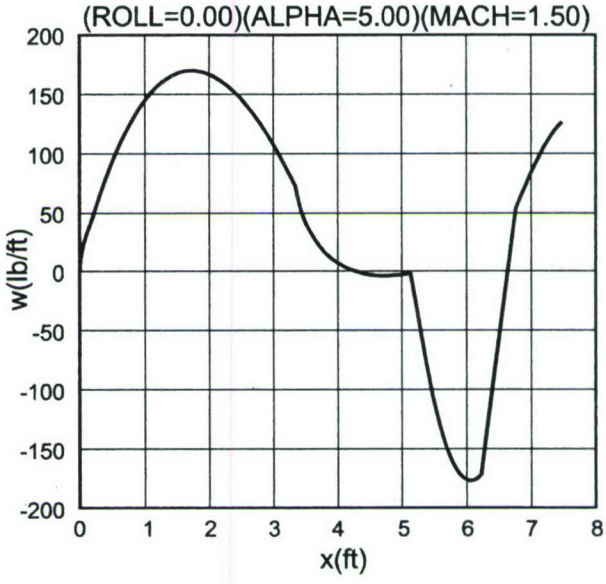

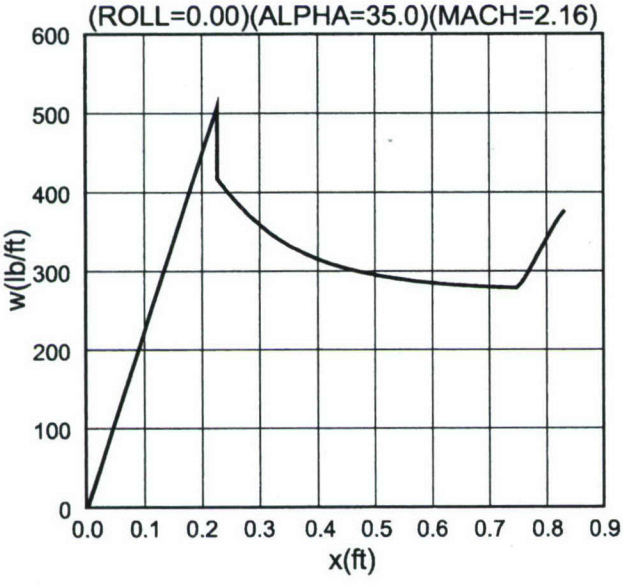

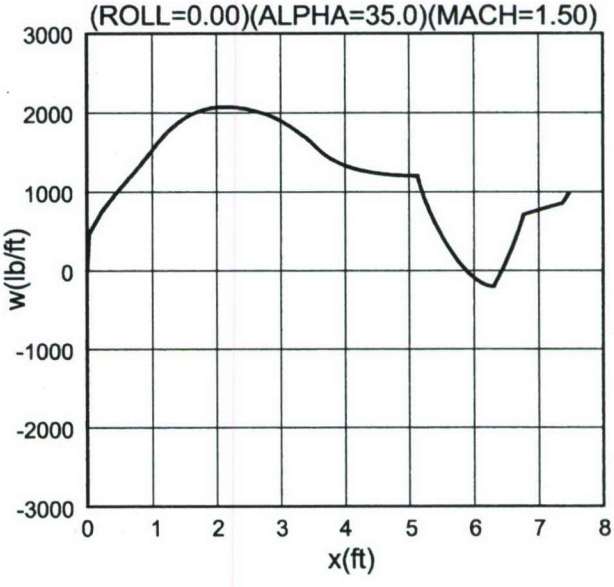

FIGURE 14. LOCAL LOADS ON TWO BODY TAIL CONFIGURATIONS AT SMALL AND LARGE ANGLES OF ATTACK

Method 2 of Figure 12 uses the summation approach of Reference 32 to compute pitch damping moment. Using the local load W(X) of Figure 14, the pitch damping moment for a body-tail configuration is:

$$C_{M_q} + C_{M_{\dot{\alpha}}} = \frac{-2}{\sin\alpha}\left[\sum_{i=1}^{N}\frac{W(X_i)\Delta X_i}{Q_\infty A_{ref}}\left(\frac{X_i - X_{CG}}{d_{ref}}\right)^2 + C_{N_{W(B)}}\left(\frac{X_{CP} - X_{CG}}{d_{ref}}\right)^2_{W(B)}\right] \qquad (20)$$

Equation (20) was used to compute pitch damping on the ANF at $M_\infty = 2.0$ where $W(X_i)$, $C_{N_{W(B)}}$ and $(X_{CP})_{W(B)}$ were all nonlinear values from the AP09. Also, body-wing interference is included in the body pitch damping integration since it is included in the body loads. As seen in Figure 12, Method 2 is much better than Method 1 and agrees with the NOL and BRL data quite well but falls below the AEDC data. A couple of points need to be made about the Method 2 results of Figure 12. First, it was found that the AP09 code needed to be modified to compute local values of C_{N_α} versus the secant slope of C_{N_α}, which is what the AP05 does. Secondly, it was found the overall configuration C_{N_α} gave slightly improved results compared to using individual C_{N_α} values of $C_{N_{W(B)}}$ and C_{N_B}. Thirdly, Equation (20) assumes the lifting surface is a point source as opposed to distributing the load analogous to the body. In checking out the validity of treating the wing or canards as a point source, it was found that when the root chord was small compared to the body reference length, errors of 1 percent or less typically occurred for the pitch damping term of the lifting surface. However, when the root chord was large compared to the body reference length, errors in pitch damping could be fairly large. As a result, the load on both the forward and aft lifting surfaces will be divided into 100 equal chord-wise intervals. Equation (20) then becomes for a body-tail case

$$C_{M_q} + C_{M_{\dot{\alpha}}} = \frac{-2}{\sin\alpha}\left[\sum_{i=1}^{N}\frac{W(X_i)\Delta X_i}{Q_\infty A_{ref}}\left(\frac{X_i - X_{CG}}{d_{ref}}\right)^2 + 2C_{N_{W(B)}}\sum_{i=1}^{100}\left(\frac{(X_{CP})_i - X_{CG}}{d_{ref}}\right)^2\frac{(A_W)_i}{A_W}\right] \qquad (20A)$$

Equation (20) is of course generalized for a wing-body-tail in a similar fashion as Equation (18). Also $(A_W)_i$ of Equation (20A) is the area of the individual wing panel compared to the wing area of a single wing, $A_W/2$ and thus the factor 2 for the wing-body term.

The third method shown in Figure 12 utilizes the improved pitch damping moment improvements discussed in Sections 21 – 27 and relates the improved zero AOA pitch damping to the local conditions at a higher AOA. In reviewing Reference 36 in more detail, the pitch damping moment was derived based on the assumption that the local velocity and dynamic pressure at a point on the body or tail fin was the same as the freestream values so that the dynamic pressure, Q, would cancel out when nondimensionalizing the moment equation to obtain pitching moment. That is, the pitching moment for a wing-body-tail configuration about some reference point is:

$$M = -\left[N_B(X_{CP} - X_{ref})_B + (N_{C(B)} + N_{B(C)})(X_{CP} - X_{ref})_C + (N_{W(B)} + N_{B(W)})(X_{CP} - X_{ref})_W + N_{CW}(X_{CP} - X_{ref})_W\right] \qquad (21)$$

Equation (21) can be rewritten in coefficient form as:

$$C_M = -\frac{Q_L}{Q_\infty}\left[C_{N_B}\left(\frac{X_{CP}-X_{ref}}{d_{ref}}\right)_B + \left(C_{N_{C(B)}}+C_{N_{B(C)}}\right)\left(\frac{X_{CP}-X_{ref}}{d_{ref}}\right)_C + \left(C_{N_{W(B)}}+C_{N_{B(W)}}+C_{N_{CW}}\right)\left(\frac{X_{CP}-X_{ref}}{d_{ref}}\right)_W\right] \tag{22}$$

Equation (22) assumes all normal force coefficient terms have been referenced to the appropriate reference areas for simplicity.

Furthermore, putting Equation (22) in slope form on the right side and using only the tail term for simplicity we have

$$C_{M_T} = -\frac{Q_L}{Q_\infty}\left[\left(C_{N_\alpha}\right)_{W(B)} + \left(C_{N_\alpha}\right)_{CW}\right]\left(\frac{X_{CP}-X_{ref}}{d_{ref}}\right)_T \Delta\alpha_T \tag{23}$$

where

$$\Delta\alpha_T \cong \frac{q}{V_L}\left(\frac{X_{CP}-X_{ref}}{d_{ref}}\right)_T \tag{24}$$

Now $C_{M_Q} = \dfrac{\partial C_M}{\partial\left(\dfrac{qd}{2V_\infty}\right)}$, so Equation (23) becomes after substituting in Equation (24) and taking the derivative,

$$\left(C_{M_Q}\right)_T = -2\left[\left(C_{N_\alpha}\right)_{W(B)} + \left(C_{N_\alpha}\right)_{CW}\right]\left(\frac{X_{CP}-X_{ref}}{d_{ref}}\right)^2 \frac{Q_L}{Q_\infty}\frac{V_\infty}{V_L} \tag{25}$$

Equation (25) applies only to the tail term but the factor

$$\frac{Q_L V_\infty}{Q_\infty V_L} \tag{26}$$

would multiply all terms of Equation (22) if expanded similarly to Equation (25). We will now look at defining the Equation (26) term.

Now

$$\frac{Q_L}{Q_\infty} = \frac{\frac{1}{2}\rho_L V_L^2}{\frac{1}{2}\rho_\infty V_\infty^2} = \left(\frac{P_L}{T_L}\right)\left(\frac{V_L^2}{V_\infty^2}\right)\left(\frac{T_\infty}{P_\infty}\right) \tag{27}$$

But

$$C_P = \frac{P_L - P_\infty}{\frac{1}{2}\rho_\infty V_\infty^2} \tag{28}$$

So that

$$P_L = \frac{1}{2}\rho_\infty V_\infty^2 C_P + P_\infty \tag{29}$$

Using Equation (29) into (27) we have:

$$\frac{Q_L}{Q_\infty} = \left(\frac{V_L}{V_\infty}\right)^2 \left(\frac{T_\infty}{T_L}\right)\left(\frac{\gamma M_\infty^2}{2} C_P + 1\right) \tag{30}$$

Now we will make a couple of approximations where

$$V_L \cong V_\infty \cos\alpha \tag{31}$$

$$C_P = 2\sin^2\alpha \tag{32}$$

Equation (32) is the Newtonian flow approximation which in principal is derived based on infinite Mach numbers. In practice, the author has found success in using the Equation (32) down to low supersonic Mach numbers. Also

$$\frac{T_\infty}{T_L} = \frac{1 + \frac{\gamma - 1}{2} M_L^2}{1 + \frac{\gamma - 1}{2} M_\infty^2} \tag{33}$$

Substituting Equation (33), (32), and (31) into Equation (30), and utilizing Equation (31), Equation (26) becomes

$$\frac{Q_L V_\infty}{Q_\infty V_L} = \cos\alpha \left[\frac{1+\frac{\gamma-1}{2} M_\infty^2 \cos^2\alpha}{1+\frac{\gamma-1}{2} M_\infty^2} \right] \left[1+\gamma M_\infty^2 \sin^2\alpha\right] \tag{34}$$

One approach is thus to use Equation(34) to multiply the pitch damping moment at near zero deg AOA for a given freestream Mach number and AOA to get the nonlinear value of pitch damping moment. This method is referred to as Method 3 of Figure 12. The zero AOA values of $C_{M_q} + C_{M_{\dot{\alpha}}}$ come from the AP09 code as modified by the Section 2.1 – 2.6 methods and these values are multiplied by the factors of Equation (34).

In viewing the Method 3 of Figure 12 it is clear it agrees with the AEDC data better than either Method 1 or 2. It is also clear that the reason such a simple formula works so well is the similarity of the nose loading in Figure 14 in going from low to high AOA. Method 3 tends to average out a lot of the data in Figure 12, but it follows the general trends of the data. While not shown, the data of Reference 21 actually goes to 85 deg AOA with a maximum in pitch damping occurring around 45 deg AOA and then declining. Equation (34) follows this trend as well. Hence, it is believed Equation (34) does in fact capture much of the physics of why pitching damping increases with AOA.

The major limitation of Equation (34) is the use of Newtonian Theory to predict pressure coefficient. Unfortunately, there are no local slope pressure predictors for low Mach number. As a result, to utilize Method 3 in a robust sense with respect to Mach number, we must find a complimentary factor for lower Mach numbers, which is primarily AOA dependent. To do this, Figure 15 shows a plot of the Equation (34) versus Mach number for various AOAs. As seen in Figure 15, Equation (34) decreases significantly with Mach number. Equation (34) is used down to a Mach number of 1.5, where it is believed Newtonian Theory becomes questionable. From $M_\infty = 1.5$ to 0, it is assumed the value of Equation (34) goes to one in a linear sense. Also of note in Figure 15 is the fact that Equation (34) reaches a maximum at $\alpha = 45$ deg and declines to zero at $\alpha = 90$ deg.

Both Methods 2 and 3 are new or improved methods to predict nonlinear pitch damping. It is unclear, based on the Figure 12 comparison to wind tunnel data, which method is best. As a result, both methods will be compared to available wind tunnel data on other configurations in the results and discussion sections before any conclusions are drawn. However, it is worth while to point out some of the strengths of both Methods 2 and 3.

Method 2 is very robust in the sense it will handle all AOAs (0–90 deg) and Mach numbers (0–20) and roll orientations (0 deg, 45 deg), control deflections and multi-fin options that the AP09 code allows. Method 2 also calculates local body pitch damping moments. It has much less empiricism than Method 3 does. On the other hand, it was much more involved and difficult to implement than Method 3, even though the AP09 code already had all the nonlinear static aerodynamics and structures loads available for $M_\infty \geq 1.2$.

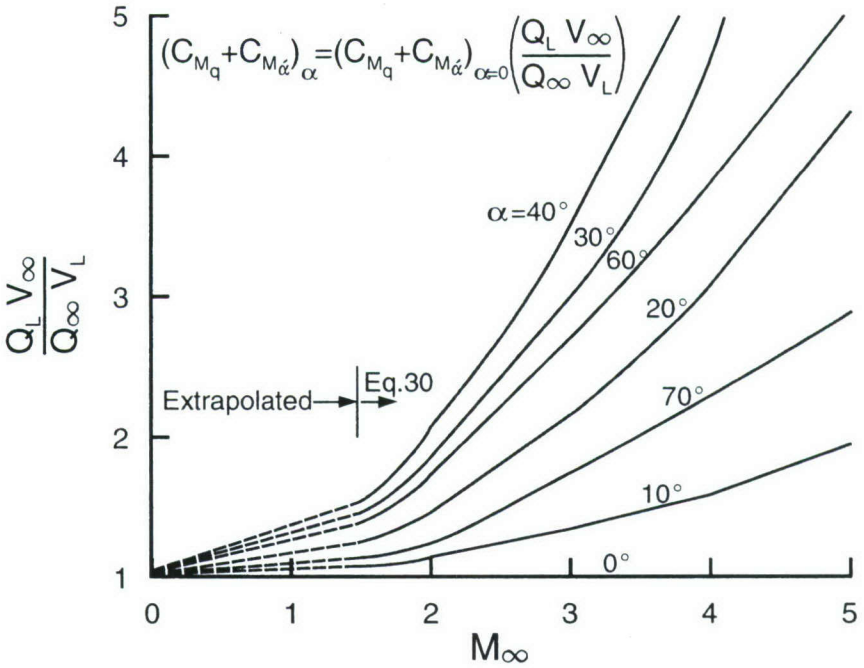

FIGURE 15. APPROXIMATE RELATIONSHIP TO ALLOW PITCH DAMPING NONLINEARITIES TO BE ESTIMATED BASED ON $C_{M_q} + C_{M_{\dot{\alpha}}}$ AT AOA ZERO

Method 3 utilizes the original time dependent linear solution for C_{M_α} and rotational pitching rate C_{M_q} from linear theory. Method 3 utilizes the improvements in pitch damping due to long boattails derived for the AP09. Method 3 was also much easier to implement than Method 2. Figure 16 summarizes the Methods 2 and 3 approaches.

Method 2 – Use Static Aerodynamics Completely

- Uses all nonlinear static aerodynamics of AP09 and structural loads to distribute body loads
- Very robust in α, M_∞, δ, Φ, number of fins
- Distributes fin loads over 100 equally space chordwise locations
- Predicts local body pitch damping
- Has minimum empiricism
- More difficult to implement than Method 3

Method 3 – Uses Quaisi-Time Dependent Wing Alone Solution and Combines with Improved Empirical Body Alone Pitch Damping

- Uses all improved body alone pitch damping of AP09 for $\alpha = 0$ deg
- Uses Quaisi-Time dependent wing alone solution
- Uses a simple method to relate zero α aero to AOA
- More empirical and somewhat less robust (no Φ dependence) than Method 2

FIGURE 16. SUMMARY OF METHOD 2 AND 3 APPROACHES TO PREDICT NONLINEAR PITCH DAMPING MOMENTS

2.9 NEW METHOD TO PREDICT NONLINEAR ROLL DAMPING

Roll damping prediction in the Aeroprediction Code, like pitch damping, had remained basically the same since the AP77[38]. However, with the attention given to cheaper unguided weapons in the last 10 years, renewed interest has been placed on roll damping. The original AP77 developed an approximate method to calculate roll damping based on three dimensional thin wing theory supersonically[39,40] and lifting surface theory subsonically[41]. For roll damping, the lifting surfaces were assumed to extend all the way to the body centerline and the r/s effect of the fins as well as the number of fins were accounted for by slender body theory (see Reference 2, page 43). The body roll damping, which is basically negligible compared to the fins was estimated empirically[42].

The improvements discussed in Section 2.5 of this report add significant improvement to the near zero AOA prediction of roll damping moments when the configuration has a long boattail. For many of the unguided weapons, they can experience high AOA due to launch conditions and in some cases due to low static margins. A combination of events can lead to reduced accuracy and in the worst case scenario, instability. It is therefore important to be able to predict roll damping at AOA in order to understand the flight performance of primarily unguided fin stabilized weapons and, to a lesser extent, guided weapons near launch.

A literature survey was conducted for nonlinear roll damping and the references found will be broken down into experimental and theoretical categories. References 22, 24, 26 and 43-53 are the experimental references found for the nonlinear roll damping. References 54-57 are nonlinear theoretical models and References 58-62 are linear theoretical or experimental data reports of interest. References 22 and 47 gives experimental values of roll damping to high AOA for the Army-Navy-Finner (ANF) and a modified version of the ANF (MANF). Roll damping of the ANF were given for Mach numbers of 0.22 and 2.5 and for the MANF at Mach numbers of 0.6, 0.9, 1.15, 1.3, 1.5, 1.76, 2.0 and 2.5. The roll damping measurements were made using a base sting as opposed to a leeward plane strut mount as done for pitch damping Hence, not as much interference from the sting onto the model should be present as for the pitch damping measurements.

Reference 43 compliments References 22 and 47 in that it gives roll damping results for the ANF determined earlier (1964) from the Naval Ordnance Laboratory Tunnel. Roll damping data are given at $M_\infty = 0.22$ for AOA −10 deg to +60 deg, at $M_\infty = 0.77$ for AOA −10 to +10 deg, at M = 2.54 for AOA −10 to +26 deg, and at $M_\infty = 4.1$ for AOA 0 to 22 deg. It is safe to say the ANF and MANF configurations have the most extensive roll damping data base available when one combines References 43 and 47.

Reference 24 gives the roll damping measurements for the 81mm Australian Mortar at $M_\infty = 0.5$ to 0.95 at $\alpha = 0$, 5 and 10 deg AOA. However, the report notes the M = 0.9 and 0.95 results are questionable due to wind tunnel transonic wall effects.

Reference 26 summarizes the Navy investigations up through 1959 of the MK 82 Low Drag Bomb. Roll damping data of Reference 26 include Mach numbers of 0.8 at α = 0-35 deg AOA and Mach number 0.6-1.4 at $\alpha = 0$ deg. Reference 48 presents a complimentary set of data

for the Fixed Fin and Inflatable Stabilizer Retarder candidates for the MK 82 Low Drag Bomb. Roll damping results are given for Mach number 0.4 to 1.3 at AOA of 0, 10, and 20 deg.

References 49 and 50 give component build-up roll damping data for a canard-control missile at $M_\infty = 0.1$ and AOA 0 to 30 deg. Several points are noteworthy in these two references. First, Reference 49 showed roll damping for body-canard, body-tail and canard-body-tail with and without control deflection. Results indicate the canard shed vortices almost eliminate the roll damping of the tail surfaces. The second point of note was the roll damping measurements for the canard-body-tail configuration of References 49 and 50 agree up to AOA 25 deg but, whereas Reference 49 shows C_{ℓ_p} continuing its negative magnitude increase at AOA 30 deg, Reference 50 showed C_{ℓ_p} approaching zero at AOA 30 deg. No explanation was given for the large divergence in C_{ℓ_p} at AOA 30 deg between the two references.

The remaining nonlinear data sets are unclassified but limited distribution. Hence, one can discuss these data but cannot show the specific data or configuration without approval from its source. Reference 44 gives wind tunnel measurements of the 2.75 Wrap Around Fin Rocket at $M_\infty = 4.25$ and AOA 0 to 10 deg. Instead of C_{ℓ_p} increasing in magnitude with AOA as would be expected, this report shows a decrease. It is not clear why, leading one to feel suspect of the results. Reference 51 gives results of a folding fin 2.75 inch diameter rocket at Mach number 2.5 to 4.5 for AOA −5 deg to +5 deg. Roll damping trends increase in magnitude with AOA as would be expected for these high Mach numbers. References 52 and 53 give the transonic and supersonic wind tunnel test results of several axisymmetric bomblet munition models. Roll damping results are given for Mach numbers 0.4 to 2.5 and for AOA 0 to 11 deg. Results follow the trends one would expect. One thing nice about the results of the References 52 and 53 is test data is available for very low aspect ratio 6 fin configurations. The final two limited distribution nonlinear roll damping data reports are References 45 and 46. References 45 and 46 are for mortar configurations where Mach number varies from 0.5 to 1.05 and AOA 0 to 14 deg.

To summarize the nonlinear roll damping data available, it is fair to say that only two configurations (ANF and MANF) have a fairly extensive data base available. Portions of other data bases are available, but quite limited. What is needed is a component data base similar to References 49 and 50 that extend the aspect ratio of the wings, along with Mach number and AOA range. Not having such a data base will hamper a semiempirical model development and hender the accuracy of any model developed. However, a nonlinear semiempirical model for roll damping prediction is a goal of this work. The model can be refined and improved upon as more data becomes available.

The available nonlinear theoretical approaches for roll damping are even more limited than the experimental data bases. Reference 54 gave a revised equation for roll which includes not only C_{ℓ_δ} and C_{ℓ_p} but C_ℓ as well. Also the equation is a function of roll orientation and AOA. Unfortunately, the new nonlinear roll equation is of no value to predict nonlinear roll damping.

References 55 and 56 appear to be the most rigorous attempt to define nonlinear roll damping moments found in the literature. Oberbampf[55,56] made several fairly significant

assumptions in his theoretical development however. The assumptions include no effect of the fin on the body and a simplified lifting theory for the wing alone solution, as opposed to a more rigorous lifting surface or three dimensional thin wing theory approach. On the other hand, Oberkempf's method made an assumption for boundary layer separation which allowed him to bring into play the viscous effects at AOA and roll (since local AOA on a wing is a function of both α and Φ). References 55 and 56 showed reasonable comparisons of theory and experiment to the ANF and several other configurations at a limited set of conditions.

The last nonlinear method is given in Reference 57. The theory is compared to experiment on a couple of examples[57] with reasonable success; however, the theory is not defined in Reference 57 so it is assumed the Reference 57 theory is not available in the open literature.

Before leaving the literature survey on nonlinear roll damping, several references for zero AOA roll damping are worthy of note. First is Nicholaides[58], et al method to compute low AOA roll damping. The most interesting point about Reference 58 was not the theoretical method, but he showed a component buildup of roll damping on the ANF with body-tail, body-wing (wing same size as the tail); and body-wing-tail. Reference 58 indicated that at M = 1.95, the tail surfaces were only 14 percent as effective in roll damping in the wing-body-tail (WBT) arrangement as in the body tail configuration. At M = 1.73, no tail roll damping effectiveness was shown in the WBT arrangement. Hence, Reference 59 like Reference 49, showed a large loss in roll damping of the tail surfaces due to wing or canard shed vortices.

Reference 59 gave roll damping flight test results of a wing-body-tail configuration similar to the seasparrow missile. In using the AP05 code to compare theory to measurements, it is clear that there was a large loss in roll damping due to wing shed vortices. Reference 59 also indicated a substantial loss in roll damping due to aeroelastic effects.

Prakash[60] derived a simple approach to predict C_{ℓ_p} based on linearized wing theory and incorporation of wing-body and body-wing interference effects. He showed slightly improved results compared to Oberkampf[55] at supersonic speeds but results much too high subsonically. The AP77[38] results were the best overall of all the theories shown in Reference 60.

Eastman[61] showed that roll damping moment could be correlated quite well to roll driving moment for cruciform missiles. His formulation gave

$$C_{\ell_p} = -2.15(\bar{y}/d)C_{\ell_\delta} \tag{35}$$

where $\bar{y}$ is the radial distance from the body centerline to the exposed wing centroid. Examples of several configurations where C_{ℓ_δ} were known were shown to compare well to the simple correlation Equation (35). Mikhail[62] then extended Eastman's[61] theory to multiple fins that could be planar, wrap around, or offset from the body centerline.

To summarize the literature review of experimental data and analytical approaches for nonlinear roll damping, it is fair to say that the data bases are very limited and the theoretical

methods are even more limited. There was no robust theoretical method at all that could handle wing-body- tail configurations, which is the goal of the present work.

Before we discuss analytical approaches to model nonlinear roll damping, it is appropriate to discuss some of the physical phenomena that we will attempt to model in an approximate sense. The physics are Mach number, AOA, roll rate, and configuration dependent. Figures 17 and 18 attempt to illustrate some of the physical phenomena that occur when a missile rolls. For supersonic flow, shocks occur both on the nose of the body and the leading edges on the canards and wings. Under certain conditions, these shocks may intersect a lifting surface, creating significant nonlinearities. In addition to the body vortices, each canard sheds a vortex at about 80 percent of the span. This vortex path will be slightly curved due to the roll and will intersect a tail surface(s). Typically the intersection will occur on the outer part of the tail where the load on the tail due to roll (see Figure 17B) is the highest, thus having the largest impact on the roll damping of the tail since the vortex lift is always opposite the wing lift. Also, for lift, only two wing shed vortices need to be considered whereas for roll, all vortices from the forward lifting surfaces adversely impact the roll damping of the tail surfaces.

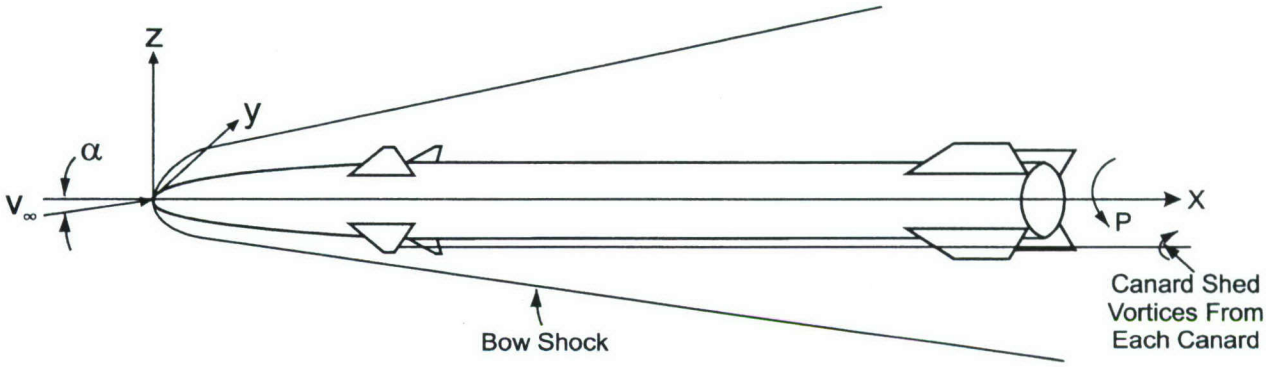

A. Rolling Cruciform Canard-Body-Tail Configuration at Supersonic Mach Number

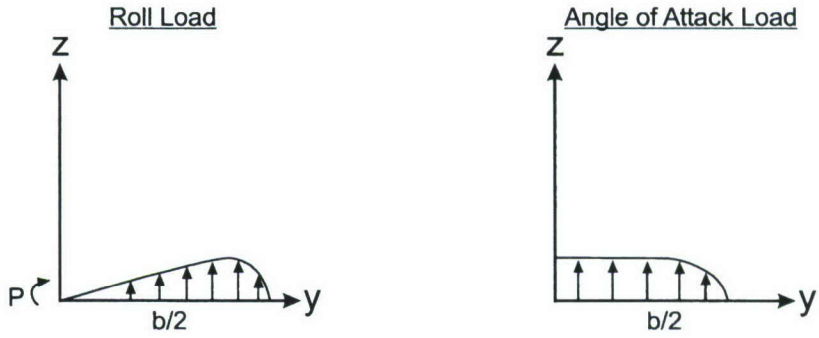

B. Wing Load Due to Roll And Angle of Attack

FIGURE 17. SOME OF THE PHYSICAL PHENOMENA THAT OCCUR ON A ROLLING MISSILE

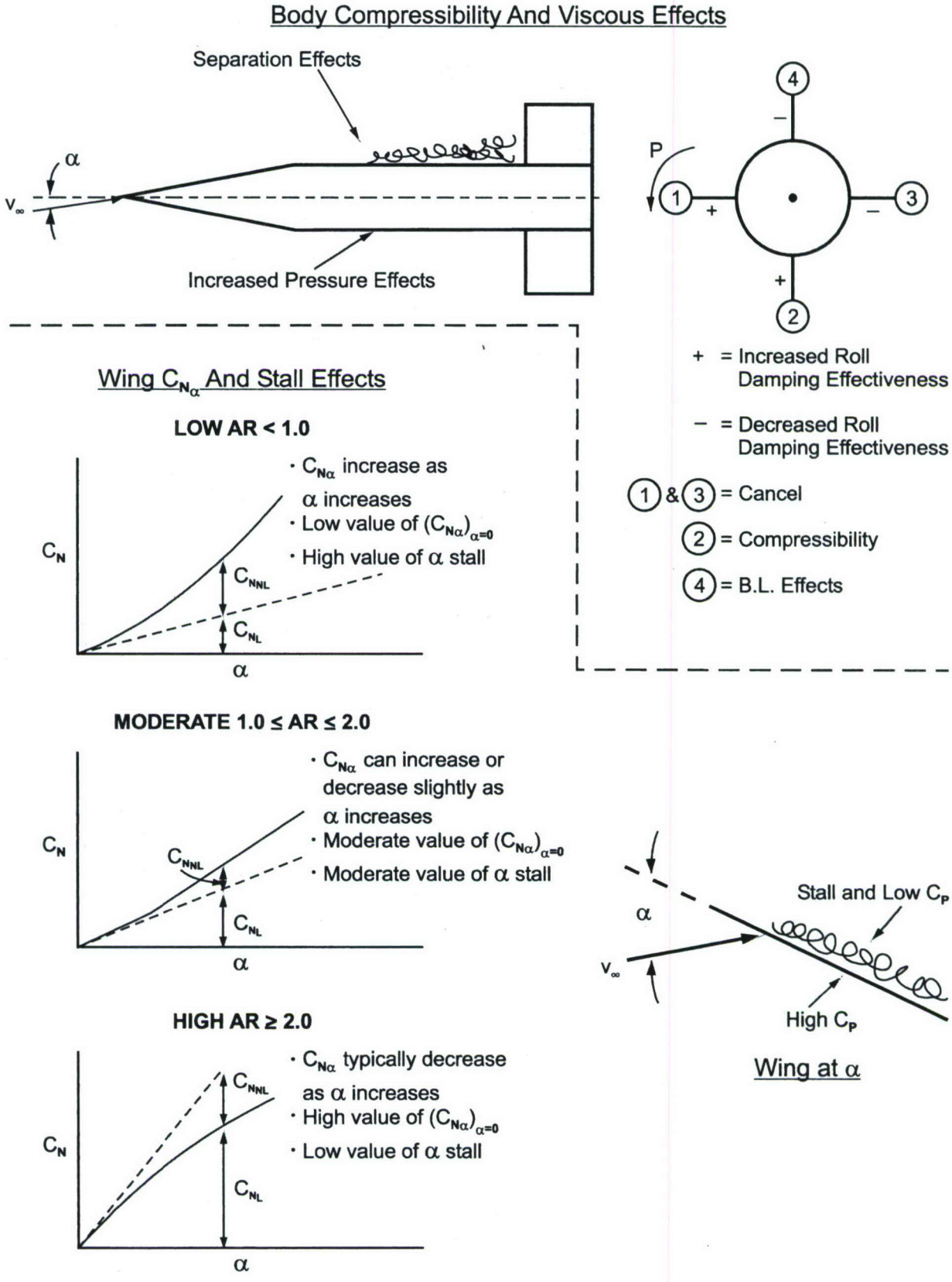

FIGURE 18. SOME PHYSICAL PHENOMENA AFFECTING ROLL DAMPING

Another physical phenomena that occurs at subsonic up to low supersonic speeds is asymmetric shedding of vortices. This phenomena typically starts around 25 deg AOA and reaches a maximum around 45 deg AOA and then goes to zero around 65 deg AOA. While not mentioned in References 49 and 50 as to why C_{ℓ_p} was so different at $\alpha = 30$ deg between the two identical tests, the fact the results were identical at $\alpha = 25$ deg makes one suspicious of the asymmetric vortex as a possible source of the large difference in C_{ℓ_p}.

Wing stall is also a physical phenomena which affects C_{ℓ_p}, particularly at subsonic Mach numbers. Wing stall is a function of the wing aspect ratio (see Figure 18), Mach number and AOA. For aspect ratio ($AR \geq 2.0$) wing stall typically occurs at 10-15 deg AOA at subsonic Mach numbers whereas for low aspect ratio ($AR \leq 0.5$) wing stall is hardly noticeable at any AOA. Moderate aspect ratio wings are in between the low and high aspect ratio extremes. At high Mach number ($M > 2.0$), stall on wings in not nearly as noticeable due to the high dynamic pressures in the windward plane dominating the flowfield.

Another physical phenomena for wing-body-tail configurations is the fact that all forward lifting surfaces will shed vortices when rolling and these vortices will all adversely impact the roll damping effectiveness of the tail surfaces. As AOA increases, the impact of the forward shed vortices will diminish and the effectiveness of the tail surfaces on roll damping will improve.

Dynamic pressure (see Figure 18) plays a significant role in roll damping effectiveness. At low AOA, all forward fins are effective in providing roll damping whereas as AOA increases, the fins in the windward plane become more effective and the fins in the leeward plane become less effective in providing roll damping. At lower Mach number, where dynamic pressure is the lowest, the roll damping can actually decrease with AOA whereas at higher Mach number, the windward plane fins tend to dominate and hence the roll damping generally increases with increasing AOA. If the fins are located on a boattail or flare, roll damping typically will decrease or increase respectively due to the lower or higher dynamic pressure on the boattail or flare. Boattail effects were accounted for in Section 2.5 but effects of a fin located on a flare must be considered in any new methodology. Figure 19 summarizes the physical phenomena that must be accounted for in an effective semiempirical model for roll damping prediction.

- Asymmetric shed body vortices ($25 \text{ deg} < \alpha < 65 \text{ deg}$; $M_\infty < 2.0$)
- C_{N_α} of wing (AR, M_∞) and stall
- Angle of attack and dynamic pressure
  (All fins effective at $\alpha = 0$; windward plane fins at moderate to high α)
- Canard shed vortices (all forward fins shed vortices in roll, impact on tail surfaces at point of maximum normal force due to roll)
- Fins on boattail or flare

FIGURE 19. SUMMARY OF PHYSICAL PHENOMENA THAT AFFECT ROLL DAMPING MOMENT

One now must translate the physical phenomena into a mathematical model which hopefully will approximate roll damping in a robust sense for weapon configurations. The improvements discussed in Section 2.5 should allow reasonable accuracy for roll damping of body tail configurations near $\alpha = 0$. However, account of the adverse effect of canard/wing shed vortices on the tail surfaces has not been attempted nor has AOA or flare effects been accounted for. Thus the goal will be to extend the good zero AOA roll damping prediction capability to missiles with two sets of lifting surfaces and to weapons at AOA.

The first problem to be dealt with is the canard shed vortices. There are 3 sets of data (Reference 49, 58, and 59) that have roll damping at zero AOA for configurations with two sets of lifting surfaces. Moreover, two of the data sets (References 49, 58) have component buildup data for roll damping that clearly shows the loss of tail effectiveness for roll damping when the forward lifting surfaces are placed on the wind tunnel model. The approach taken here to model the loss of roll damping on the tail surfaces due to wings or canards is to use the analogy to the loss of lift on the tail surfaces due to the wings or canards. However, the effect on the tail surfaces needs to be doubled to account for the fact that all forward lifting surfaces impact the tail surfaces in roll, not just the surfaces that are affected by the flow normal to the body as is the case in calculating normal force. Also, a factor needs to be applied to the wing shed vortex effect on the roll damping of the tail fins to account for the fact the vortices hit the tail fin where the load due to roll is highest. A model which appears to account for the loss of roll damping on the tail fins due to wing/canard shed vortices is:

$$\left(C_{\ell_P}\right)_{TM} = \left(C_{\ell_P}\right)_{TU}\left[\frac{C_{N_{T(B)}} + \Delta C_{N_{B(T)}} + (NC)C_{N_{T(V)}}}{C_{N_{T(B)}} + \Delta C_{N_{B(T)}}}\right] \tag{36}$$

where subscript TM and TU stand for tail modified and unmodified respectively.

Several points are worthy of note in Equation (36). All the normal force terms in Equation (36) contain all the nonlinearities in AOA, Mach number, and configuration geometry at both $\Phi = 0$ and 45 deg. $C_{N_{T(V)}}$ thus already contains canard/wing size and location in the calculation of downwash for both roll angles of 0 and 45 deg. The NC that multiples $C_{N_{T(V)}}$ accounts for four shed vortices impacting the tail versus two for the $C_{N_{T(V)}}$ along with an additional factor of two for the vortex impacting the tail at the largest load due to roll. If the canards or wings are not cruciform, then NC is replaced by the number of canards or wings present. Finally, a constraint is placed on the factor in Equation (36) that multiplies $\left(C_{\ell_P}\right)_{TU}$ that does not allow the factor to go negative, creating a positive roll damping of the tail fins. Of course if there are no canards or wings present, the factor multiplying $\left(C_{\ell_P}\right)_{TU}$ in Equation (36) will be 1.0 and there will be no change in the value of $\left(C_{\ell_P}\right)_{TM}$.

A convenient way to model the nonlinear effects of dynamic pressure on the roll damping moment is to increase the zero AOA value of C_{ℓ_P} by Equation (34), in analogy to pitch damping. However in using Equation (34) in conjunction with C_{ℓ_P} at $\alpha = 0$, one must keep in

mind the fact that C_{ℓ_P} at $\alpha = 0$ assumes all four fins are effective whereas at AOA the leeward plane fins become increasingly ineffective. Furthermore, at low subsonic speeds, wing stall becomes a more important issue, in some cases actually decreasing the magnitude of C_{ℓ_P} as the AOA approaches stall. Hence, a model to modify Equation (34) as AOA increases and Mach number decreases is needed. An approximate model that focuses in on the compressibility and separation physical phenomena discussed earlier is given by:

$$C_{\ell_P} = \left(C_{\ell_P}\right)_{\alpha=0} \left\{ 0.3 \left[\left(\frac{Q_L}{Q_\infty} \right) - 1 \right] \left(\frac{b}{d_{ref}} \right)^{3/4} - 0.2 M_N + 1 \right\} \tag{37}$$

$\left(C_{\ell_P}\right)_{\alpha=0}$ of Equation (37) is the improved value of roll damping moment discussed in Section 2.5. Q_L/Q_∞ of Equation (37) is defined by (34), omitting the term V_∞/V_L from the equation so that

$$Q_L/Q_\infty = \left[\frac{1 + \frac{\gamma - 1}{2} M_\infty^2 \cos^2 \alpha}{1 + \frac{\gamma - 1}{2} M_\infty^2} \right] \left[1 + \gamma M_\infty^2 \sin^2 \alpha \right] \tag{38}$$

Equation (38) is plotted in Figure (20) for convenience. Note that V_∞/V_L was omitted from Equation (34) because there was no oscillation motion involved in the roll damping motion derivation, unlike pitch damping (see Equation (23) and (24)). M_N of Equation (37) is the Mach number normal to the body $M_\infty \sin \alpha$.

Some explanation is in order for the derivation of Equation (37). Referring to Figure 18, Equation (37) attempts to address the physical phenomena of increases in roll damping due to compressibility in the windward plane (the first term inside the outer bracket of Equation (37)) and the loss of the effectiveness of the leeward plane fins due to being in the low pressure region (the second term inside the outer bracket of Equation (37)). Of course, if AOA is zero, both the first and second terms of Equation (37) are zero and the Equation (37) reverts back to the zero AOA value of roll damping. Notice in Figure 18 the effect on each fin in roll as AOA increases. As AOA increases, those fins heading in the direction of increased dynamic pressure become more effective in roll damping (fins ① and ②) whereas those fins heading into a region of lower dynamic pressure (fins ③ and ④) become less effective in roll damping. Equation (37) assumes fins ① and ③ cancel each other out whereas fin ② increases roll damping and fin ④ decreases roll damping. Actually, Equation (37) allows for 30 percent of the windward plane to increase and 20 percent of the leeward plane to decrease roll damping with the other 50 percent of the fins cancelling each other out. Initially, a value of 0.25 was assigned to both the windward and leeward plane fins but in comparison to data, the 0.3/0.2 split appeared to be a better fit. Also the term $(b/d_{ref})^{3/4}$ recognizes the fact that longer span fins are more effective than shorter span fins in producing roll damping. Also note that Equation (37) does not account directly for the

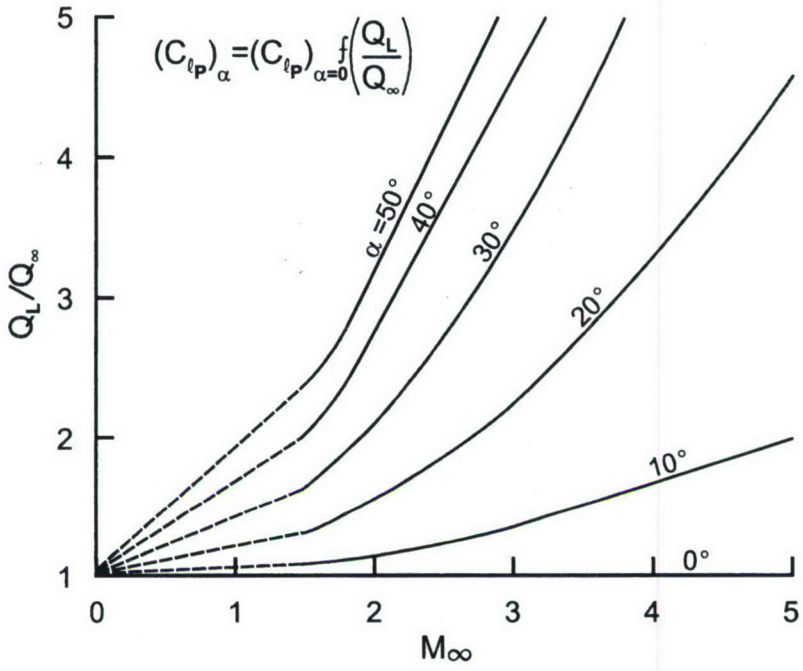

FIGURE 20. APPROXIMATE RELATIONSHIP TO ALLOW ROLL DAMPING NONLINEARITIES TO BE ESTIMATED BASED ON C_{ℓ_P} AT AOA ZERO

wing C_{N_α} and wing stall physics of Figure 18. Finally, if the fins are located on a flare, the effective AOA is $\alpha + \theta_f$ where θ_f is the flare angle. Thus a fin located on a flare will be in a region of higher dynamic pressure. The effect of fins on a boattail were accounted for in the improved zero AOA value of C_{ℓ_P} discussed in Section 2.5. Equation (37) will be referred to as Method 1 for nonlinear roll damping predictions.

A second method to predict nonlinear roll damping utilized the idea of Eastman[61] (Equation (35)), but extends Eastmans approach in the nonlinear AOA range. Initially Equation (35) was tried directly where C_{ℓ_δ} was computed using the nonlinear values of C_{ℓ_δ} using the fourth order wing along solution in the aeroprediction code (see Reference 2, pp 200-208). Using the Eastman approach directly met with some success, but overpredicted roll damping significantly for configurations with long boattails, in analogy to the AP05. An approach which appears to offer more promise, however, is given by:

$$C_{\ell_P} = (C_{\ell_P})_{\alpha=0} + 4.3\left[(C_{N_\delta})_{\alpha=0} - (C_{N_\delta})_\alpha\right]\left(\frac{\bar{y}}{d_{ref}}\right)^2 (MFF)\, f(\alpha) \qquad (39)$$

where $f(\alpha) = 1 - \dfrac{.02|\alpha - \theta_f|}{(\bar{y}/d_{ref})}$; $f(\alpha) \geq 0.5$

Equation (39) utilizes the zero AOA value of roll damping based on the improvements in roll damping discussed in Section 2.5 and uses the Eastman[61] approach to compute the change in roll damping due to AOA and nonlinear effects from stall. In particular, Equation (39) addresses the physical phenomena of nonlinear wing lift with aspect ratio and AOA, and to some extent stall, of Figure 18 by using the nonlinear wing alone lift methodology of Reference 2. The MFF of Equation (39) is the multi-fin factors of Figure 9 and $f(\alpha)$ is the viscous effects of boundary layer separation in the leeward plane. Notice that $f(\alpha)$ is allowed to decrease the nonlinear term of roll damping as much as 50 percent.

The question naturally arises as to whether Methods ① or ② are superior to one another or if each method is superior in a given region. Figure 21 addresses this question. In utilizing Methods ① and ②, it was found Method ① was superior for higher aspect ratio configurations ($AR \geq 1.0$) where the normal Mach number was greater than about 0.6. This would imply the physical phenomena of compressibility and viscous separation in the leeward plane were the dominant physics involved for this class of configurations and freestream conditions. On the other hand, it was found that Method ② was superior to Method 1 for low values of normal Mach ($M_N \leq 0.2$) numbers or aspect ratio ($AR \leq 0.5$). The implication here is that for this class of configurations and freestream conditions, wing nonlinear lift curve slope and viscous effects are the dominant physics involved. It was found that for regions in between where Methods ① and ② were best, a blend of Methods ① and ② worked well. Referring to Figure 21, in region ③ we have:

$$C_{\ell_p} = (1) + \left(\frac{1 - AR}{0.5}\right)((2) - (1)) \tag{40A}$$

Where ① and ② refers to Methods ① and ② respectively. Likewise for region ④ of Figure 21, we have:

$$C_{\ell_p} = (1) + \left(\frac{0.6 - M_N}{.40}\right)((2) - (1)) \tag{40B}$$

Equations (40A) and (40B) imply that all the physical phenomena of Figure 17 and 18 are important in the transitions regions ③ and ④ of Figure 21.

Suffice it to say that Figure 21 and Equations (36), (37), (39) and (40) were derived based on a meager amount of experimental data. It is believed that the present semi-empirical method to predict nonlinear roll damping on wing-body-tail configurations is a good first cut. However, as more data becomes available, Figure 21 and Equation (40) could be revised.

AP09 Nonlinear Roll Damping Model

① Compressibility and separation major phenomena

$$C_{\ell_P} = \left(C_{\ell_P}\right)_{\alpha=0} \left\{0.3\left[\left(\frac{Q_L}{Q_\infty}\right)-1\right]\left(\frac{b}{d_{ref}}\right)^{3/4} - M_N + 1\right\}; M_N \geq 0.61$$

$$AR \geq 1.0$$

② Wing $C_{N\delta}$ and viscous effects major phenomena

$$C_{\ell_P} = \left(C_{\ell_P}\right)_{\alpha=0} + 4.3\left[\left(C_{N_\delta}\right)_{\alpha=0} - \left(C_{N_\delta}\right)_{\alpha}\right]\left(\frac{\bar{y}}{d_{ref}}\right)^2 (MFF) f(\alpha); M_N \leq 0.2$$

$$AR \leq 0.5$$

Where: $f(\alpha)=1-0.02\,|\alpha-\theta_f|/(\bar{y}/d_{ref})$

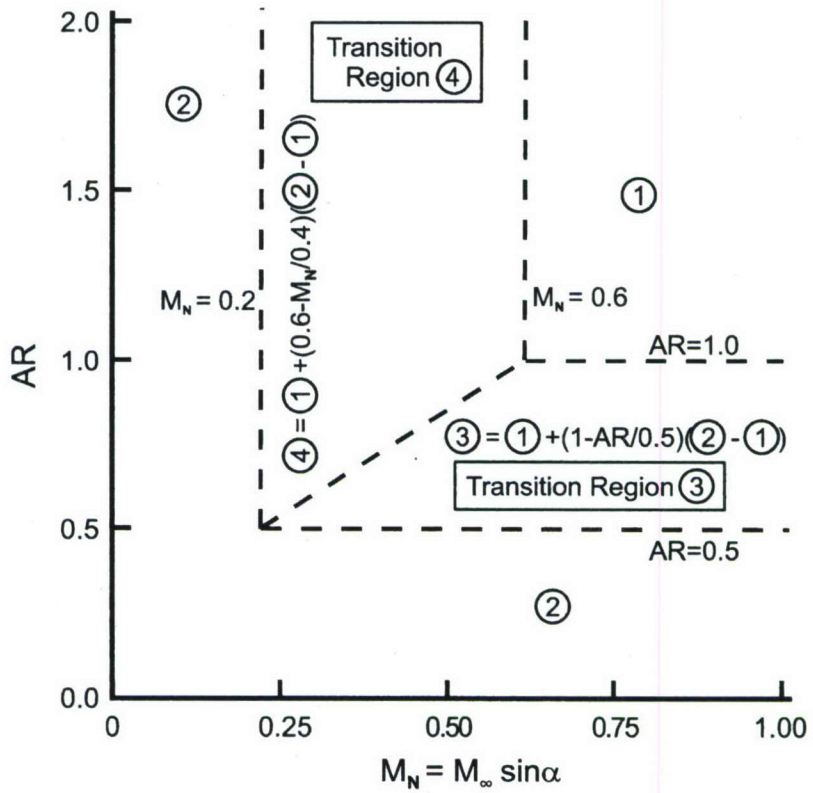

FIGURE 21. AREA OF APPLICABILITY OF METHODS ① AND ② TO PREDICT ROLL DAMPING AS FUNCTON OF ASPECT RATIO AND NORMAL MACH NUMBER

2.10 TANGENT SLOPE FOR C_{N_α} and C_{M_α}

It was mentioned earlier that in order to get the most accurate values of pitch damping, the correct value of C_{N_α} was needed. The AP05 and all prior versions of the APC used the secant slope for both C_{N_α} and C_{M_α}. That is:

$$C_{N_\alpha} = \frac{C_N}{\sin\alpha}, C_{M_\alpha} = \frac{C_M}{\sin\alpha}$$

Also, the center of pressure was defined in terms of pitching moment and normal force. That is:

$$X_{CP}/d = -C_M/C_N$$

The strict definition of static stability requires a positive pitching moment and a negative pitching moment coefficient derivative. The strict definition of static margin is defined as

$$X_{CP}/d = -C_{M_\alpha}/C_{N_\alpha}$$

where $C_{M_\alpha} = \frac{dC_M}{d\alpha}$ and $C_{N_\alpha} = \frac{dC_N}{d\alpha}$ are the tangent slopes.

There are several reasons the AP05 and prior versions of the APC used the secant slope versus the tangent slope for normal force and pitching moment coefficient slopes as well as using the pitching moment and normal force to define center of pressure. First of all, it is easier to obtain the secant slope of both C_{N_α} and C_{M_α} from theory and experiment than the tangent slope. Secondly, the secant slope is a smoother curve when plotted versus angle of attack or Mach number since no derivative is involved in the slope definition. Finally, the secant slope and tangent slope are basically equal at small angles of attack. However, the secant slope will allow the true value of static margin to be computed at AOA near zero. The secant slope can give a positive static margin at some conditions where the tangent slope will give unstable conditions.

The tangent slope for C_{N_α} and C_{M_α} has one major problem, noise in the data. The noise in the slopes comes from three factors. First, as alpha approaches 90 deg, C_{N_α} and C_{M_α} should approach zero, which can cause problems for the center of pressure prediction. Secondly, for moderate to large wing aspect ratios, wing stall occurs at lower Mach numbers which can have a dramatic effect on tangent slopes of C_N and C_M. Finally, when the flow transitions on the body from supercritical to subcritical, the normal force can vary substantially. Again the derivative of C_N can have a large variation.

The AP09, while using the tangent slopes for C_{N_α} and C_{M_α}, will try to smooth out some of the variation in the center of pressure by blending in the secant slopes as AOA increases. Thus for alpha less than 30 deg, the tangent slopes will be used to compute X_{CP}/d. For alpha greater than 30 deg, a blend of tangent and secant slopes will be used, and at alpha greater than 70 deg, secant slopes only will be used for static margin calculations.

3.0 RESULTS AND DISCUSSION

The results of the new methods developed in Section 2 will be presented in terms of the methods of Sections 2.1 – 2.7 broken down by the Major Weapons categories benefiting from the new technologies, namely spin stabilized projectiles, mortars and low drag bombs. Results of the new nonlinear methods for pitch and roll damping moments will then be discussed separately.

Many of the configurations that aerodynamics were available for are limited distribution. The limited distribution statement is generally for Department of Defense (DOD) agencies and the DOD contractors. As a result, for configurations that have limited distribution statements, or have proprietary information, no aerodynamics or configuration geometry will be shown. The references for each case will be given for those who want to view the configurations and their aerodynamics and are able to access the reports. For limited distribution configurations, error comparisons can be given for each configuration. Results of the AP05 and AP09 aerodynamic predictions compared to experimental data will be shown in terms of the error comparisons. Here the errors are defined for each aerodynamic coefficient as:

$$\text{percent error} = \frac{\left|C_{exp} - C_{Theory}\right|}{C_{exp}} \times 100 \tag{41}$$

For center of pressure, the errors will be defined in terms of percent of body length.

That is:

$$\frac{\left[(X_{CP})/d\right]_{error}}{\ell} = \frac{\left|\dfrac{(X_{CP})_{exp}}{d} - \dfrac{(X_{CP})_{Theory}}{d}\right|}{\ell} \times 100 \tag{42}$$

The errors of Equations (41) and (42) can be defined for C_A, $\left(C_{N_\alpha}\right)_{\alpha=0}$ and X_{CP}/d for spin stabilized projectiles and other weapons defined to fly at small AOA and then averaged for several Mach numbers. For weapons designed to fly at higher AOA, errors averaged over AOA and Mach numbers is more appropriate than averaging over Mach numbers only for low AOA data.

In addition to error comparisons of the AP05 and AP09 compared to experimental data, improvements in error of the AP09 over the AP05 for various aerodynamic coefficients can be defined as:

$$\text{AP09 improvement in aerodynamics over the AP05} = \frac{\text{AP05 avg error (in percent)} - \text{AP09 avg error (in percent)}}{\text{AP05 avg error in percent}} \quad (43)$$

Equation (43) can be used for each of the aerodynamic coefficients that were computed by each code.

3.1 SPIN STABILIZED PROJECTILES

Four projectiles will be considered, the Army 155 mm[15], M33[16] and the Navy 5"/54[17] and Hi Frag[18] projectiles. Of the four projectiles, only the M33 is published in an unlimited distribution format. For the M33 configuration, aerodynamics and configuration geometry can be shown. All four projectiles have boattails, so results with the AP05 and AP09 will differ, particularly for Mach numbers below 2.0.

The first case considered is the Army 155 mm[15]. Figure 22 shows the error results comparing the AP05 and AP09 predictions compared to experiment for C_A, $(C_{N_\alpha})_{\alpha=0}$ and X_{CP}/d. Here, since the experimental data was range data, an AOA of 2 deg was used in the aerodynamic calculations for C_{N_α} and X_{CP}/d. The 155mm configuration has a very short boattail so the AP09 improvement in C_{N_α} and X_{CP}/d is not very large as seen in Figure 22. Note that in examining Figure 22, the C_A errors for both the AP05 and AP09 are the same and below the ±10 percent criteria desired. If not for the two large errors at the $M_\infty = 0.8$ and 0.9, the average error on C_A would be only 3.1 percent. Also of note is the fact that the average C_{N_α} errors for both the AP05 and AP09 are below the ±10 percent criteria desired for the Aeroprediction Code. Also note the AP09 lowers the C_{N_α} error by about 25 percent compared to the AP05. Finally, the center of pressure error for both the AP05 and AP09 are larger than the ±4 percent of body length desired due to large errors in the transonic flow region. On the other hand, the AP09 lowers the center of pressure error by 0.9 percent of the body length or about 15 percent.

The next configuration considered is the M33 projectile[16]. Figure 23 shows the M33 configuration along with comparisons of AP05 and AP09 predictions compared to experimental data. Since the data is averaged range data, values of C_{N_α} and X_{CP}/d were computed at 2 deg AOA. Figure 24 then gives the error comparisons of the AP05 and AP09 at each 0.1 Mach number interval for $M_\infty = 0.5$ to 2.5. The M33 configuration has a 0.78 cal boattail. Note in comparing the AP05 and AP09 predictions to averaged experimental data in Figure 23 and more specifically in Figure 24, that both the AP05 and AP09 give good predictions of C_A and C_{N_α}. However, the AP09 reduces the average center of pressure error of the AP05 from 5.4 to 3.5 percent of the body length. This 35 percent reduction in center of pressure error for the AP09 brings the overall average below the desired criteria of ± 4 percent of body length.

M_∞	C_A Errors (in percent)		$(C_{N_\alpha})_{\alpha\approx 2}$ Errors (in percent)		X_{CP}/d Errors (percent of body length)	
	AP05	AP09	AP05	AP09	AP05	AP09
0.5	3.3	3.3	2.3	3.5	2.0	2.9
0.6	8.1	8.1	4.7	1.2	2.6	4.8
0.7	16.7	16.7	1.2	1.8	2.4	5.9
0.8	40.0	40.0	0.6	1.8	1.5	1.5
0.9	42.0	42.0	5.6	2.8	3.3	3.1
1.0	8.7	8.7	9.4	8.9	15.9	9.7
1.1	1.0	1.0	13.3	13.3	17.8	13.0
1.2	6.4	6.4	13.3	9.0	13.4	10.1
1.3	5.0	5.0	10.7	7.4	12.1	9.5
1.4	1.7	1.7	8.3	5.1	10.6	8.4
1.5	0.3	0.3	5.4	2.7	8.8	6.8
1.6	0.3	0.3	2.7	0.8	6.6	5.3
1.7	0.3	0.3	0.4	0.8	4.8	4.0
1.8	0.6	0.6	0.7	1.5	3.3	2.9
1.9	0.3	0.3	1.1	1.4	2.6	2.4
2.0	0.3	0.3	2.9	2.9	2.2	2.2
2.1	0.3	0.3	2.1	2.1	2.9	2.6
2.2	0.7	0.7	0.7	0.7	3.1	3.1
2.3	1.1	1.1	1.0	1.0	3.3	3.3
2.4	1.5	1.5	2.8	2.8	3.1	3.1
Avg	6.9	6.9	4.6	3.4	6.1	5.2

FIGURE 22. ERROR COMPARISONS OF AP05 AND AP09 AERODYNAMICS TO DATA[15] FOR THE 155MM PROJECTILE

The third configuration to compare AP05 and AP09 static aerodynamic predictions to data is the 5"/54 MK 41 Navy Projectile[17]. This configuration also has a fairly short boattail, similar to the 155mm round. Figure 25 compared the error predictions of the AP05 and AP09 to experimental data[17]. Note the axial force average error is higher than the previous two cases due to the large errors subsonically. However, the average error is still within the ±10 percent desired accuracy level. Also note that the average C_{N_α} and X_{CP}/d errors of the AP09 are reduced considerably from those of the AP05. An average error reduction of C_{N_α} of 3 percent (or a 41.7 percent reduction in error) for the AP09 over the AP05 is seen in Figure 25. Both the AP05 and AP09 average errors are within the ±10 percent guideline. The center of pressure error reduction for the AP09 over the AP05 is 33.7 percent. However, the AP09 center of pressure average error of 6.5 percent of the body length is still greater than the desired ±4 percent ℓ. In fairness, spin stabilized projectiles are generally between 4 and 6 cal in length. Thus an error of only about 0.2 cal is allowed if we are to stay within the ±4 percent ℓ desired accuracy criteria. In general, the ±4 percent desired accuracy level is easier to meet for a missile which is longer and has fins than a shorter body alone configuration.

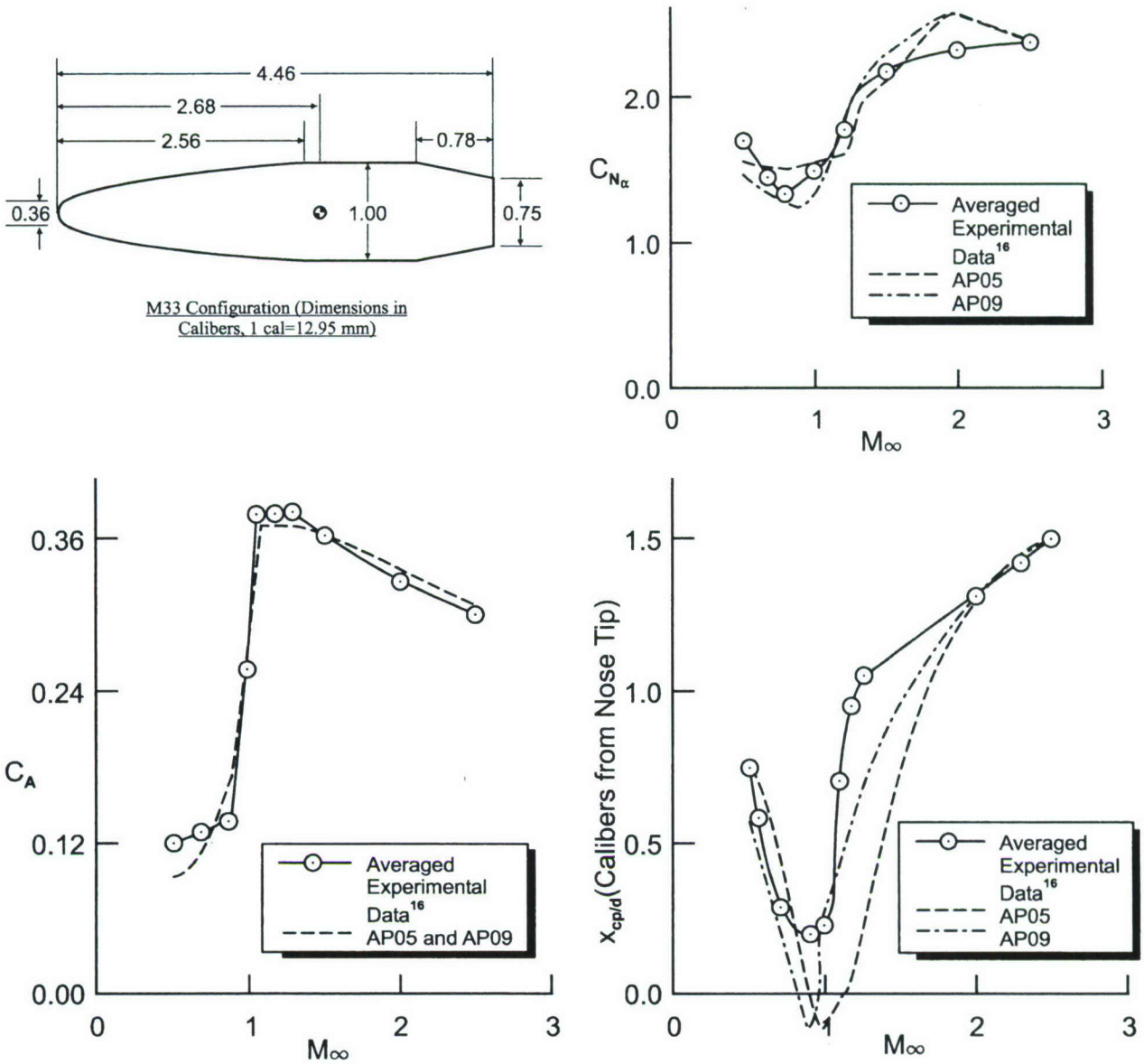

FIGURE 23. COMPARISON OF AP05 AND AP09 AERODYNAMIC PREDICTIONS TO EXPERIMENTAL DATA FOR M33 PROJECTILE

It is interesting to note that Reference 63 compared the range of the 5"/54 MK 41 projectile to range tables and an error only 1.37percent was obtained at maximum range conditions. This is in contrast to the average axial force error of 7.9 percent of Figure 25. The reason for the lower range error than axial force average error is two fold. First, the projectile spends little time in the Mach 0.6 to 1.0 range where the axial force errors are the largest. Secondly, the axial force errors at any given Mach number are not always positive or negative and therefore can cancel each other out over the flight of the projectile. Reference 63 showed an average range error of 9.21 percent using the GE Spinner code[5] and a range error of 9.96 percent using the McDrag[64] prediction for C_A.

M_∞	C_A Errors (in percent)		$(C_{N\alpha})_{\alpha=0}$ Errors (in percent)		X_{cp}/d Errors (percent of body length)	
	AP05	AP09	AP05	AP09	AP05	AP09
0.5	19.2	19.2	6.7	9.6	0.2	4.3
0.6	17.9	17.9	1.9	8.4	0.7	5.8
0.7	11.7	11.7	5.5	5.5	3.4	5.4
0.8	1.5	1.5	10.4	0.7	2.2	4.9
0.9	15.0	15.0	15.7	1.4	3.1	6.3
1.0	16.4	16.4	4.0	3.3	7.2	1.8
1.1	2.7	2.7	1.2	4.3	15.2	6.5
1.2	2.1	2.1	8.5	4.5	19.3	8.3
1.3	0.5	0.5	4.7	5.2	16.4	7.6
1.4	1.0	1.0	3.9	5.4	13.7	6.5
1.5	2.2	2.2	3.2	5.0	11.4	5.4
1.6	2.0	2.0	0.9	6.3	8.1	4.0
1.7	1.4	1.4	4.0	7.8	5.4	2.7
1.8	0.9	0.9	6.6	8.7	2.9	1.6
1.9	0.3	0.3	8.6	9.5	0.7	0.2
2.0	1.2	1.2	9.8	9.8	0.9	0.9
2.1	1.6	1.6	8.1	8.1	0.7	0.7
2.2	1.6	1.6	5.9	5.9	0.2	0.2
2.3	2.3	2.3	3.8	3.8	0.2	0.2
2.4	2.6	2.6	1.3	1.3	0.5	0.5
2.5	3.0	3.0	0	0	0.7	0.7
Avg	5.1	5.1	5.5	5.5	5.4	3.5

FIGURE 24. ERROR COMPARISONS OF AP05 AND AP09 AERODYNAMICS TO DATA[16] FOR THE M33 PROJECTILE

M_∞	C_A Errors (in percent)		$(C_{N_\alpha})_{\alpha=2}$ Errors (in percent)		X_{C_P}/d Errors (percent of body length)	
	AP05	AP09	AP05	AP09	AP05	AP09
0.6	17.2	17.2	4.2	4.8	-	-
0.7	22.9	22.9	1.2	5.5	2.1	2.5
0.8	36.6	36.6	2.4	6.1	8.5	11.7
0.9	40.7	40.7	8.0	0.1	10.0	6.9
1.0	15.3	15.3	9.8	8.8	18.8	9.6
1.1	2.1	2.1	9.8	11.2	18.5	10.2
1.2	1.9	1.9	16.5	5.8	16.5	8.5
1.3	2.2	2.2	17.0	5.1	14.8	8.8
1.4	0.3	0.3	13.1	4.1	14.0	8.7
1.5	2.7	2.7	12.2	3.9	12.9	8.1
1.6	2.7	2.7	9.3	1.6	11.5	7.7
1.7	2.5	2.5	6.9	0.0	9.4	6.3
1.8	2.3	2.3	4.5	1.5	7.9	5.4
1.9	2.0	2.0	2.6	3.0	6.2	4.0
2.0	1.7	1.7	0.4	4.7	5.0	3.5
2.1	0.7	0.7	2.2	4.4	5.8	4.2
2.2	0.4	0.4	3.6	1.4	6.0	4.2
2.3	0.0	0.0	5.0	5.0	6.3	4.6
2.4	0.4	0.4	6.7	1.8	6.0	4.4
2.5	1.6	1.6	8.8	4.2	5.6	4.2
Avg	7.9	7.9	7.2	4.2	9.8	6.5

FIGURE 25. ERROR COMPAISONS OF AP05 AND AP09 STATIC AERODYNAMICS TO DATA[17] FOR THE 5"/54 MK 41 PROJECTILE

The final projectile case to consider is the Navy Hi Frag[18]. This configuration has a full one caliber boattail and thus the improvements in the AP09 for long boattails should start to be seen for this configuration. Figure 26 compares the AP05 and AP09 static aerodynamic errors as a function of Mach number. As seen in the figure, the AP09 and AP05 once again do a good job in predicting axial force coefficient. However, only the AP09 does a good job in predicting C_{N_α} and X_{CP}/d. Note the AP09 reduces the average C_{N_α} and X_{CP}/d errors of the AP05 by 69 percent and 85 percent respectively. The AP09 also brings C_{N_α} and X_{CP}/d well within the desired accuracy goals of ±10 percent and ±4 percent of body length respectively.

M_∞	C_A Errors (in percent)		$(C_{N_\alpha})_{\alpha\approx 2}$ Errors (in percent)		X_{CP}/d Errors (percent of body length)	
	AP05	AP09	AP05	AP09	AP05	AP09
0.5	3.6	3.6	3.1	10.9	5.8	6.5
0.6	0.0	0.0	5.4	5.4	4.6	4.0
0.7	4.5	4.5	7.8	1.6	1.0	0.4
0.8	6.7	6.7	14.7	0.0	11.9	0.4
0.9	12.6	12.6	10.7	3.8	16.3	1.0
1.0	11.3	11.3	30.0	8.5	31.0	1.7
1.1	3.4	3.4	29.0	11.0	26.3	1.9
1.2	4.7	4.7	22.9	1.6	14.8	3.3
1.3	4.6	4.6	19.2	0.5	13.5	1.5
1.4	1.0	1.0	16.8	1.4	10.4	0.4
1.5	2.1	2.1	13.1	3.7	10.8	0.0
1.6	3.5	3.5	11.1	2.2	8.8	1.0
1.7	4.3	4.3	10.9	0.4	6.5	1.0
1.8	5.5	5.5	9.6	1.6	4.6	0.8
1.9	4.9	4.9	8.8	2.7	2.9	0.4
2.0	3.1	3.1	7.8	3.0	4.0	0.2
2.1	4.4	4.4	10.4	5.8	1.3	0.2
2.2	5.3	5.3	10.1	5.0	1.5	0.0
2.3	6.3	6.3	9.7	5.0	1.3	0.2
2.4	6.8	6.8	9.0	4.3	1.3	0.0
2.5	5.8	5.8	8.7	4.0	1.2	0.6
2.6	5.9	5.9	8.4	4.0	1.0	1.2
Avg	5.0	5.0	12.6	3.9	8.2	1.2

FIGURE 26. ERROR COMPARISONS OF AP05 AND AP09 STATIC AERODYNAMICS TO DATA[18] FOR THE NAVY HI-FRAG PROJECTILE

Figure 27 now averages the errors for 4 projectile configurations for both the AP05 and AP09 compared to data. As seen in the table, the overall axial force coefficient error for both the AP05 and AP09 is 6.2 percent. The normal force coefficient slope error of the AP09 is 4.3 percent compared to 7.5 percent for the AP05 or a 42.7 percent reduction. The largest error

Configuration	C_A Errors (in percent)		AP09 Imp. over AP05 (in percent)	$C_{N\alpha}$ Errors (in percent)		AP09 Imp. over AP05 (in percent)	X_{CP}/d Errors (percent of body length)		AP09 Imp. over AP05 (in percent)
	AP05	AP09		AP05	AP09		AP05	AP09	
1. 155 mm[15]	6.9	6.9	0.0	4.6	3.4	26.1	6.1	5.2	14.8
2. M33[16]	5.1	5.1	0.0	5.5	5.5	0.0	5.4	3.5	35.2
3. 5"/54 MK41[17]	7.9	7.9	0.0	7.2	4.2	41.7	9.8	6.5	33.7
4. Hi Frag[18]	5.0	5.0	0.0	12.6	3.9	67.4	8.2	1.2	85.4
Average	6.2	6.2	0.0	7.5	4.3	42.7	7.4	4.1	44.6

FIGURE 27. COMPARISON OF AVERAGE STATIC AERODYNAMIC PREDICTION ERRORS OF AP05 AND AP09 COMPARED TO EXPERIMENTAL DATA FOR FOUR BOATTAILED PROJECTILES

reduction was for the Hi Frag projectile which had the largest boattail. The average center of pressure error for the AP09 was 4.1 percent, close to the goal of ±4 percent, whereas the AP05 center of pressure error was 7.4 percent, well above the ±4 percent goal. The AP09 thus decreased the average center of pressure error of the AP05 by 44.6 percent.

In summary, the improvements in body alone normal force and center of pressure prediction for projectile configurations with boattails has provided substantial improvement in the AP09 prediction accuracy for these coefficients compared to the AP05. The largest error improvements occurred for the longest boattail case. No changes in axial force prediction errors was seen between the AP05 and AP09 for spin stabilized projectiles.

3.2 MORTAR CONFIGURATIONS

Several mortar configurations will be considered to compare the AP09 static and dynamic aerodynamics to both the AP09 and experimental data. All mortar cases have a limited distribution statement, so only errors of AP05 and AP09 predictions will be given. The specific configurations and their aerodynamics can be found in the references that are given for each case.

Most mortar configurations, as seen in Fig. 1, consist of a forebody, short afterbody, boattail, followed by a boom with fins attached. The geometry of the mortar is only allowed exactly in the Aeroprediction Code where second-order-shock expansion theory is used, or around $M_\infty \geq 2.0$. On the other hand, typical mortar flight regimes are $M_\infty \leq 1.1$. The bottom line is that the mortar configuration must be forced into a nose, afterbody, boattail shape in order to allow the Aeroprediction Code to compute aerodynamics for $M_\infty \leq 2.0$. This means the boattail must be modified to include the length of the boom.

The user of the Aeroprediction Code can expect slightly higher errors for configurations where the geometry is modified to fit within the context of the required nose, afterbody, boattail

format than those configurations where no geometry modifications are needed. It is the goal of the present work to reduce the errors of the computation process as much as possible through the new methodology. The new methodology attempts to account primarily for the viscous effects present on mortars and other long boattail cases that the AP05 and prior versions of the Aeroprediction Code do not completely account for.

The first mortar case considered is the 81 MM Improved Mortar Projectile. This is an Australian mortar round and the static and dynamic aerodynamics are given in References 65 and 24 respectively. Reference 65 gives results for Mach numbers 0.5, 0.7, 0.8, 0.9, 0.95. However, Reference 65 notes that the M = 0.9 and 0.95 static aerodynamic results are somewhat questionable due to transonic wind tunnel wall effects so only the M_∞ = 0.5, 0.7 and 0.8 static results will be considered. Results are given for AOA to about 5 deg. The roll and pitch damping results are given in Reference 24 and accuracy of the wind tunnel results are stated to be ±10 percent for roll damping and ±20 percent for pitch damping. Wind tunnel wall interference and roll bearing friction were the major areas of concern in the dynamic derivative experimental results.

Figure 28 gives the error comparisons of the static and dynamic aerodynamic comparisons of the AP05 and AP09 predictions compared to experiment[65,24]. In viewing the AP09 errors compared to the AP05 errors, it is seen the AP09 lift, roll and pitch damping are significantly better than the AP05 predictions and slightly superior for drag and center of pressure prediction. More specifically, the average lift (or normal force since AOA is near zero) error of the AP09 represents a 58.9 percent reduction over the AP05 error, the roll damping and pitch damping errors of the AP09 are 67.6 and 96.8 percent lower that the AP05, respectively. It should be kept in mind when viewing the roll and pitch damping results that the experimental data errors are estimated at ±10 percent and ±20 percent for roll and pitch damping respectively.

The next two mortar examples are from Reference 66. Both these cases have higher aspect ratio fins due to folding versus fixed fins. The first configuration has an aspect ratio of 3.77 (Figure 29) and the second an aspect ratio of 4.86 (Figure 30). Hence, the changes in the multi-fin factors discussed in Section 2.4 will have no impact on the results presented in Figures 29 and 30 since the Section 2.4 changes impacted aspect ratio of one and lower only at subsonic Mach numbers. All the other Section 2 methods will have an impact on the results of the Figures 29 and 30 cases though. On the other hand, the high drag fin numbers as well as the design of the boom will present problems for both the AP05 and AP09 predictions. Reference 66 gave only static aerodynamics for all configurations.

In examining the Figure 29 results for the lower aspect ratio case, it is seen the AP09 improves the average predictions for C_A and C_N. X_{CP} is about the same for the AP05 and AP09. On the other hand, neither the AP05 or AP09 average errors for C_A, C_N or X_{CP} fall within the desired accuracy boundaries for static aerodynamics. These goals are ±10 percent for average accuracy of C_A and C_N and ±4 percent ℓ for X_{CP}. In examining the Figure 29 results in more detail, it is seen that C_A prediction on average is quite good at low AOA but deviates from experiment at high AOA. Both the AP05 and AP09 C_A predictions are lower than data at higher AOA, probably due to the geometry of the fin hub being more of an issue at higher AOA than at

Static Aerodynamics

M_∞	α	C_D Errors (in percent)		C_L Errors (in percent)		X_{C_P}/d Errors (percent of body length)	
		AP05	AP09	AP05	AP09	AP05	AP09
0.5	0	36.9	17.1	0.0	0.0	1.9	0.9
	2	35.1	21.0	76.9	29.2	2.0	1.5
	4	23.2	12.0	86.7	39.8	2.9	2.9
	5	18.5	9.2	90.7	43.8	2.6	2.8
0.7	0	11.2	4.9	0.0	0.0	1.1	1.9
	2	10.9	4.1	27.4	4.8	0.2	0.3
	4	0.6	9.4	34.7	6.6	0.8	0.8
	5	4.8	12.5	36.7	15.2	0.8	0.9
0.8	0	6.1	7.9	0.0	0.0	7.0	3.4
	2	1.7	10.3	7.8	0.0	4.8	1.4
	4	2.8	11.6	18.3	10.9	3.4	0.0
	5	8.9	10.3	20.9	13.6	3.3	0.3
Avg		13.4	11.6	33.3	13.7	2.6	1.4

Dynamic Derivatives

M_∞	Roll Damping Errors (in percent)		Pitch Damping Errors (in percent)	
	AP05	AP09	AP05	AP09
0.5	46.9	8.6	282.7	14.2
0.7	39.0	13.9	214.9	2.0
0.8	34.3	16.4	199.5	6.0
Avg	40.1	13.0	232.4	7.4

FIGURE 28. ERROR COMPARISONS OF AP05 AND AP09 STATIC AND DYNAMIC AERODYNAMICS TO EXPERIMENT[24,65] FOR THE AUSTRAILIAN 81MM MORTAR ROUND

M_∞	α	C_A Errors (in percent)		C_N Errors (in percent)		X_{C_P} Errors (percent of body length)	
		AP05	AP09	AP05	AP09	AP05	AP09
0.4	0	16.1	8.3	0.0	0.0	11.3	8.1
	5	7.4	5.8	56.0	36.0	7.8	3.6
	10	1.5	1.0	28.3	10.0	0.4	5.0
	15	14.5	11.2	20.0	3.0	3.2	8.2
	20	29.6	23.4	30.3	4.4	4.6	11.0
0.61	0	9.7	2.3	0.0	0.0	11.3	9.3
	5	4.9	0.2	50.0	34.6	6.8	4.4
	10	8.5	5.3	26.7	13.3	0.0	2.9
	15	20.0	18.0	18.0	1.0	3.4	5.4
	20	31.3	26.8	30.7	4.3	3.6	8.1
0.76	0	7.1	0.0	0.0	0.0	11.1	12.6
	5	0.9	5.5	46.4	42.9	6.1	7.6
	10	12.9	14.9	31.7	28.3	0.4	1.1
	15	24.2	23.8	16.0	13.0	3.7	2.0
	20	35.6	33.4	13.6	7.9	5.2	4.9
Avg		14.9	12.3	24.5	13.2	5.3	6.3

FIGURE 29. ERROR COMPARISONS OF AP05 AND AP09 STATIC AERODYNAMICS TO DATA[66] FOR THE XM984 MORTAR MUNITION CONFIGURATION 194411

M_∞	α	C_A Errors (in percent)		C_N Errors (in percent)		X_{CP} Errors (percent of body length)	
		AP05	AP09	AP05	AP09	AP05	AP09
0.4	0	12.1	4.5	0.0	0.0	2.9	1.9
	5	7.0	2.3	4.4	7.1	3.5	3.6
	10	0.2	1.0	9.2	1.1	8.3	8.5
	15	15.3	12.6	20.8	5.6	10.7	10.0
	20	27.8	22.0	26.1	0.6	12.3	11.7
0.61	0	5.9	1.5	0.0	0.0	2.2	3.1
	5	1.4	3.3	30.0	10.0	3.7	2.6
	10	8.9	10.2	5.9	2.4	8.8	7.6
	15	23.4	21.7	10.8	0.0	9.6	8.1
	20	31.5	27.2	18.2	1.2	12.0	10.4
0.76	0	0.2	7.3	0.0	0.0	3.5	5.2
	5	6.3	11.0	24.4	21.8	0.9	1.4
	10	17.2	19.1	17.5	16.3	5.7	2.7
	15	29.5	29.3	11.7	9.2	8.5	4.9
	20	37.4	35.6	6.5	1.2	10.6	6.5
Avg		14.3	13.9	12.4	5.1	6.8	5.8

FIGURE 30. ERROR COMPARISONS OF AP05 AND AP09 STATIC AERODYNAMICS TO DATA[66] FOR THE XM984 MORTAR MUNITION CONFIGURATION 194451

lower AOA. The normal force predictions are all higher than data would suggest at lower AOA. It is suspected the AP05 and AP09 predictions for the body is the problem here. As might be expected, the center of pressure predictions at low AOA are too stable as a result of the overprediction of body alone normal force.

Figure 30 presents the second case considered from Reference 66. Results for the AP05 and AP09 predictions are generally better for this case than the Figure 29 case due to larger tail fins and less impact of the body lift. The AP09 gives improved results over the AP05 for the axial and normal force coefficients as well as the center of pressure. The AP09 normal force predictions fall within the desired accuracy guidelines discussed earlier whereas the axial force and center of pressure are slightly outside the desired accuracy goals.

It should be pointed out that the results of Figures 29 and 30 were computed using optimized values of critical crossflow Mach number and Reynolds numbers for both the AP05 and AP09. Values of R_{N_c} of 1×10^5 and ΔM_{N_c} of -0.24, -0.18 and -0.14 were used for Mach numbers of 0.4, 0.61 and 0.76 respectively. The results also accounted for perturbation inputs for the hub pins.

The next two mortar examples are lower aspect ratio cases, similar to the Figure 28 case. Aspect ratios for these two cases from Reference 45 and 46 are 0.86 and 0.68 respectively and therefore all the modifications made to the AP05 to form the AP09 should be utilized for these two configurations. Wind tunnel results are available for AOA 0 to 16 deg and Mach numbers

0.3 to 1.05. Also dynamic as well as static aerodynamics are available so the roll and pitch damping modifications to the AP05 will be used. Mach numbers of 0.5, 0.7, 0.9, and 1.05 will be considered for validation of the new methodology in the AP09. The pitch damping for the Reference 45 configuration was measured in the tunnel (but at M = 0.5 only) whereas the pitch damping for the Reference 46 configuration was computed (presumably) based on static wind tunnel test results.

Figure 31 compares the errors of the AP05 and AP09 to experimental data for the aspect ratio 0.86 configuration of Reference 45. In general, the axial force predictions of both the AP05 and AP09 were 10 to 20 percent higher than the wind tunnel results. The reason for the discrepancy is not clear. One possibility is corrections made to the sting balance measurements for base drag and skin friction drag. Experience has shown the Aeroprediction Code compares best to direct sting balance measurements because of the difficulty in accurately measuring base pressure on a model where the base diameter is close to the sting diameter (desire a 3 to 1 ratio for accurate base pressure measurements) and also the difficulty obtaining accurate base pressure measurements as a function of AOA. Many times for simplicity, measurements are made at zero AOA and applied to all AOA, which is not correct since base pressure changes with AOA.

The second point to note in Figure 31 is the significant improvement in normal force and center of pressure prediction of the AP09 over the AP05. The normal force coefficient predictions of both the AP05 and AP09 are high compared to data, but the discrepancy is more reasonable with the AP09. The center of pressure prediction, which is probably the most important of the static aerodynamics, is predicted very well by the AP09 and is well within the desired ±4 percent of body length accuracy criteria for X_{CP}.

The final point to be made in the Figure 31 is the fact the AP09 makes significant improvements in both roll and pitch damping prediction compared to the AP05. The AP05 predicts roll damping too high by a factor of two and pitch damping too high by a factor of three whereas the AP09 improves the dynamic derivative accuracy significantly. It should be pointed out that the Aeroprediction Code prediction in Figure 31 and 32 are for the linear term of the pitch and roll damping in contrast to the static aerodynamics where both linear and nonlinear terms are predicted. Unfortunately, the pitch damping derivatives of the Figure 31 case were only measured at low Mach numbers so only one data point exists for comparison to AP05 and AP09 results.

Figure 32 presents the error comparisons of the AP05 and AP09 to experimental data for the aspect ratio 0.68 case of Reference 46. Comments regarding this case are similar to those of Figure 31. The axial force is high for both the AP05 and AP09. The increase in axial force coefficient made in the AP09 for body tail configurations, actually made the comparisons to data worse for the Figure 31 and 32 case compared to the AP05 in contrast to other mortar cases considered. The normal force coefficient error in the AP09 was reduced in half compared to the AP05, and most importantly, the center of pressure error was reduced by 4.4 percent of the body length in the AP09 compared to the AP05. Finally, the AP09 roll damping and pitch damping are in reasonable agreement to the Reference 46 results whereas the AP05 is high by a factor of 2 to 3.

Static Aerodynamics

M_∞	α	C_A Errors (in percent)		C_N Errors (in percent)		X_{Cp} Errors (percent of body length)	
		AP05	AP09	AP05	AP09	AP05	AP09
0.5	0	22.4	7.2	0.0	0.0	14.7	2.5
	4	23.0	14.2	64.4	12.6	14.6	0.7
	8	16.2	16.2	62.1	16.8	13.6	2.0
	12	3.0	12.5	53.3	19.0	12.1	2.5
	16	11.2	17.5	39.7	10.2	10.3	2.3
0.7	0	19.4	4.5	0.0	0.0	10.4	5.0
	4	20.0	10.2	52.2	18.9	11.1	0.8
	8	13.1	10.1	49.2	20.3	11.0	0.9
	12	0.7	4.1	41.3	18.0	9.8	1.5
	16	13.3	2.1	27.9	10.6	8.1	1.2
0.9	0	15.9	1.6	0.0	0.0	1.8	5.7
	4	15.7	4.7	34.4	29.1	2.3	0.9
	8	15.3	1.5	39.4	35.5	3.3	1.1
	12	3.6	2.5	26.6	24.9	3.3	1.7
	16	5.1	0.0	13.2	13.5	1.9	1.1
1.05	0	14.9	6.1	0.0	0.0	1.1	3.9
	4	15.7	7.0	20.2	18.8	5.0	0.9
	8	10.6	2.5	19.7	19.3	6.6	3.3
	12	3.7	4.0	11.9	12.8	6.3	3.6
	16	1.3	6.6	0.0	2.4	4.1	2.0
Avg		12.2	8.4	27.8	14.1	7.6	2.1

Dynamic Aerodynamics

M_∞	C_{ℓ_p} Errors (in percent)		C_{M_q} Errors (in percent)	
	AP05	AP09	AP05	AP09
0.5	87.4	26.0	314.7	13.3
0.7	105.7	38.0	-	-
0.9	112.0	35.0	-	-
1.05	112.9	42.9	-	-
Avg	104.5	35.5	314.7	13.3

FIGURE 31. ERROR COMPARISONS OF AP05 AND AP09 STATIC AND DYNAMIC AERODYNAMICS TO DATA[45] FOR THE PGMM CONFIGURATION 11111

Static Aerodynamics

M_∞	α	C_A Errors (in percent)		C_N Errors (in percent)		X_{C_P} Errors (percent of body length)	
		AP05	AP09	AP05	AP09	AP05	AP09
0.5	0	31.6	15.4	0.0	0.0	11.8	5.3
	4	24.0	23.3	65.7	14.4	12.6	1.7
	8	28.5	28.8	65.6	20.0	11.7	1.1
	12	16.7	27.5	56.5	18.8	10.2	0.5
	16	0.8	18.9	40.7	13.0	8.2	1.3
0.7	0	25.8	10.2	0.0	0.0	7.7	7.5
	4	27.9	17.2	52.6	18.4	9.6	2.0
	8	22.5	19.4	56.1	24.4	9.8	0.4
	12	11.5	16.9	45.8	20.8	8.6	1.1
	16	6.0	6.8	31.9	14.2	6.9	0.7
0.9	0	0.0	9.5	0.0	0.0	2.3	6.6
	4	0.5	9.5	40.0	28.5	3.1	0.5
	8	2.3	9.9	45.5	36.4	4.5	1.9
	12	0.8	13.9	29.5	25.6	4.3	2.4
	16	17.3	6.8	12.7	11.9	2.6	1.5
1.05	0	3.7	11.2	0.0	0.0	1.3	6.5
	4	3.0	10.5	21.7	12.7	4.0	0.4
	8	5.9	12.7	21.6	17.6	5.9	2.4
	12	11.1	17.6	14.9	13.8	5.9	3.1
	16	18.6	25.1	2.2	2.9	4.1	2.0
Avg		17.6	20.8	30.1	14.7	6.8	2.4

Dynamic Aerodynamics

M_∞	C_{ℓ_p} Errors (in percent)		C_{M_q} Errors (in percent)	
	AP05	AP09	AP05	AP09
0.5	90.3	27.8	242.9	5.1
0.7	108.2	38.8	222.2	2.4
0.9	97.6	29.8	188.8	17.8
1.05	112.9	38.2	165.3	8.8
Avg	102.3	33.7	204.8	8.5

FIGURE 32. ERROR COMPARISONS OF AP05 AND AP09 STATIC AND DYNAMIC AERODYNAMICS TO DATA[46] FOR THE PGMM CONFIGURATION 51511

The last mortar configuration considered is the 60 MM M49A4 case. The configuration details and static aerodynamics for $M_\infty = 0.3$ and 0.48 to AOA 20 deg are given in Reference 67. The M49A4 configuration is very short (less than 5 cal in length), but has a long boattail and boom. Figure 33 gives the error comparisons of the AP05 and AP09 compared to experiment. As seen in the figure the axial and normal force prediction errors of the AP09 are reduced by 41.2 and 68.8 percent respectively over the AP05 predictions. Note the very large center of

M_∞	α	C_A errors (in percent)		C_N errors (in percent)		X_{CP} errors (percent body length)	
		AP05	AP09	AP05	AP09	AP05	AP09
0.3	0	0.9	1.3	0	0	84.2	14.5
	5	6.1	0.6	39.0	1.0	76.6	8.0
	10	7.2	3.3	52.3	15.0	74.4	5.9
	15	29.3	17.6	48.5	19.7	72.1	3.1
	20	49.8	31.6	45.3	22.7	71.3	1.4
0.48	0	8.8	3.1	0	0	90.7	18.0
	5	1.7	3.5	37.5	0	80.7	6.5
	10	13.8	10.8	46.0	11.9	75.6	4.0
	15	31.6	21.4	42.9	17.6	73.1	4.1
	20	52.1	36.0	44.0	23.0	70.9	1.4
Avg		20.3	12.7	35.6	11.1	77.0	6.7

FIGURE 33. ERROR COMPARISONS OF AP05 AND AP09 STATIC AERODYNAMICS TO DATA[67] FOR THE 60MM M49A4 MORTAR

pressure errors of the AP05, which is caused by the body alone center of pressure predicted to be 17 cal ahead of the nose at low AOA. The AP09 predicts the body alone center of pressure about 3 cal ahead of the nose near $\alpha = 0$. The net result is a center of pressure error of 6.7 percent of the body length for the AP09, compared to the very large errors of the AP05.

Figure 34 gives a summary of the static and dynamic aerodynamic prediction errors of the AP05 and AP09 for mortar configuration. Note there are 6 configurations for static aerodynamics and only 3 for dynamic derivatives. As seen in the summary table, axial force coefficient for the AP09 is only slightly superior to the AP05, with the AP09 being superior on 4 cases and inferior to the AP05 on the other 2 configurations. The AP09 normal force and center of pressure prediction on average are much better than the AP05. The AP05 normal force prediction error is cut in half by the AP09 (12.0 versus 27.3 percent) and the center of pressure error is reduced by over 75 percent (4.1 versus 17.7 percent of body length). The area of largest improvement of the AP09 over the AP05 is dynamic derivatives. The C_{ℓ_p} errors are reduced from 82.3 to 27.4 percent and the C_{M_q} errors are reduced from 241.8 to 9.7 percent when using the AP09 compared to the AP05. It is therefore clear that the AP09 shows substantial improvement over the AP05 on all mortar aerodynamics except for axial force where the AP09 shows only a small improvement in accuracy over the AP05.

3.3 LOW DRAG BOMB CONFIGURATIONS

Five bomb configurations will be considered, four of which are from unlimited distribution documentation and one from limited distribution documentation. For the unlimited distribution configurations, plots of data and configurations can be shown along with the error analysis that is shown for limited distribution configurations.

Static Aerodynamics

Configuration	C_A Errors (in percent)		AP09 Imp. Over AP05 (in percent)	C_N Errors (in percent)		AP09 Imp. Over AP05 (in percent)	X_{CP}/d Errors (percent of body length)		AP09 Imp. Over AP05 (in percent)
	AP05	AP09		AP05	AP09		AP05	AP09	
1. 81 mm Mortar[65]	10.1	9.5	5.9	33.3	13.7	58.9	2.6	1.4	46.0
2. XM 984 (194441)[66]	15.1	11.8	21.9	24.5	13.2	46.1	5.3	6.3	-18.2
3. XM 984 (194541)[66]	14.4	11.5	20.1	12.4	5.1	58.9	6.8	5.8	14.7
4. PGMM (11111)[45]	12.2	17.5	-43.4	27.8	14.1	49.3	7.6	2.1	72.3
5. PGMM (51511)[46]	13.1	19.6	-49.6	30.1	14.7	51.2	6.8	2.4	64.7
6. M49A4[67]	21.6	12.7	41.2	35.6	11.1	68.8	77.0	6.7	91.3
Average	14.4	13.8	4.2	27.3	12.0	56.0	17.7	4.1	76.8

Dynamic Derivatives

Configuration	C_{ℓ_p} Errors (in percent)		AP09 Imp. Over AP05 (in percent)	C_{M_q} Errors (in percent)		AP09 Imp. Over AP05 (in percent)
	AP05	AP09		AP05	AP09	
1. 81 mm Mortar[24]	40.1	13.0	67.6	232.4	7.4	96.8
2. PGMM (11111)[45]	104.5	35.5	66.0	288.3	13.3	95.3
3. PGMM (51511)[46]	102.3	33.7	61.1	204.8	8.5	95.8
Average	82.3	27.4	66.7	241.8	9.7	96.0

FIGURE 34. COMPARISON OF AVERAGE STATIC AND DYNAMIC AERODYNAMIC PREDICTION ERRORS OF AP05 AND AP09 COMPARED TO EXPERIMENT FOR SEVERAL MORTAR ROUNDS

The first bomb configuration considered is the General Purpose Low Drag Bomb (GPLDB) which is described in References 26, 68-71. References 26, 68-70 are unlimited distribution and Reference 25 is limited distribution. The drawings of the configuration and charts of aerodynamics will therefore come from References 26, 68-70. However, the aerodynamic error analysis of the static aerodynamics will come from Reference 71. Unfortunately Reference 71 was for static aerodynamics only, so error comparisons for roll and pitch damping will be taken from References 26 and 68.

Figure 35 shows the wind tunnel model of Reference 26 along with the AP09 approximation. The GPLDB actually is an ogive from the nose to a point mid way back on the boattail where a straight conical section begins. The AP09 thus approximated the MK 82 GPLDB as a nose that extended up to approximately where the maximum diameter occurred,

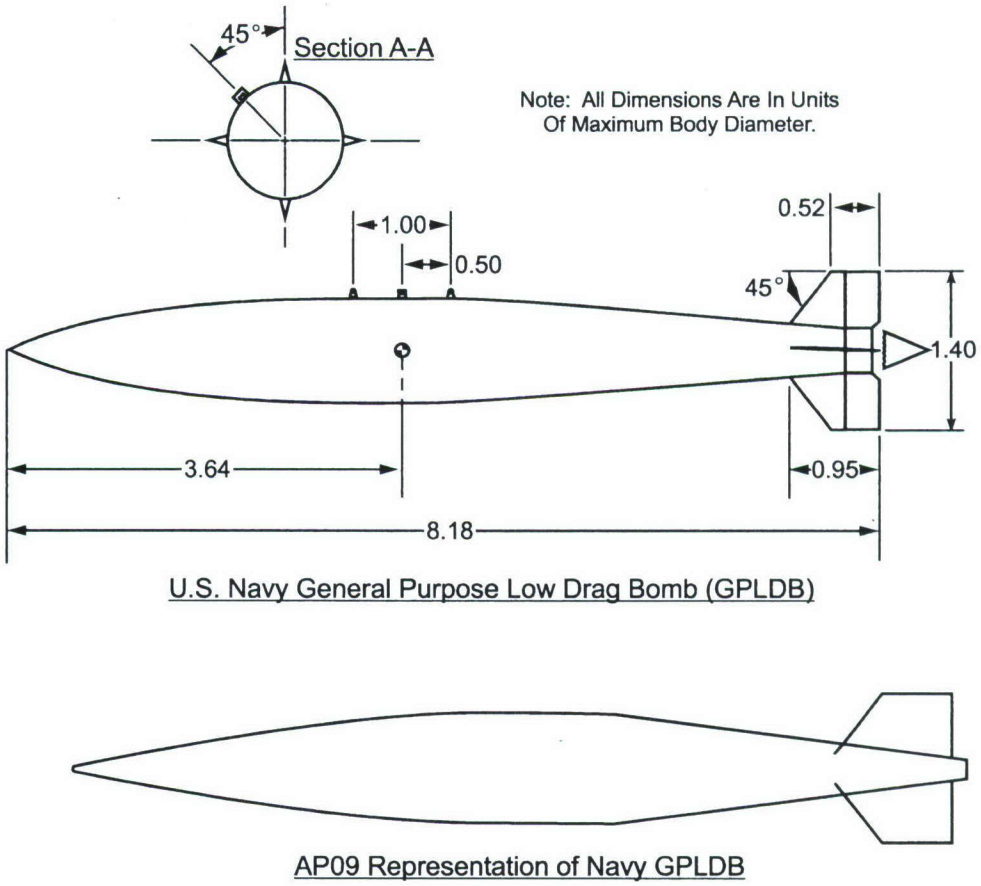

FIGURE 35. U.S. NAVY LOW DRAG BOMB AND AP09 REPRESENTATION

followed by an afterbody and a conical boattail. The boattail angle was selected to be identical to that on the GPLDB and thus the afterbody length was defined by the boattail angle and nose length.

Figures 36 and 37 show a comparison of the AP05 and AP09 C_N and X_{CP} to experiment[26] at Mach numbers of 0.8, 1.56 and 2.16 and AOA 0 to 20 deg. Note the AP05 and AP09 normal force coefficients are nearly identical but the AP09 gives improved center of pressure prediction over the AP05 at all three Mach numbers considered. Figure 38 shows comparisons of pitch and roll damping between experiment and the AP05 and AP09 predictions. Note the significant improvement in dynamic derivative predictions of the AP09 over the AP05, and in particularly the pitch damping predictions.

Figure 39 now gives specific error comparisons of the AP05 and AP09 to full scale static aerodynamic data of Reference71 and scaled wind tunnel model dynamic derivative data of Reference 26. Note the AP09 gives some slight improvement in all static aerodynamics (C_A, C_N and X_{CP}/d) predictions compared to the AP05. Also note both the AP05 and AP09 predictions of C_N and X_{CP}/d are within the desired accuracy bounds of ±10 percent and 4 percent ℓ_B respectively. The final point to make from Figure 39 is the large improvement in accuracy of roll and pitch damping of the AP09 compared to the AP05.

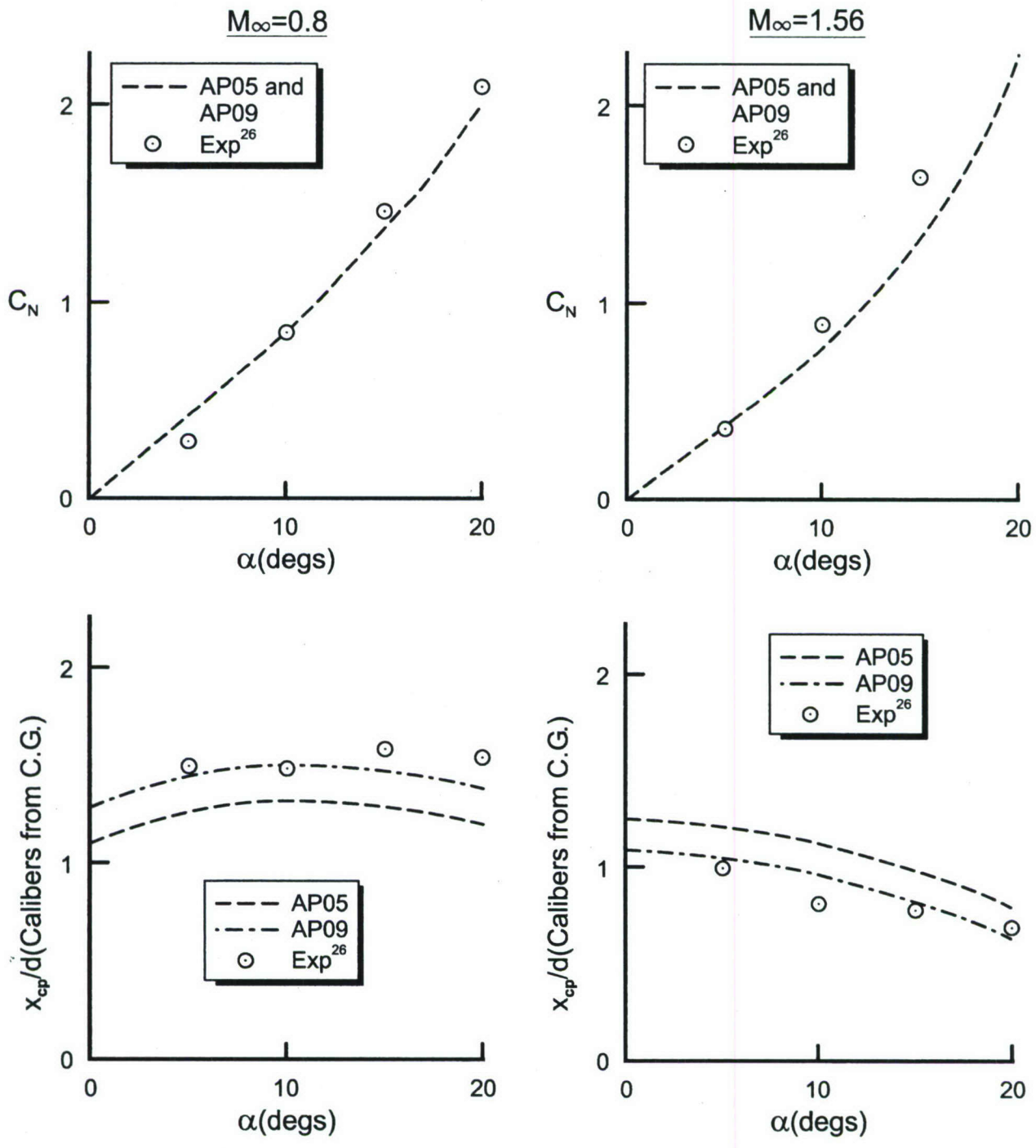

FIGURE 36. NORMAL FORCE AND CENTER OF PRESSURE COMPARISONS OF AP05 AND AP09 TO EXPERIMENT (Φ=0°) FOR GPLDB

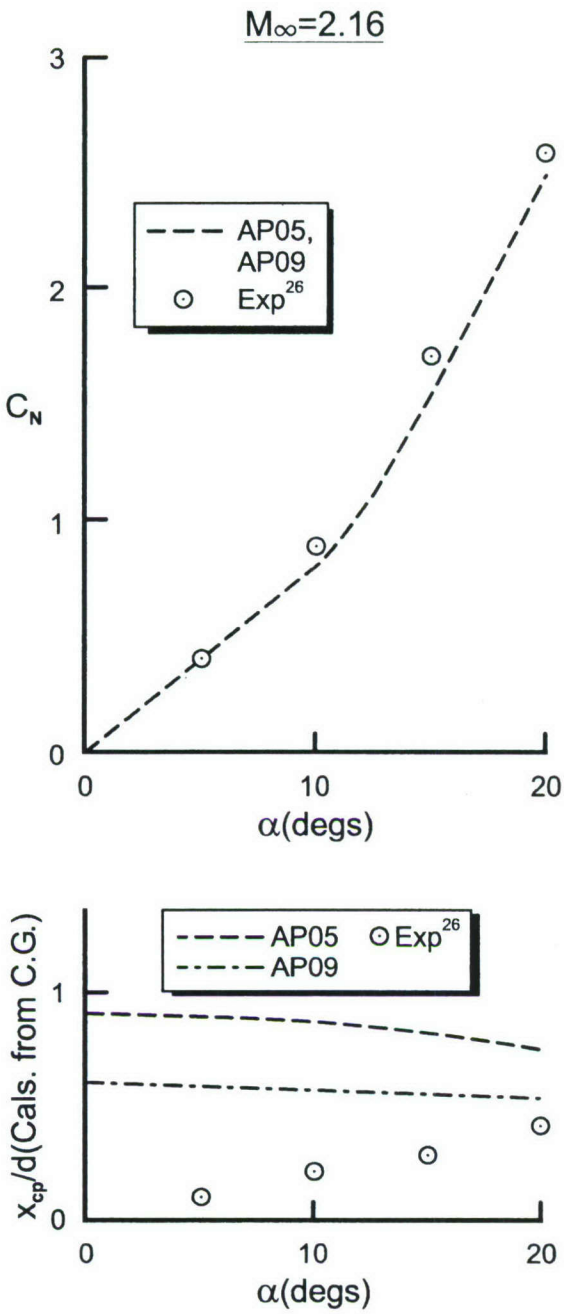

FIGURE 37. NORMAL FORCE AND CENTER OF PRESSURE COMPARISONS OF AP05 AND AP09 TO EXPERIMENT FOR GPLDB (Φ=0°)

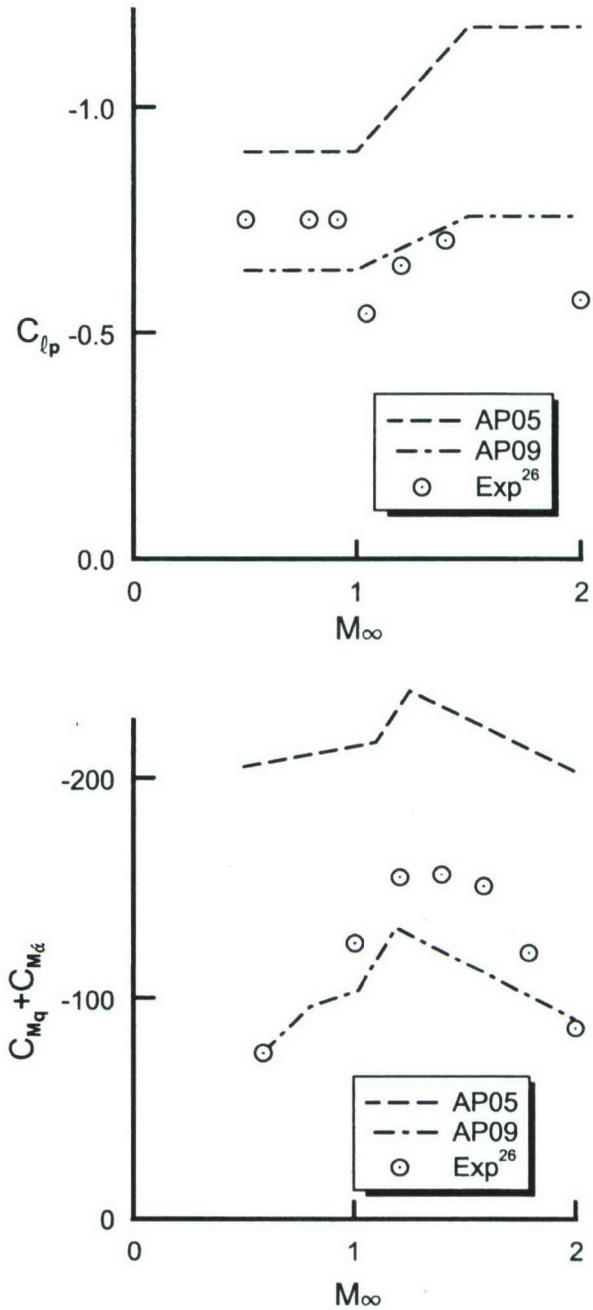

FIGURE 38. ROLL AND PITCH DAMPING COMPARISONS OF AP05 AND AP09 TO EXPERIMENT FOR GPLDB (α=0°)

Based on AEDC Data[71]

M_∞	α	C_A Errors (in percent)		C_N Errors (in percent)		X_{C_P}/d Errors (percent of body length)	
		AP05	AP09	AP05	AP09	AP05	AP09
0.6	0°	12.5	12.5	0	0	1.8	1.2
0.8	↓	6.1	6.1	↓	↓	2.9	0.8
0.9	↓	13.1	13.1	↓	↓	2.0	1.2
1.1	↓	1.1	1.1	↓	↓	1.1	0.7
1.3	↓	9.3	9.3	↓	↓	0.6	0.2
1.5	↓	11.5	11.5	↓	↓	8.9	3.0
0.6	8°	13.8	10.6	14.0	1.8	1.7	0.5
0.8	↓	10.0	1.2	6.7	3.3	1.2	1.1
0.9	↓	14.5	14.6	4.4	2.9	0.4	3.3
1.1	↓	1.9	1.9	7.5	7.5	1.9	3.1
1.3	↓	17.8	17.8	1.5	0.0	2.4	2.0
1.5	↓	9.7	15.8	20.7	22.4	3.7	1.1
0.6	16°	33.8	6.9	11.3	0.8	2.9	1.1
0.8	↓	31.1	12.0	2.1	2.1	0.2	2.1
0.9	↓	46.1	46.2	3.7	12.4	2.9	4.1
1.1	↓	4.2	4.2	6.4	5.1	6.1	4.9
1.3	↓	15.1	15.1	10.6	10.0	5.1	3.9
1.5	↓	11.1	0.6	7.9	10.8	1.4	3.3
0.6	24°	72.8	26.7	7.3	1.3	3.0	1.8
0.8	↓	60.0	26.5	2.7	3.1	1.2	2.9
0.9	↓	46.6	46.9	9.4	4.9	3.2	4.4
1.1	↓	0.5	0.5	2.4	2.0	4.8	4.5
1.3	↓	21.6	21.6	8.7	8.1	3.1	2.6
1.5	↓	31.7	15.9	5.3	8.4	0.5	3.9
Average		17.3	10.7	5.5	4.5	2.6	2.4

Based on NOL Data[26]

M_∞	C_{ℓ_P} Errors (in percent)		$C_{M_q} + C_{M_{\dot{\alpha}}}$ Errors (in percent)	
	AP05	AP09	AP05	AP09
0.6	20.0	14.7	173.1	1.3
0.8	21.3	13.3	180.0	38.7
0.9	21.0	10.7	170.0	35.0
1.1	39.0	1.7	45.3	28.0
1.3	48.6	4.3	46.7	19.4
1.5	64.7	14.7	44.3	24.5
Average	35.8	9.9	109.9	24.5

FIGURE 39. ERROR COMPARISONS OF AP05 AND AP09 AERODYNAMICS TO DATA FOR MK82 GPLDB

It was found in actual flight tests that some GPLDB's would go unstable in flight due to a smaller than desired static margin. As a result, three alternative MK 82 designs were investigated to improve the reliability of the GPLDB. These concepts were investigated aerodynamically and therefore comparisons of aerodynamics of these three concepts will be given here. Actually, only one of the concepts is a boattailed low drag concept whereas the other two designs are based on an inflatable stabilizer at the rear that converts into a conical flare with 8 fins for increased static stability and damping characteristics.

Figure 40 presents the Fixed Fin (FF) candidate replacement for the MK 82 GPLDB along with the AP09 approximation. The nose and afterbody length of the FF and AP09 approximation are identical. However, the AP09 approximates the boattail length as including all length past the end of the afterbody, including the straight section the fins rest on. The FF design has 4 fins, just like the MK 82 GPLDB. Figure 41 shows a comparison of C_{N_α}, X_{CP}/d, C_{ℓ_p} and $C_{M_q} + C_{M_{\dot{\alpha}}}$ predictions of the AP05 and AP09 compared to experiment. Once again, the AP09 predictions are superior to the AP05 for all aerodynamics. The most notable aerodynamic improvements of the AP09 are for the static aerodynamics above M_∞ of about 0.7 and dynamic derivatives.

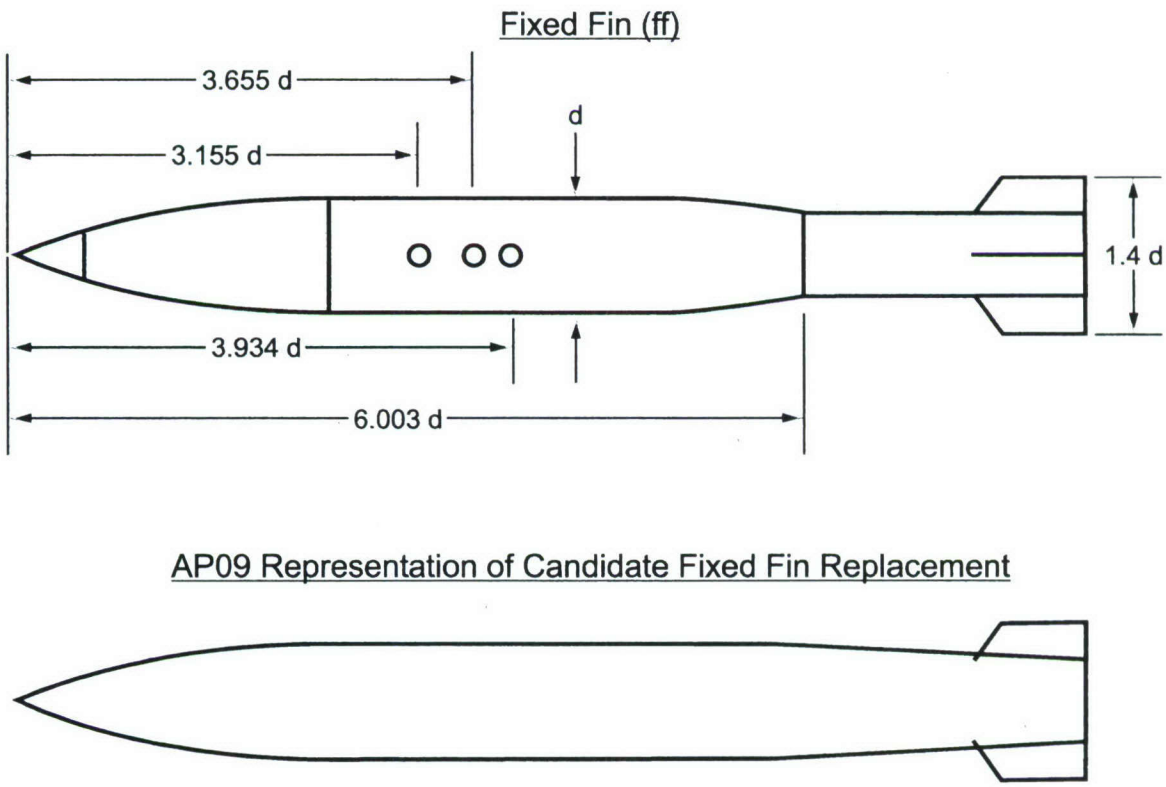

FIGURE 40. FIXED FIN CANDIDATE REPLACEMENT FOR MK82 GPLDB (CG=3.934D)

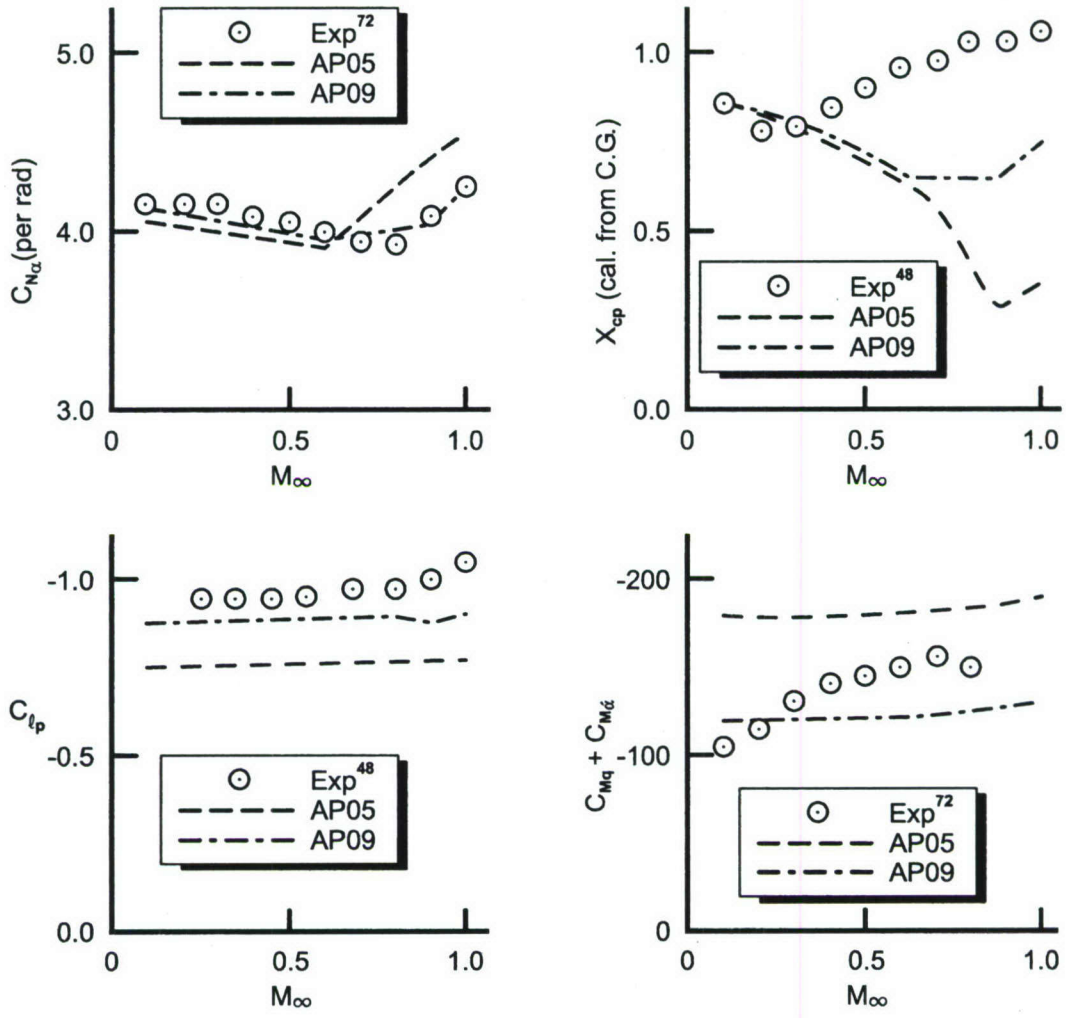

FIGURE 41. COMPARISON OF AP05 AND AP09 AERODYNAMICS TO EXPERIMENTAL DATA FOR MK82 FIXED FIN CANDIDATE REPLACEMENT FOR GPLDB (α=0°)

Figure 42 provides more detailed error analysis of the aerodynamics given in Figure 41. Note once again the average errors of all aerodynamics are reduced by the AP09 compared to the AP05, with the largest reductions on roll and pitch damping. Also, it is worth noting that both the AP05 and AP09 predict C_{N_α} and X_{CP}/d within the desired accuracy bounds of ±10 percent and ±4 percent ℓ_B respectively.

The next two configurations are actually not very low drag bombs due to the fact they have inflatable stabilizers at the end of the body, which increases the drag substantially. Nevertheless, it was believed they would be good test cases for the Aeroprediction Code, since the configurations had fairly complex geometry with 8 fins on the inflatable flare.

Figure 43 shows the first case, the Inflatable Stabilizer Retarder (ISR) with the AP09 representation at the bottom of the figure. Note the AP09 does not allow for the initial boattail followed by a flare. Only a flare or a boattail is allowed. Thus the afterbody length extends to

M_∞	C_{N_α} Errors (in percent)		X_{CP}/d Errors (in percent of body length)		C_{ℓ_p} Errors (in percent)		$C_{M_q} + C_{M_{\dot{\alpha}}}$ Errors (in percent)	
	AP05	AP09	AP05	AP09	AP05	AP09	AP05	AP09
0.1	3.9	3.9	0.7	1.2	-	-	72.3	5.7
0.2	3.1	2.2	0.4	0.7	-	-	57.4	2.6
0.3	1.9	0.5	1.3	0.9	20.0	6.3	39.2	13.8
0.4	2.2	0.2	1.9	1.7	20.0	6.3	30.0	20.0
0.5	2.7	0.5	0.4	0.4	18.9	6.3	26.2	22.1
0.6	1.8	2.5	1.3	1.3	20.0	7.3	22.7	24.0
0.7	6.0	1.5	3.0	2.6	20.0	7.3	21.7	23.7
0.8	8.1	5.8	6.8	3.4	20.6	7.2	23.3	18.0
0.9	10.0	1.7	10.6	5.2	24.5	11.2	-	-
1.0	7.8	7.5	11.2	4.4	26.7	14.3	-	-
Avg	4.8	2.6	3.8	2.2	21.3	8.3	36.6	16.2

FIGURE 42. ERROR COMPARISONS OF AP05 AND AP09 AERODYNAMICS TO DATA FOR THE MK82 FIXED FIN CANDIDATE REPLACEMENT FOR GPLDB

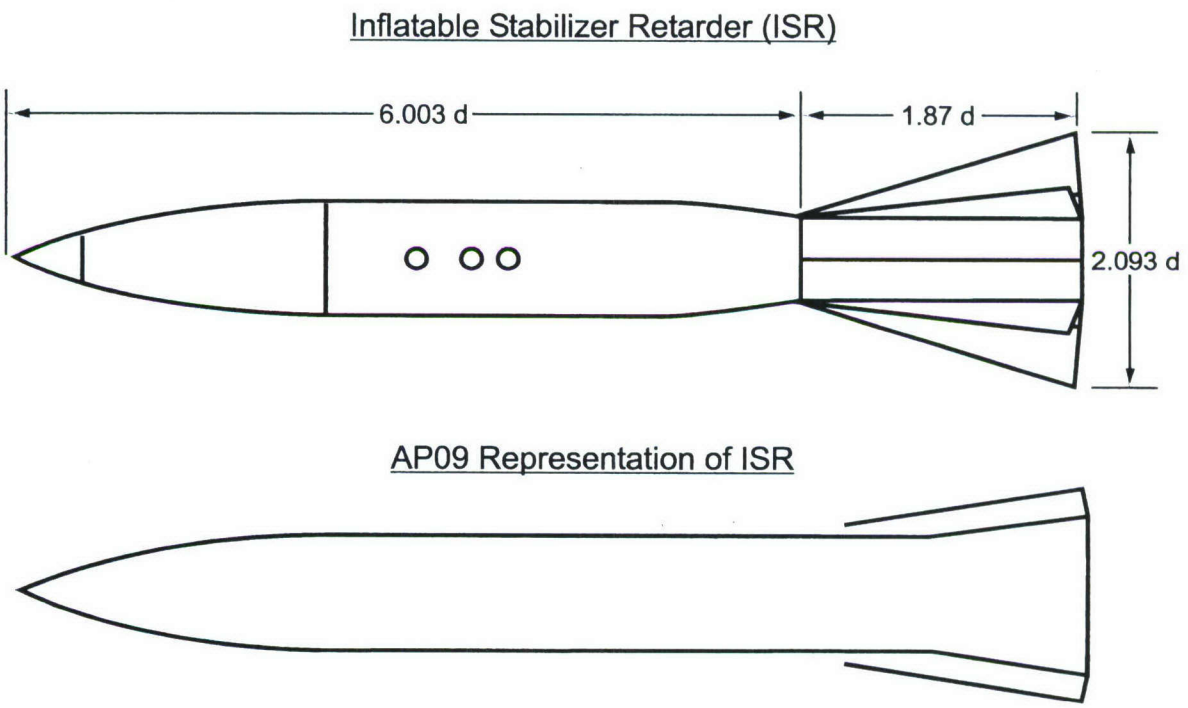

FIGURE 43. ISR CANDIDATE REPLACEMET FOR MK82 GPLDB (CG=3.655D)

the flare on the AP09 representation of the ISR. It was also found best to approximate the flare exact angle versus the exact length. Since the ISR flare starts on a smaller diameter than the AP09 flare, the AP09 flare was shorter in length than the ISR flare. On the other hand the tail fins of the ISR and AP09 have the same characteristics of span, chord, area and centroid of presented area. The fact that physically they are shown detached from the body on the AP09,

will not affect the aerodynamic calculations in the AP09. However, anytime one has to approximate a configuration in order to make it fit within the nose, afterbody, and boattail or flare restrictions of the AP09, larger error boundaries than the ±10 percent for C_A and C_N and ±4 percent ℓ_B for X_{CP}/d can be expected.

Figure 44 compares C_{N_α}, X_{CP}/d, C_{ℓ_p} and $C_{M_q} + C_{M_{\dot{\alpha}}}$ predictions of the AP05 and AP09 to data. As expected, neither the AP05 and AP09 are as accurate as desired for C_{N_α} aerodynamics due to the required geometry modifications of the code. On the other hand, X_{CP}/d, C_{ℓ_p} and $C_{M_q} + C_{M_{\dot{\alpha}}}$ predictions are reasonable. Figure 45 gives the exact accuracy comparisons of the AP05 and AP09 to data. It is seen that the average error of C_{N_α}, X_{CP}/d, C_{ℓ_p} and $C_{M_q} + C_{M_{\dot{\alpha}}}$ are about the same for the AP05 and AP09 with the AP09 giving significant improvement over the AP05 for roll damping.

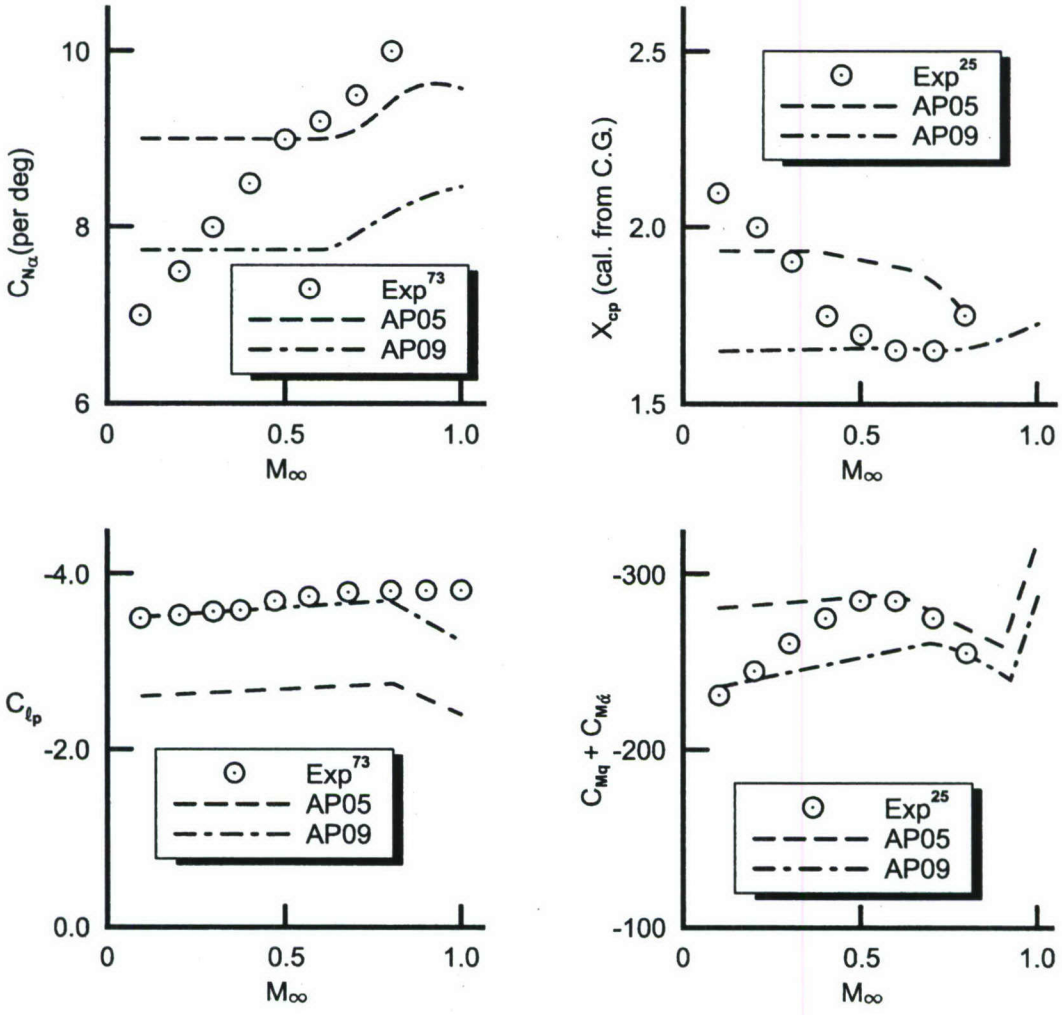

FIGURE 44. COMPARISON OF AP05 AND AP09 AERODYNAMICS TO DATA FOR ISR CANDIDATE REPLACEMENT FOR GPLDB

M_∞	C_{N_α} Errors (in percent)		X_{C_P}/d Errors (in percent of body length)		C_{ℓ_p} Errors (in percent)		$C_{M_q} + C_{M_{\dot{\alpha}}}$ Errors (in percent)	
	AP05	AP09	AP05	AP09	AP05	AP09	AP05	AP09
0.1	28.6	11.1	1.9	5.7	24.2	0.2	21.7	2.6
0.2	20.0	3.3	0.8	4.4	24.2	0.2	14.7	3.3
0.3	12.4	3.3	0.4	3.0	25.4	0.1	8.5	4.6
0.4	5.9	9.2	2.2	1.0	26.1	0.1	3.3	12.7
0.5	0.6	14.0	2.5	0.4	26.8	0.2	0.7	15.4
0.6	1.5	15.8	3.0	0.3	27.6	0.2	1.8	14.7
0.7	3.9	16.2	2.3	0.1	27.9	0.3	5.5	10.5
0.8	6.9	18.6	0.4	1.5	28.7	0.4	10.6	0.4
Avg	10.0	11.4	1.7	2.1	26.4	0.2	8.4	8.0

FIGURE 45. ERROR COMPARISONS OF AP05 AND AP09 AERODYNAMICS TO DATA FOR THE MK82 ISR CANDIDATE REPLACEMENT FOR GPLDB

The next configuration is the same as the ISR except there is an extended section prior to the retarder for increased static margin and pitch damping. The ISRE and the AP09 representation are shown in Figure 46. Similar comments in terms of the AP09 geometry simplifications apply here as to the previous ISR configuration.

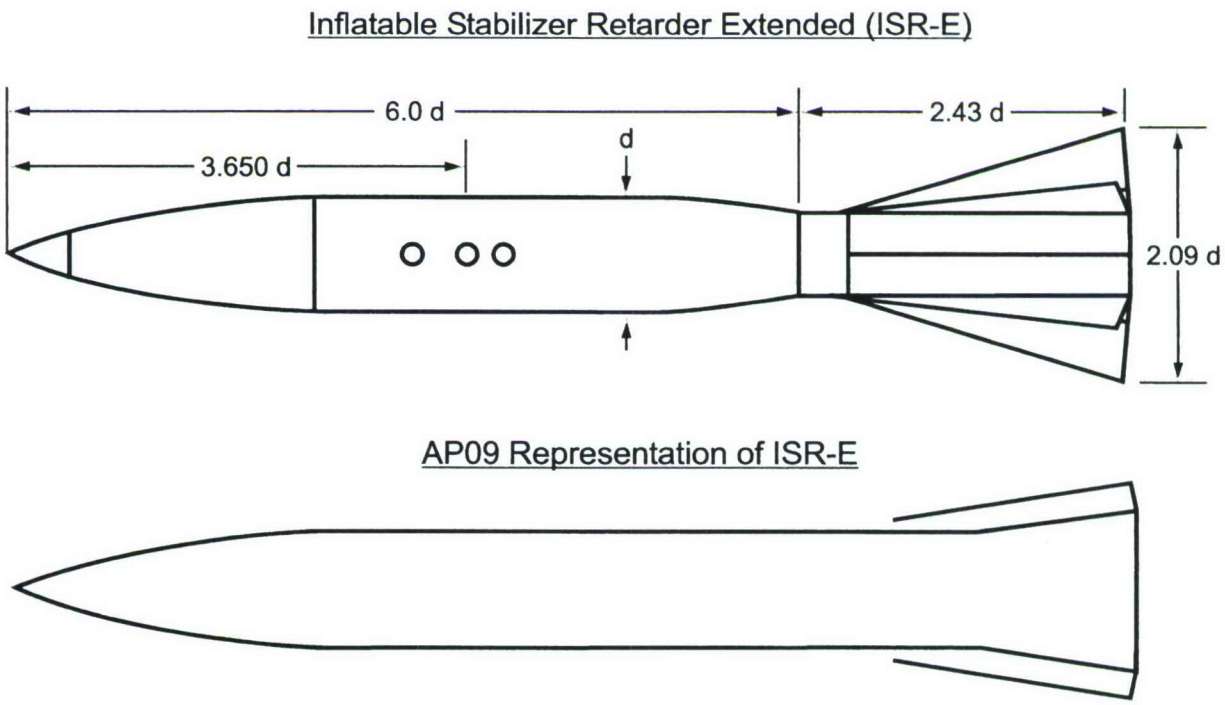

FIGURE 46. ISRE CANDIDATE REPLACEMENT FOR MK82 GPLDB (CG=3.65D)

The aerodynamic comparisons of the AP05 and AP09 to experiment for the ISRE configuration are shown in Figures 47 and 48. As seen in the figures, which have been intentionally expanded in scale, the AP05 and AP09 give reasonable predictions for C_{N_α} and X_{CP}/d. Also, the AP09 gives very good predictions of roll and pitch damping as well.

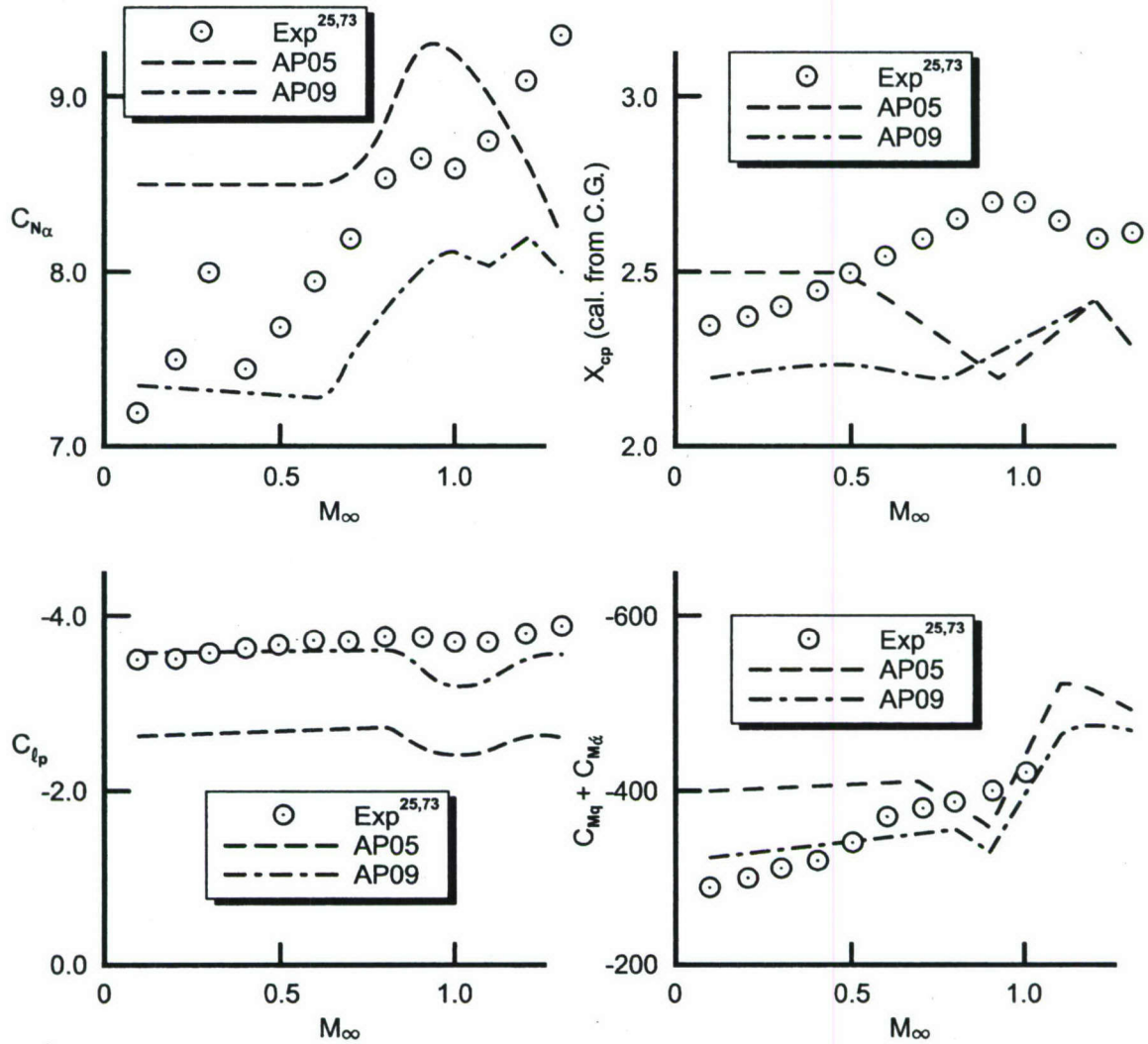

FIGURE 47. COMPARISON OF AP05 AND AP09 AERODYNAMICS TO DATA FOR ISRE CANDIDATE REPLACEMENT FOR GPLDB

The final bomb configuration is taken from References 75 and 75, both of which have a limited distributed statement. Suffice it to say, however, that this bomb possessed a fairly long boattail and the AP09 could represent the configuration with a minimum of approximation. This almost exact representation of the AP09 is in contrast to the previous two examples in particular. Figure 49 gives the error comparisons of the AP05 and AP09 to data for the M117 bomb. The only area where the AP09 gave significant improvement in accuracy over the AP05 was in C_{N_α} where the errors were cut in half. In general, both codes gave good static aerodynamics,

M_∞	C_{N_α} Errors (in percent)		X_{CP}/d Errors (in percent of body length)		C_{l_p} Errors (in percent)		$C_{M_q} + C_{M_{\dot{\alpha}}}$ Errors (in percent)	
	AP05	AP09	AP05	AP09	AP05	AP09	AP05	AP09
0.1	17.9	2.2	1.8	1.8	24.3	0.2	35.6	10.2
0.2	12.9	2.1	1.3	2.0	24.3	0.2	34.0	8.7
0.3	6.0	8.4	0.4	2.1	25.0	0.1	30.3	6.1
0.4	13.8	1.9	0.2	2.6	26.1	0.0	24.9	1.5
0.5	10.9	4.8	0.2	3.1	26.8	0.1	20.2	2.4
0.6	6.8	8.5	0.4	3.8	27.6	0.2	11.3	9.5
0.7	4.6	8.7	0.4	4.7	27.6	0.2	7.9	10.5
0.8	3.1	9.8	1.4	5.3	27.5	0.2	0.8	9.7
0.9	7.8	7.4	5.8	5.2	32.3	8.5	9.5	17.0
1.0	7.8	5.3	5.2	4.5	35.4	13.2	1.9	7.8
1.1	2.1	8.1	3.7	3.3	35.4	13.8	-	-
1.2	4.7	10.0	2.0	3.2	30.3	6.6	-	-
1.3	11.6	14.7	2.5	4.5	32.3	9.0	-	-
Avg	8.5	7.1	1.9	3.5	28.8	4.0	17.6	8.3

FIGURE 48. ERROR COMPARISONS OF AP05 AND AP09 AERODYNAMICS TO DATA FOR THE ISRE CANDIDATE SNAKEYE REPLACEMENT

M_∞	α	C_A errors (in percent)		C_N errors (in percent)		Xcp/d errors (percent body length)		C_{N_α} errors (in percent)	
		AP05	AP09	AP05	AP09	AP05	AP09	AP05	AP09
.60	0	11.9	29.8	0	0	1.1	1.3	20.5	2.7
	5			19.4	2.7	0.4	0.0		
	10			9.5	3.6	4.4	3.8		
	15			5.0	6.4	5.3	4.8		
	20			2.5	7.5	7.2	6.5		
.80	0	11.3	10.4	0	0	4.8	1.0	5.2	5.3
	5			5.1	5.1	5.1	1.9		
	10			2.2	2.2	6.8	3.6		
	15			0	0	8.0	4.8		
	20			2.5	2.0	8.6	5.5		
.95	0	22.3	7.3	0	0	6.3	0.6	1.2	6.0
	5			12.5	15.0	4.9	1.0		
	10			4.3	8.6	4.8	0.6		
	15			0.7	4.6	5.1	0.2		
	20			5.0	1.4	4.9	0.2		
1.1	0	8.5	6.8	0	0	0	5.1	1.6	2.3
	5			7.0	11.6	1.0	4.6		
	10			4.2	8.3	1.3	4.8		
	15			2.6	6.5	2.5	5.3		
	20			5.0	1.4	3.2	6.1		
1.4	0	11.9	6.3	0	0	4.6	3.2	7.8	5.1
	5			8.9	8.9	2.7	2.5		
	10			1.0	0	2.1	1.7		
	15			5.1	5.7	2.9	2.5		
	20			9.4	10.2	1.1	0.6		
Avg.		13.2	12.1	4.5	4.5	3.8	2.8	8.9	3.7

FIGURE 49. ERROR COMPARISONS OF AP05 AND AP09 AERODYNAMICS TO DATA FOR THE M117 BOMB WITH M131 FIN

although the average C_A errors slightly exceeded the accuracy goal of ±10 percent. Unfortunately, no dynamic aerodynamics were found for the M117 bomb.

Figure 50 now summarizes all the errors of the 5 bomb configurations. Only two cases have axial force data, so the accuracy averages here are not as reliable due to a smaller sample. Also, only 4 of the 5 configurations had roll and pitch damping. Several points are worth making in viewing Figure 50. First of all, the AP09 improves aerodynamic estimates of all static and dynamic predictions compared to the AP05. Errors of the AP09 are reduced by 22.4 percent for axial force, 20 percent for normal force, 7.1 percent for center of pressure, 80.1 percent for roll damping and 66.8 percent for pitch damping when compared to the AP05. Secondly, both the AP05 and AP09 give average errors within the ±10 percent desired range for C_N and ± 4 percent ℓ_B for X_{CP}/d. Thirdly, the AP09 provides significant improvement in pitch and roll damping compared to the AP05.

Bomb Static Aerodynamics Summary

Configuration	C_A Errors (in percent)		AP09 Imp. Over AP05 (in percent)	C_N Errors (in percent)		AP09 Imp. Over AP05 (in percent)	X_{CP}/d Errors (percent of body length)		AP09 Imp. Over AP05 (in percent)
	AP05	AP09		AP05	AP09		AP05	AP09	
1. MK82 GPLDB[26]	17.3	10.7	38.2	5.5	4.5	18.2	2.6	2.4	7.7
2. MK82 FF[25,72]	-	-	-	4.8	2.6	45.8	3.8	2.2	42.1
3. MK82 ISR[25,72]	-	-	-	10.0	11.4	-14.0	1.7	2.1	-23.5
4. MK82 ISRE[25,72]	-	-	-	8.5	7.1	16.5	1.9	3.5	-84.2
5. M117[74,75]	12.0	12.0	0.0	4.0	4.0	0.0	3.8	2.8	26.3
				8.9	3.7	61.2			
Average	14.7	11.4	22.4	7.0	5.6	20.0	2.8	2.6	7.1

Bomb Dynamic Aerodynamics Summary

Configuration	C_{ℓ_p} Errors (in percent)		AP09 Imp. Over AP05 (in percent)	C_{M_q} Errors (in percent)		AP09 Imp. Over AP05 (in percent)
	AP05	AP09		AP05	AP09	
1. MK82 GPLDB[26]	35.8	9.9	72.3	109.9	24.5	77.7
2. MK82 FF[25,72]	21.3	8.3	61.0	36.6	16.2	55.7
3. MK82 ISR[25,72]	26.4	0.2	99.2	8.4	8.0	4.8
4. MK82 ISRE[25,72]	28.8	4.0	86.1	17.6	8.3	52.8
Average	28.1	5.6	80.1	43.1	14.3	66.8

FIGURE 50. COMPARISON OF AVERAGE STATIC AND DYNAMIC AERODYNAMIC PREDICTION ERRORS OF THE AP05 AND AP09 COMPARED TO EXPERIMENT FOR SEVERAL BOMB CONFIGURATIONS

3.4 NONLINEAR PITCH DAMPING

Figure 12 showed the results of Methods 2 and 3 compared to experimental data for the Army-Navy-Finner (ANF) at about Mach 2.0. Figure 12 illustrated the fact that Method 2 compared closer to one set of experimental data than Method 3 whereas Method 3 compared closer to the other set of experimental data than Method 2. Both Methods 2 and 3 will therefore be compared to the remaining sets of open literature data that the authors were able to find to see if one method can be found to be superior in general to the other method.

Figure 51 compares the Methods 2 and 3 to the ANF data[20] at M_∞ = 1.58, 2.48, 2.88 and 3.24 as a function of AOA. Also shown on the figure are the AP05 results, which are independent of AOA. Note first of all the ANF pitch damping data, while varying with AOA, is not highly nonlinear. The reason for the small nonlinearity is the fact the body pitch damping increases with AOA but the wing term decreases with AOA due to the aspect ratio and the fact C_{N_α} of the wing decreases with increasing AOA. The two pitch damping terms tend to offset giving a small increase with AOA for the center of gravity (CG) selected. In comparing the AP05 and Method 2 and 3 to experimental data, it is seen both the Methods 2 and 3 follow the general trends of the data and the AP05 also gives reasonable values compared to experiment due to the relatively small nonlinearity. Method 2 is probably slightly superior to Method 3 in general, particularly at high M_∞ and AOA.

Figure 52 compares the three theoretical approaches to experimental data[20] for the ANF at M_∞ = 2.1 and AOA near zero as a function of CG location. Here it is seen Method 3 is slightly superior to both the AP05 and Method 2 compared to experiment[30].

The next case considered is an extended length (15 cal versus 10 cal) ANF (see Figure 53). Experimental data is taken from Reference 22 at M_∞ = 1.96. By extending the length of the ANF by 5 cal, it is seen the pitch damping increases greatly with AOA due to the large body term. It is also seen that Method 2, which included all the nonlinear body loads from the AP09, is clearly superior to Method 3 and the AP05.

The third configuration considered is the MK 82 Low Drag Bomb with data taken from Reference 26. Results are shown in Figure 54 for M_∞ = 2.16, 1.56 and 0.8 to AOA 40 deg. Here Methods 2 and 3 are far superior to the AP05, due in part to the large boattail. Also Method 2 is slightly better than Method 3 at M_∞ = 2.16 and 0.8 and Method 3 is slightly better than Method 2 at M_∞ = 1.56.

The fourth and final configuration where open literature data was found is the M823 Research Store with data given in References 27 and 76. Data for M_∞ = 0.7 and 0.75 is shown in Figure 54 at AOA up to 20 deg whereas Figure 55 has data at AOA about 3 deg for Mach numbers 0.6 to 1.1. In Figure 55, Method 2 is clearly superior to Method 3 and the AP05. Note the large nonlinearity in pitch damping. The large nonlinearity comes primarily from the tail term where C_{N_α} increases with AOA. Figure 56 clearly shows both Methods 2 and 3 are superior to the AP05 and fairly close to experimental data at all Mach numbers. Figure 56 also illustrates the fact the Method 2 is roll dependent whereas Method 3 is roll independent. The roll

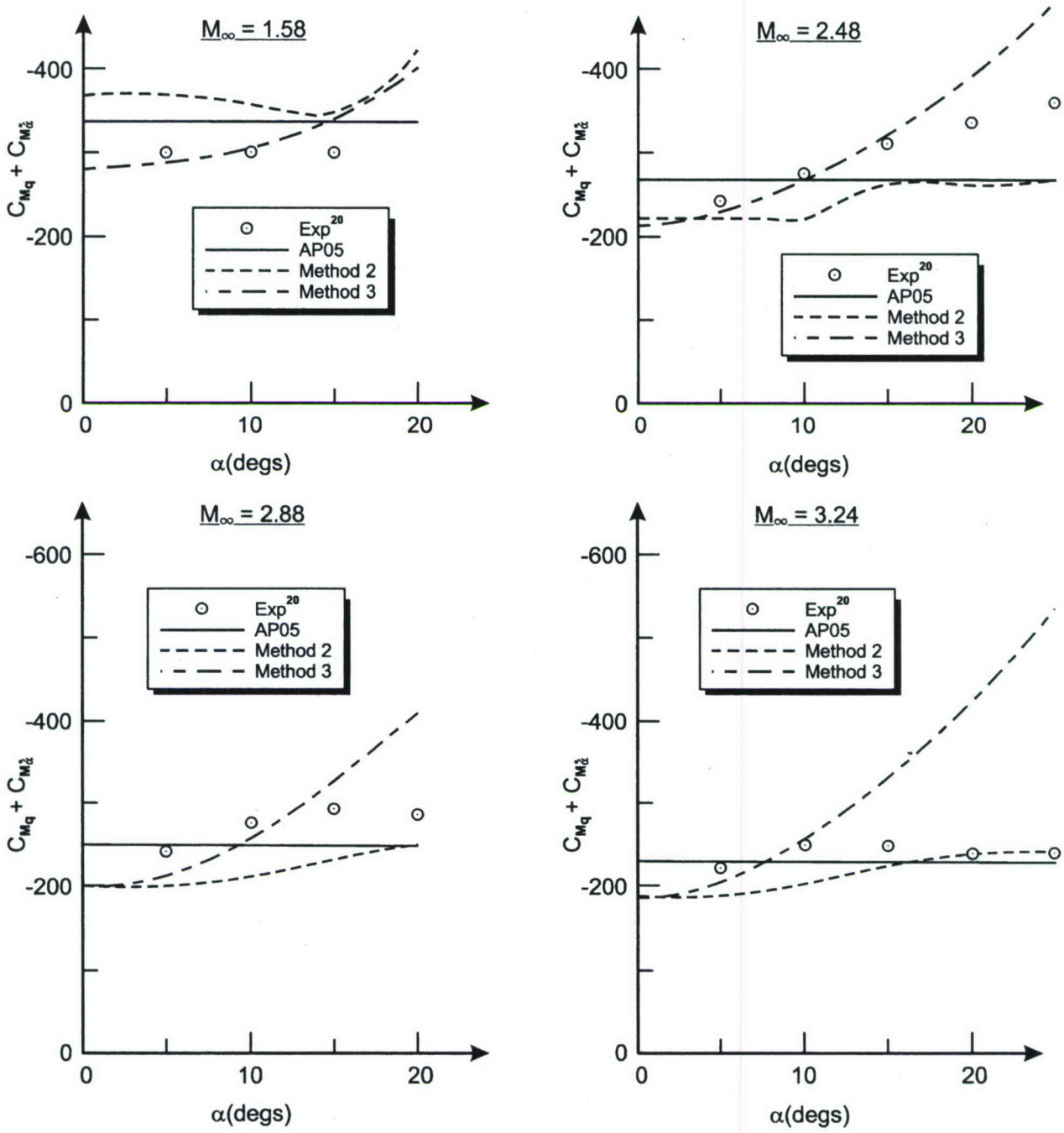

FIGURE 51. COMPARISON OF THEORY AND EXPERIMENT FOR PITCH DAMPING ON ANF

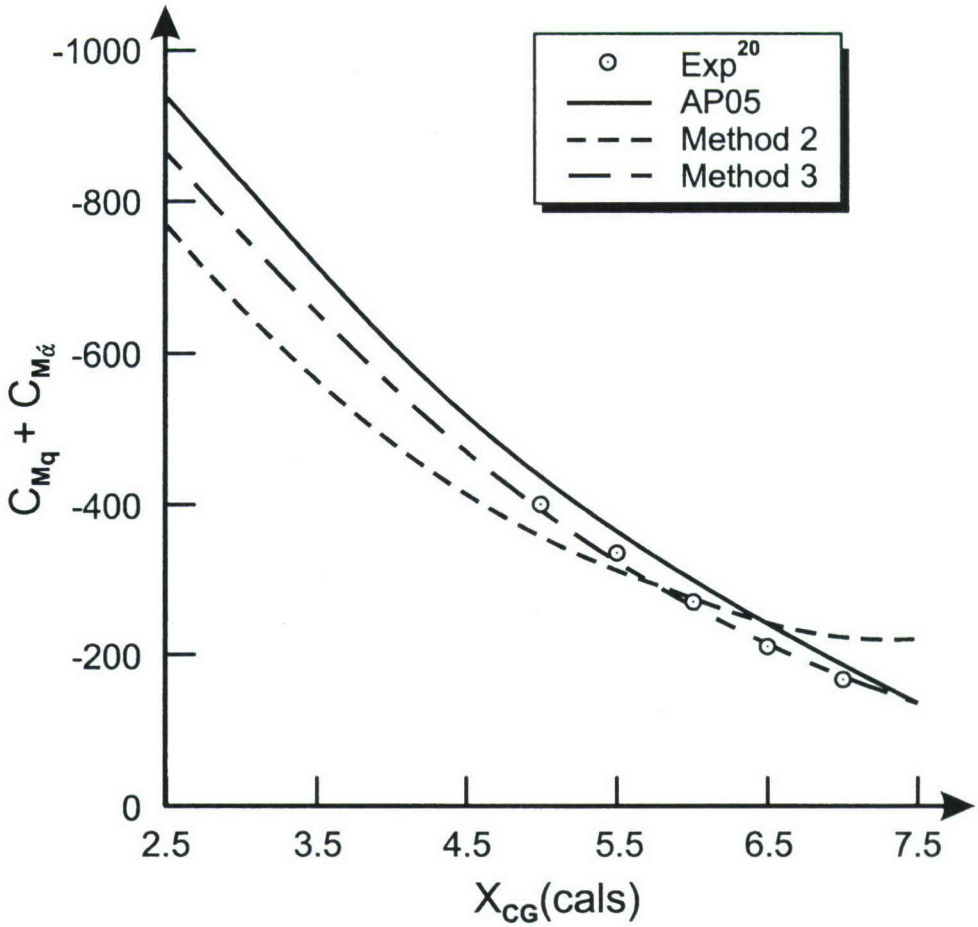

FIGURE 52. COMPARISON OF THEORY AND EXPERIMENT FOR PITCH DAMPING ON ANF WITH VARIOUS CENTER OF GRAVITY LOCATIONS (M_∞=2.1, $\alpha \approx 0^\circ$)

dependence of Method 2 comes from the difference in body-wing carryover normal force at Φ = 0 versus Φ = 45 deg roll.

The next two figures illustrate the effect of eliminating the dual accounting of the portion of body beneath the wings for pitch damping calculations using Method 3. Also included in the next two figures is the change in transonic methodology discussed in Section 2.5 where the aerodynamics are linearly interpolated between the value at the force break Mach number and the value computed at Mach 1.2. Figure 57 presents the pitch damping results of the AP05, and Methods 2 and 3 of the AP09 for the ANF. The Method 2 and 3 compare well to the NOL[20] and BRL[29] data at M_∞ = 1.5. For M_∞ < 1.5, Method 3 appears to compare better to most data, although there is one Ballistic Range data point that supports Method 2 at M_∞ = 1.0. In general, there is not enough data or consistency of data to say whether Method 2 or 3 is best. It is clear that the large discontinuity in the AP05 transonic prediction is not predicted by the new AP09 Methods 2 or 3.

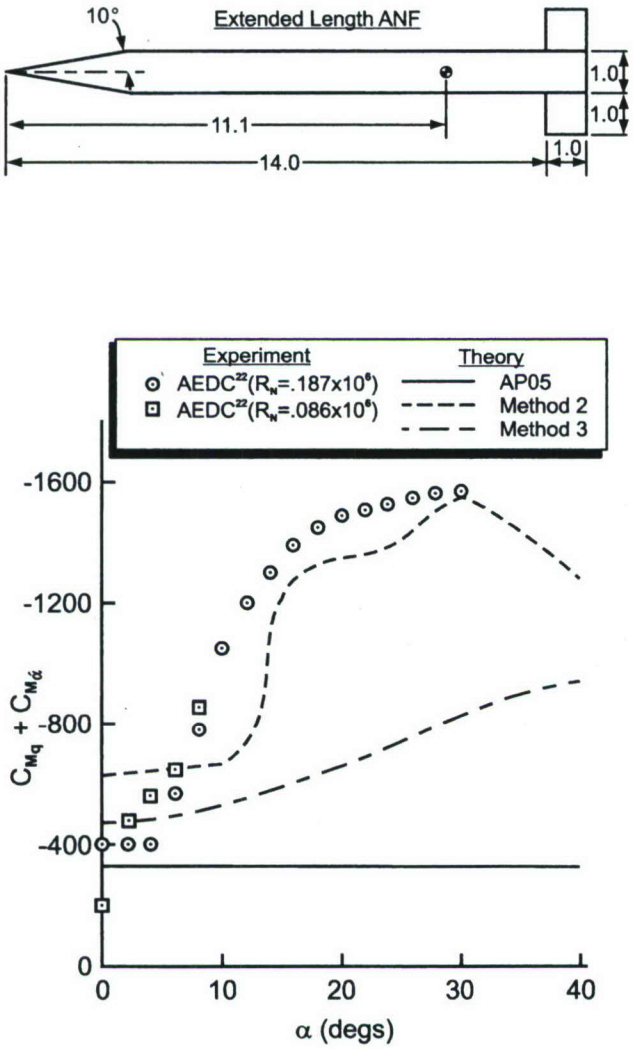

FIGURE 53. COMPARISON OF THEORY AND EXPERIMENT FOR PITCH DAMPING FOR EXTENDED LENGTH ANF (M=1.96)

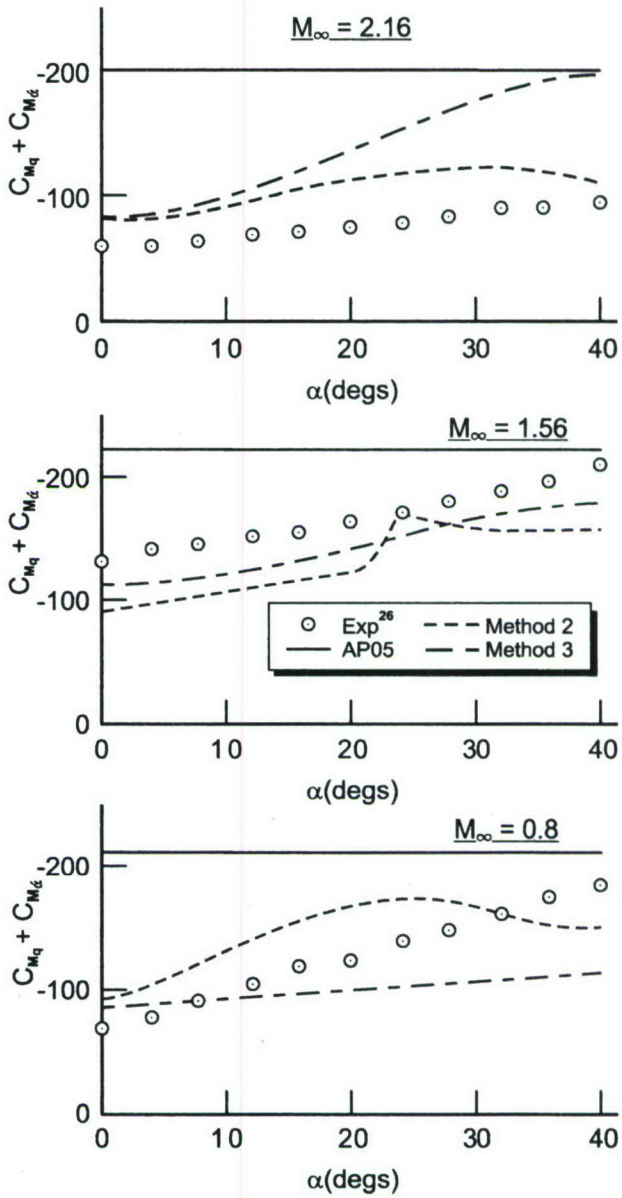

FIGURE 54. COMPARISON OF THEORY AND EXPERIMENT FOR PITCH DAMPING FOR MK82 LOW DRAG BOMB

The last case considered is the Navy Research model of Figure 58. Again, AP05 and AP09, Method 2 and 3 are compared to experiment. As seen in the figure, Methods 2 and 3 match experiment at Mach 1.5 and higher. In the transonic region, Method 2 and 3 bracket the data. At subsonic speeds, the AP05 is slightly closer to data.

In viewing the results of Figure 12 and 51-58 where two new methods to predict nonlinear pitch damping moments were compared to experimental data the following conclusions were drawn. It was found that while Method 2 was more robust and slightly

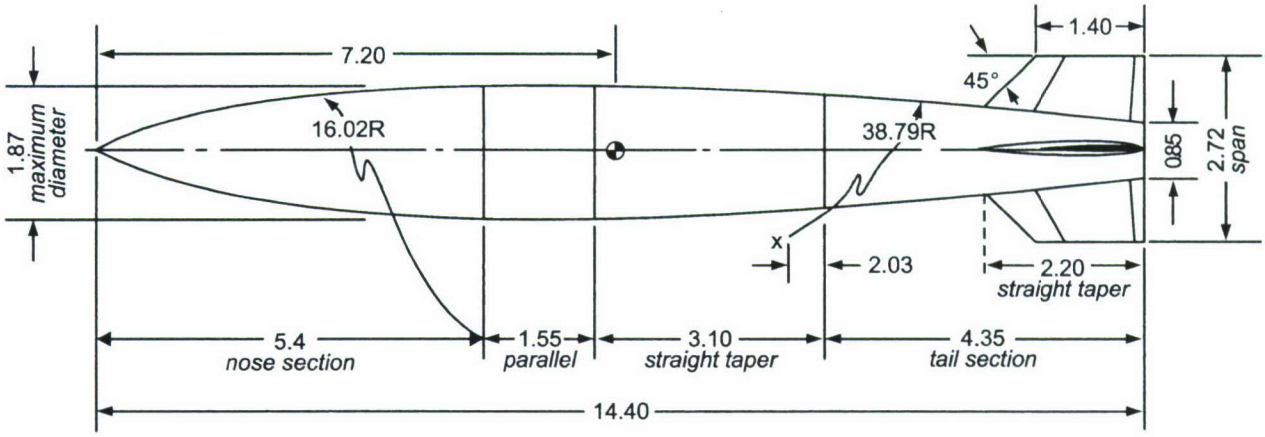

All Dimensions Are In Inches

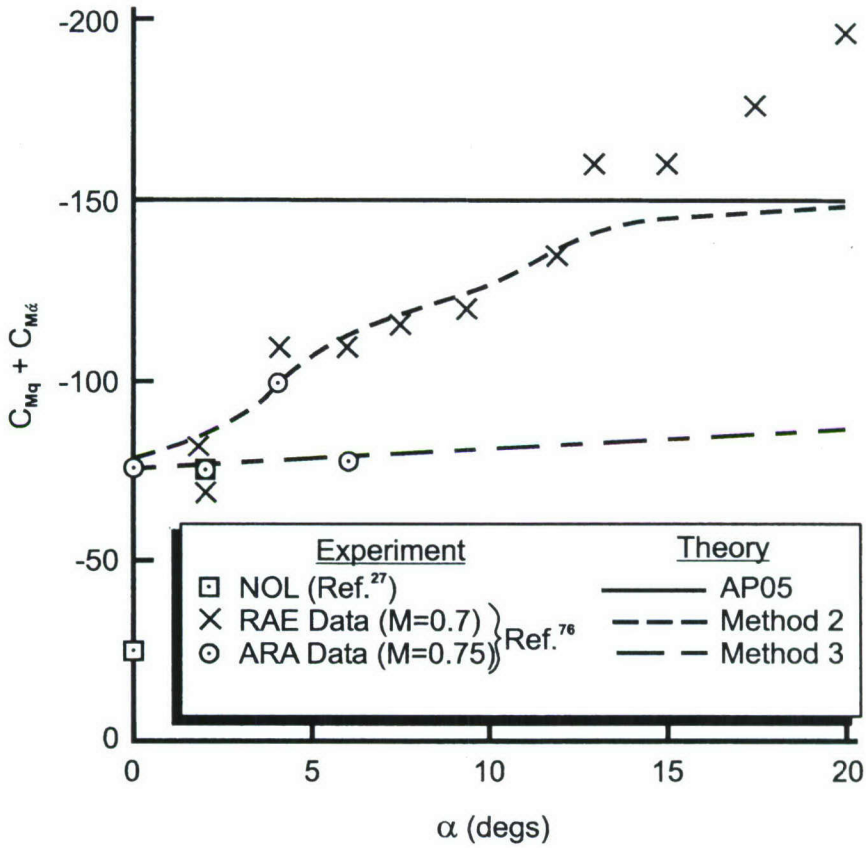

FIGURE 55. M823 RESEARCH STORE COMPARISONS OF THEORY AND EXPERIMENT FOR PITCH DAMPING

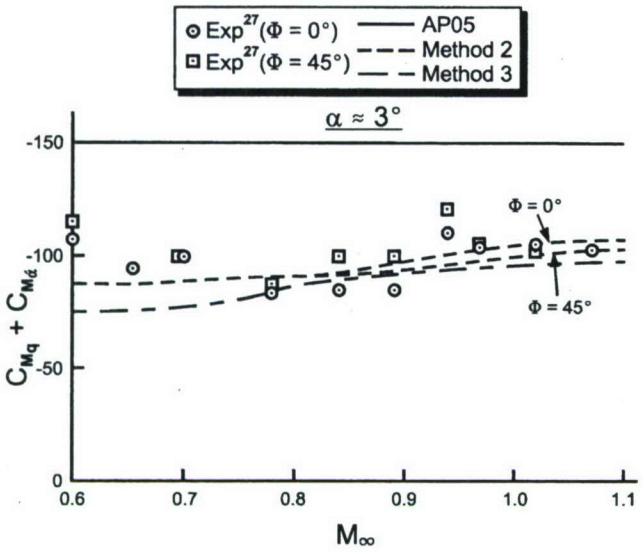

FIGURE 56. M823 RESEARCH STORE COMPARISONF OF THEORY AND EXPERIMENT FOR PITCH DAMPING (α=3°)

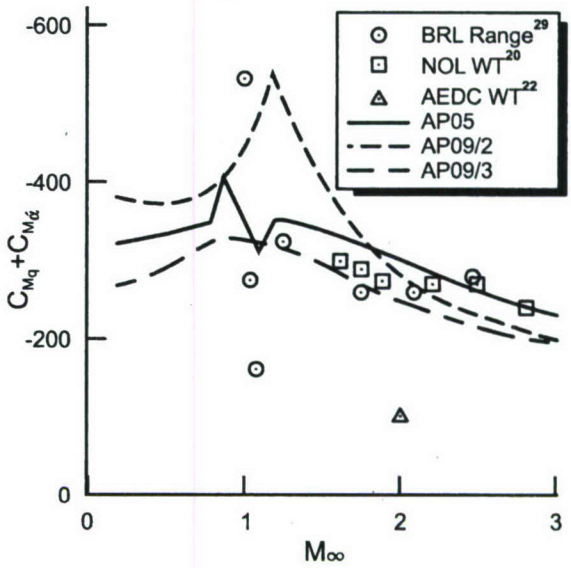

FIGURE 57. COMPARISON OF THEORY AND EXPERIMENT FOR PITCH DAMPING OF THE ANF (α≈0)

superior to Method 3 when compared to experimental data in most cases, Method 3 was superior to Method 2 in some cases. Therefore, both Methods 2 and 3 will be available in the output of the next version of the APC, the AP09.

One of the main issues encountered in assessing the two new methods was the small amount of true pitch damping data and the concerns about wind tunnel interference effects for the data that was available. A good "truth" set of pitch damping data is clearly needed that has a minimum of wind tunnel interference issues associated with it. This truth model should be backed up with Navier Stokes computations so as to minimize any wind tunnel interference issues.

3.5 NONLINEAR ROLL DAMPING

Several data sets are available to compare the new semiempirical roll damping model of Figure 21 to for accuracy and robustness. The first case considered is the ANF configuration. Comparison of the new theory to available experimental data[22,43,47] is shown in Figure 59 for M_∞ = 4.1, 2.54, and 0.22. Two sets of data are available for the M_∞ = 0.22 and 2.54 cases. One set of data is from AEDC[22,47] and the other data set from the former NOL[43] (now part of AEDC). At M_∞ = 4.1, the new theory does an excellent job of following the data up to AOA 20 deg. At M_∞ = 2.54, the AP09 does a good job in following the trends of the data and is much more accurate than the AP05. At M_∞ = 0.22, the AP09 has the correct trend at both low and high AOA but overpredicts the loss of damping as AOA increases. Referring back to Figure 21 and using the M_∞ = 2.54 case as an example, Equation (39) is used up to AOA of about 5 deg, Equation (37) is

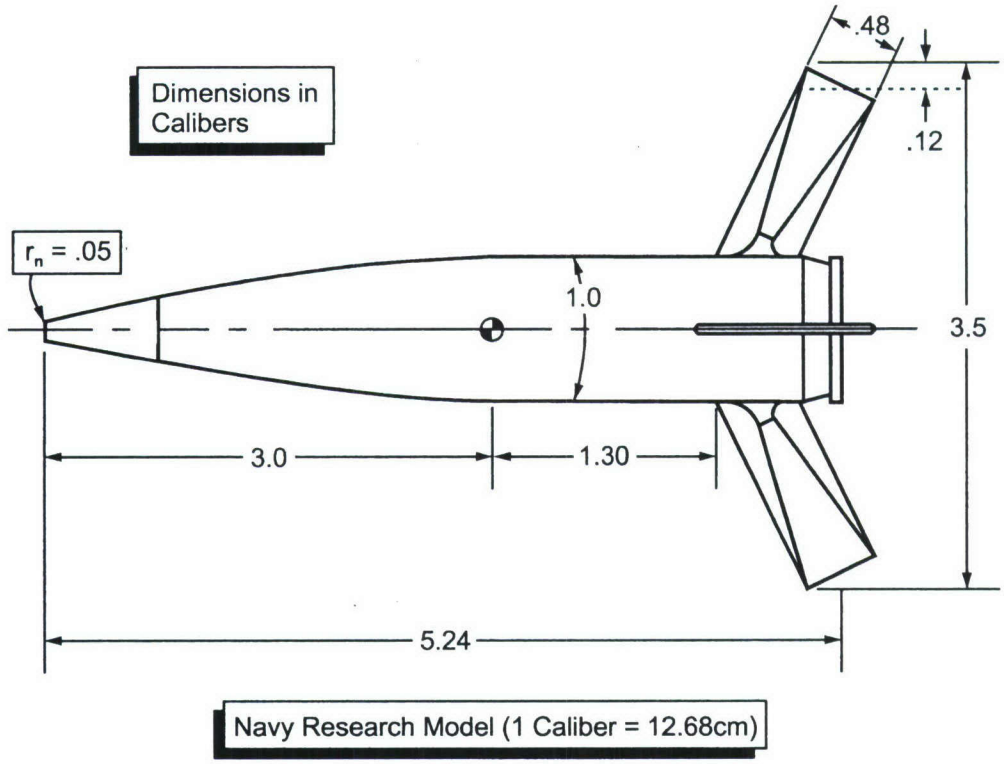

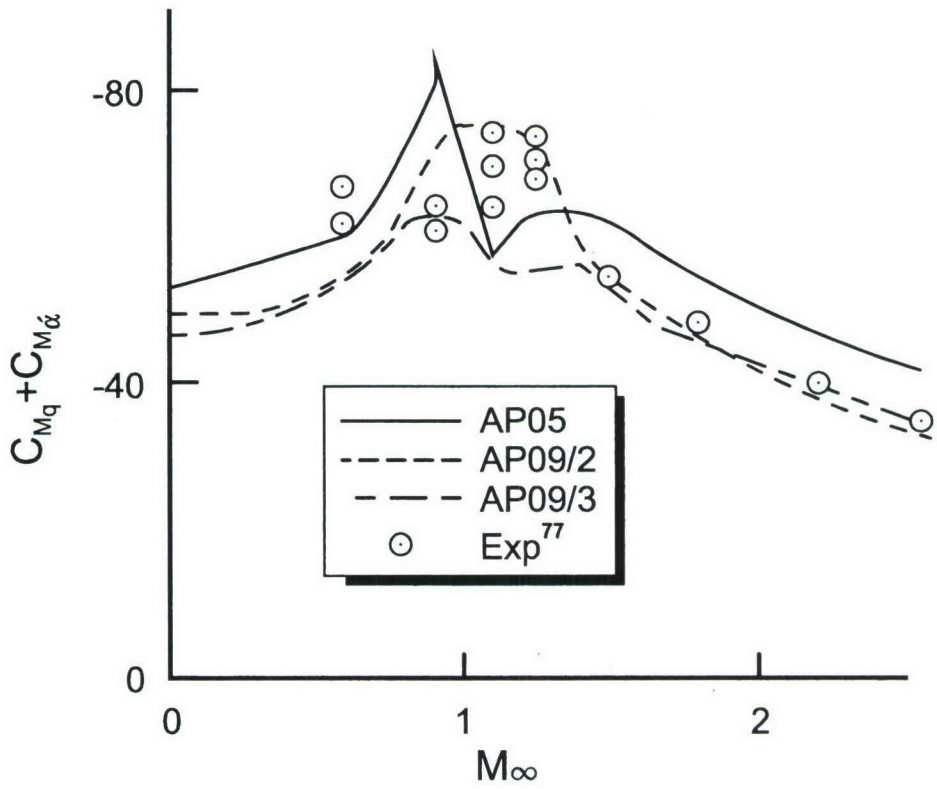

FIGURE 58. COMPARISON OF THEORY AND EXPERIMENT FOR PITCH DAMPING OF NAVY RESEARCH MODEL

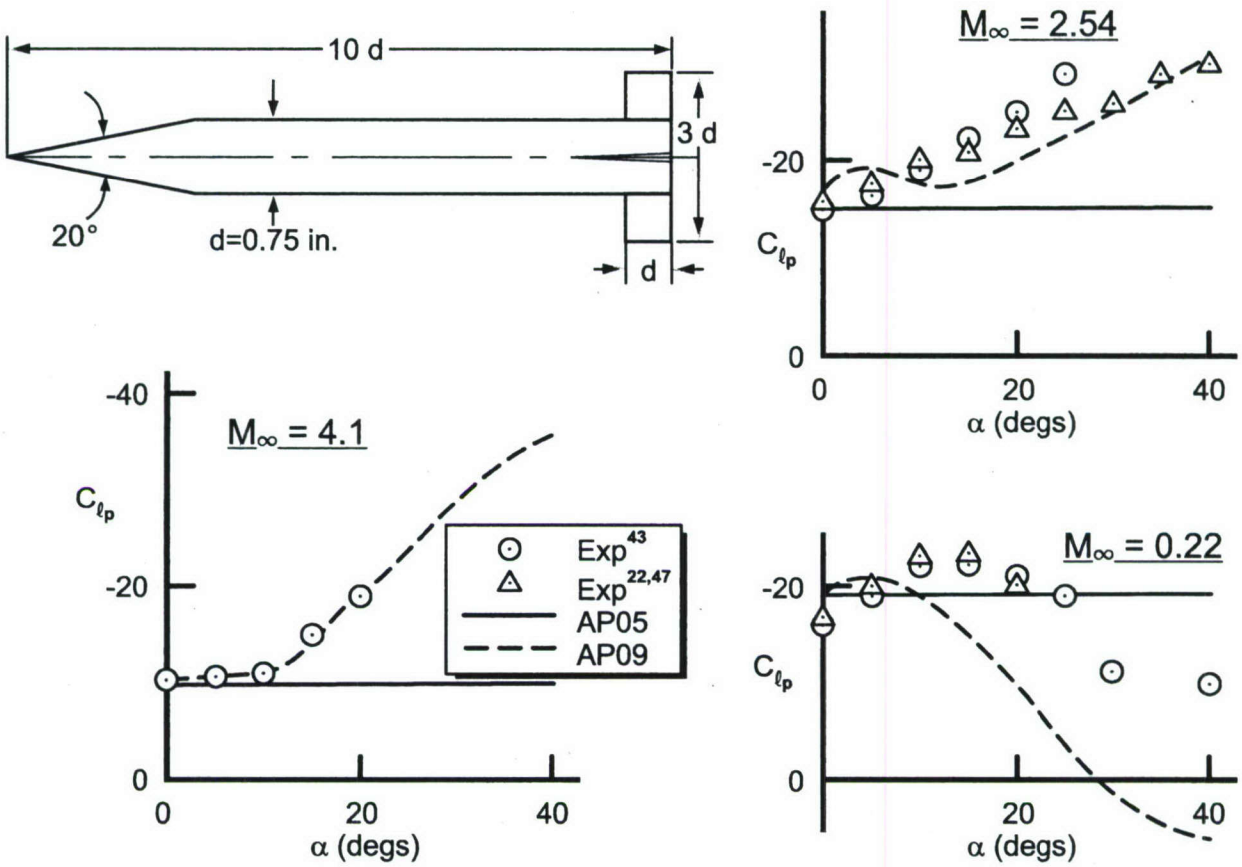

FIGURE 59. COMPARISON OF THEORY AND EXPERIMENT FOR ROLL DAMPING OF ANF

used for AOA above 14 deg and both Equations (37) and (39) are blended together for AOA in between 5 deg and 14 deg.

The second case considered is the modified finner where a more extensive data base[22,47] exists. The configuration and results of comparison of the AP05 and AP09 theories to experiment are shown in Figure 60. Results are shown for M_∞ = 0.6, 0.9, 1.3, 1.5, 2.0, 2.25 and 2.5 up to AOA 40 deg. In all cases, the AP09 gives the correct initial trend of the data and at M_∞ = 1.5, 2.0, 2.25 and 2.5 compares very well to the data. At M_∞ = 0.6 the new theory compares well to experiment up to AOA 15 deg but does not predict the sharp drop off in roll damping at α = 20 deg. At M_∞ = 0.9, the AP09 overpredicts the maximum value of C_{ℓ_p} at AOA 10 to 15 deg but predicts the C_{ℓ_p} values at high AOA quite well. At M_∞ = 1.3, predictions are excellent up to α = 20 deg where a sharp increase in C_{ℓ_p} data is noted at α = 25 deg and higher. It is not clear what causes this sharp increase in C_{ℓ_p}, but wind tunnel wall interference of the shock onto the tail is a possibility. In general, the AP09 nonlinear method is clearly superior to the linear AP05 roll damping methodology for the Figure 60 configuration.

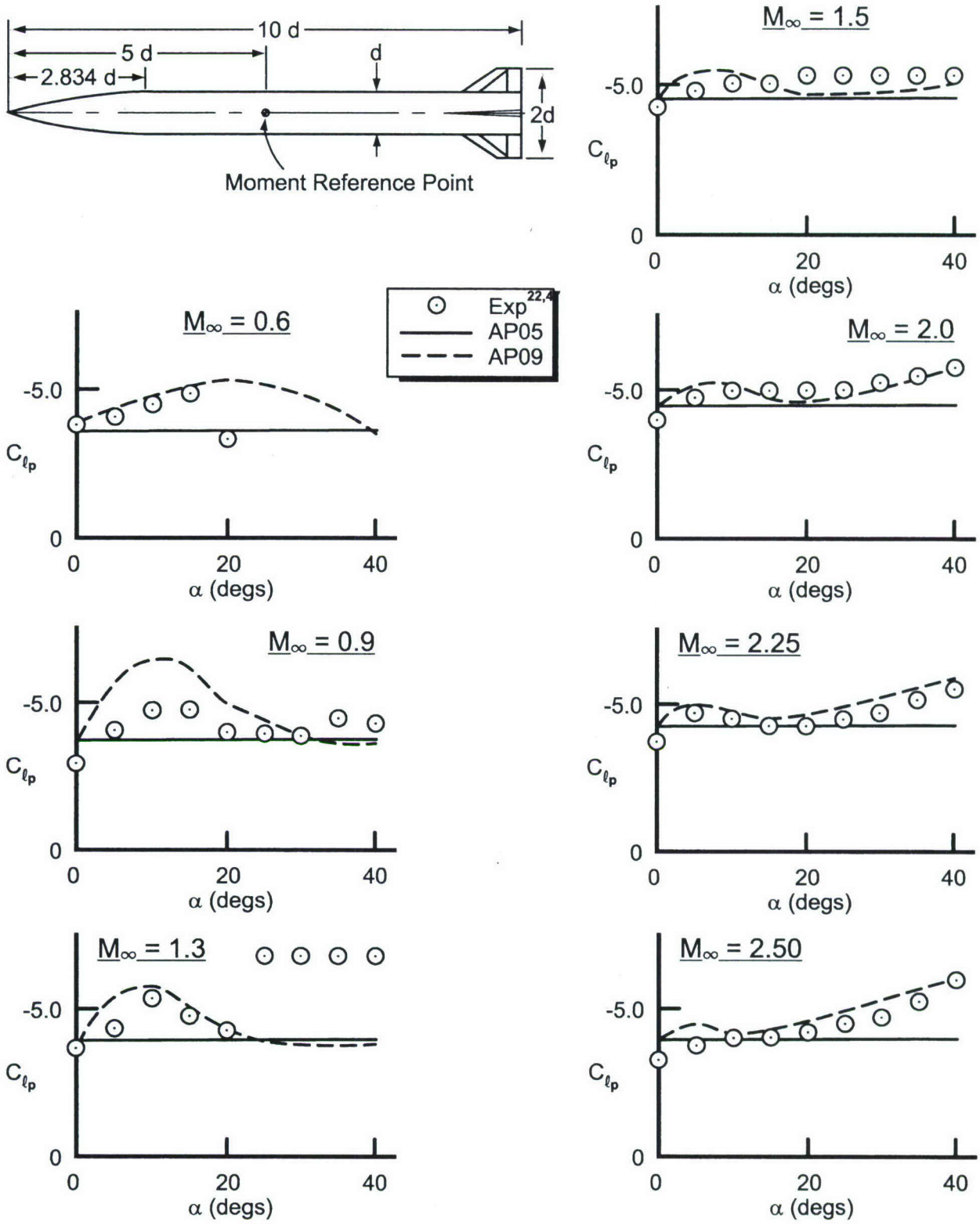

FIGURE 60. COMPARISON OF THEORY AND EXPERIMENT FOR ROLL DAMPING OF MODIFIED ARMY-NAVY-FINNER

The next three cases are for the MK 82 Low Drag Bomb and two candidate replacements for MK 82 bomb referred to as the FF and an Inflatable Stabilizer Retarder Extended (ISRE). Figure 61 compares the AP05 and AP09 predictions to roll damping experimental data[26], at M_∞ = 0.8 for AOA up to 30 deg. In general, the AP09 follows the data trends and compares quite well to the data except at α = 25 deg and higher where the theory gives too low a value of roll damping. Again, the AP09 nonlinear theory is clearly superior to the linear AP05 methodology.

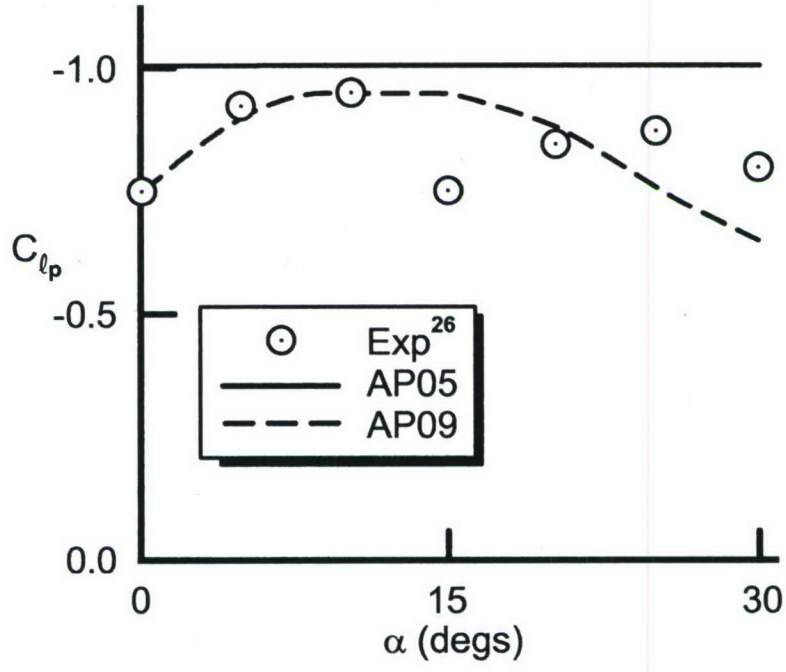

FIGURE 61. COMPARISONOF THEORY AND EXPERIMENT FOR ROLL DAMPING OF MK82 LOW DRAG BOMB (M_∞=0.8)

Figure 62 shows the comparison of the AP05 and AP09 roll damping predictions to experiment for the MK 82 candidate FF configuration at M_∞ = 0.8, 1.0 and 1.2 up to AOA 25 deg. The FF configuration has 4 fins and an enlarged view of the FF along with the AP09 representation is shown in Figure 40. In examining Figure 62, it is seen the AP09 again does a good job in following the trends of the experimental data. The AP09 predictions are slightly high for AOA greater than 10 deg but are clearly superior to the AP05 predictions except at α = 0 deg.

Figure 63 gives results for the ISRE roll damping predictions compared to experiment. The ISRE is an 8 fin configuration with a flare and the fins are located on the flare. Figure 43 gives a large view of the ISRE configuration along with the AP09 representation. C_{ℓ_p} predictions of the AP09 and AP05 are again compared to experiment at M_∞ = 0.8, 1.0,and 1.2 at AOA up to 25 deg. Here the AP09 shows significant improvement over the AP05 in roll damping predictions, even at 0 deg AOA. The reason for the AP09 improvement in roll damping prediction over the AP05 at 0 deg AOA is the fact the AP09 accounts for the flare in the Figure 21 methodology whereas the AP05 does not.

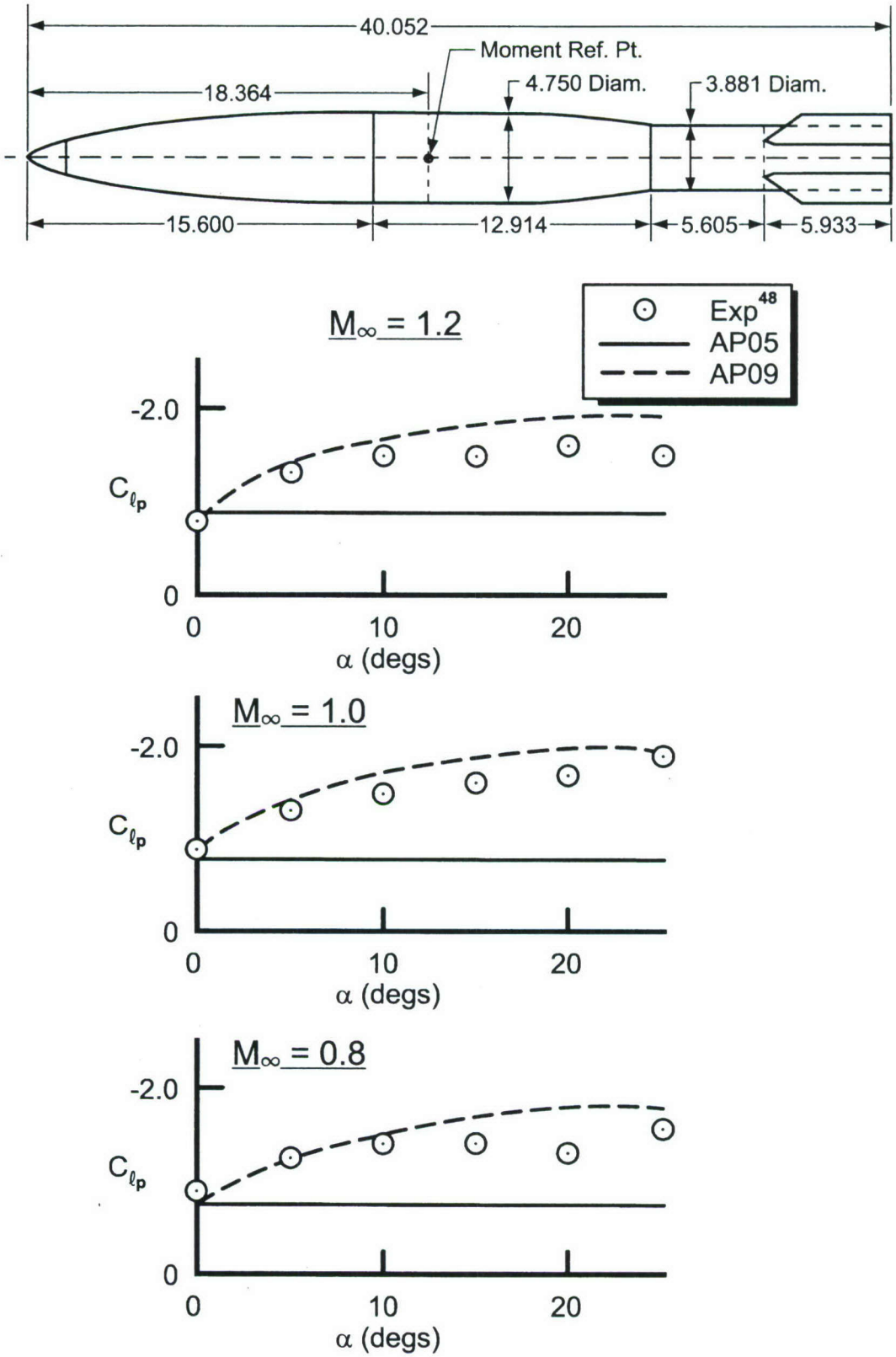

FIGURE 62. COMPARISON OF THEORY AND EXPERIMENT FOR ROLL DAMPING OF FF CANDIDATE FOR MK82 STORE

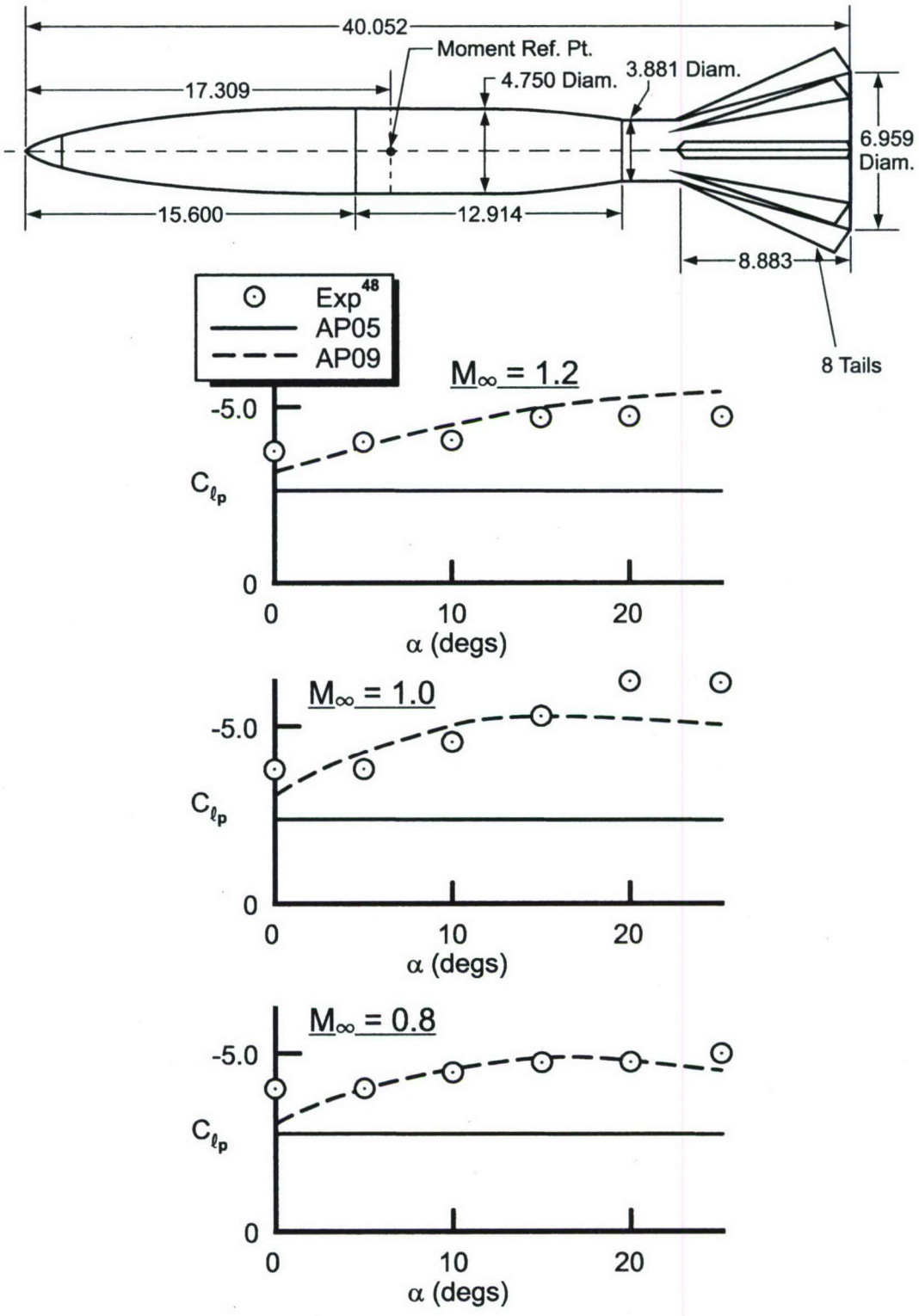

FIGURE 63. COMPARISON OF THEORY AND EXPERIMENT FOR ROLL DAMPING OF ISRE CANDIDATE FOR MK82 STORE

The next case considered is the 81 MM mortar configuration shown in Figure 64. Comparison of theory and experiment up to 10 deg AOA at $M_\infty = 0.5$ and 0.8 is shown in the figure. The data suggests a slight nonlinearity in C_{ℓ_p} with increasing AOA, but not as large as predicted by the AP09. Even so, the AP09 roll damping predictions are still superior to those of the AP05.

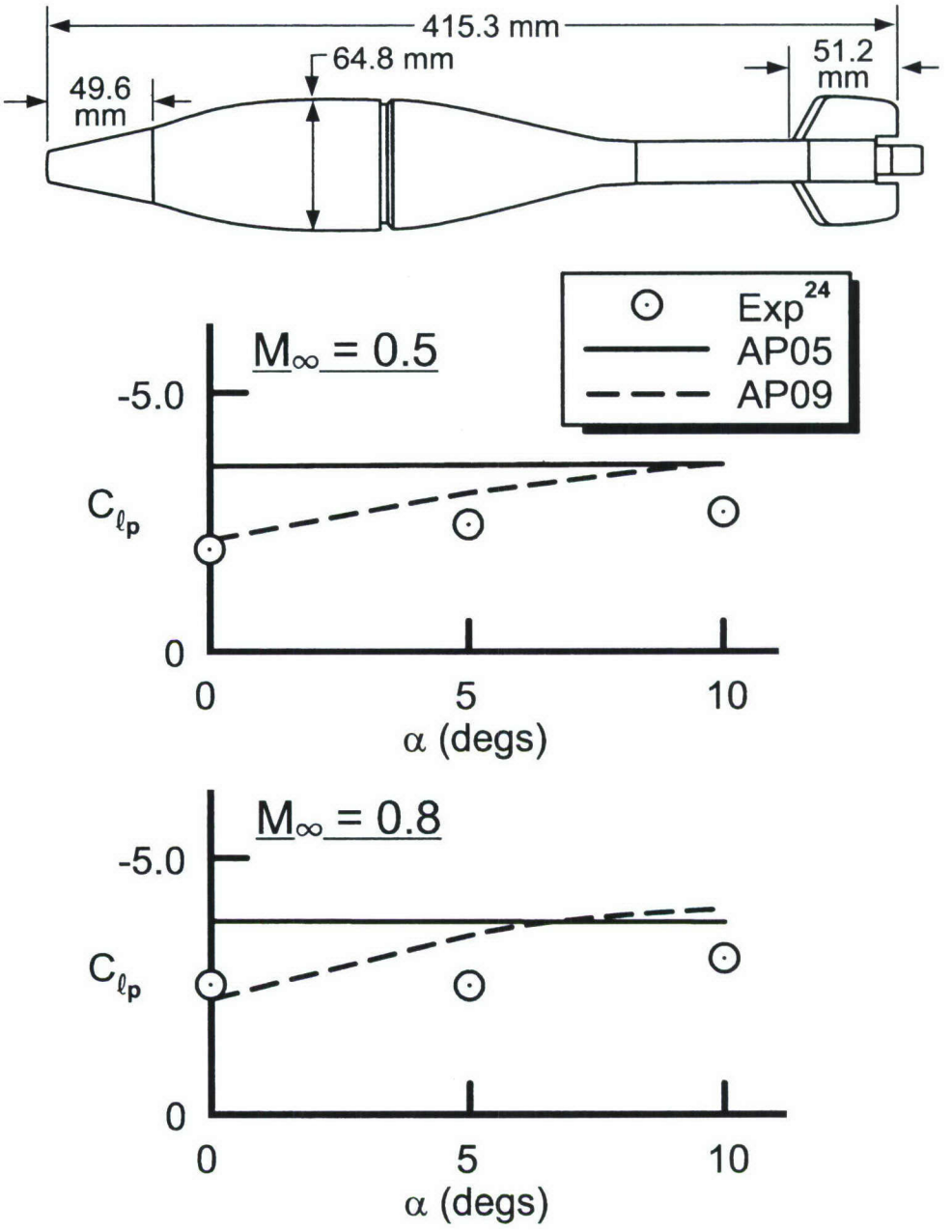

FIGURE 64. COMPARISON OF THEORYAND EXPERIMENT FOR ROLL DAMPING OF 81MM MORTAR

The next two cases illustrate the capability of the AP09 to predict roll damping of configurations that have two sets of lifting surfaces. The first case is a canard controlled missile configuration shown in Figure 65. Wind tunnel tests[49,50] were conducted in a component buildup fashion which allows comparison of the AP05 and AP09 to body-canard, body-tail and canard-body-tail configurations. Results are shown in Figure 65 at $M_\infty = 0.1$ for AOA to 30 deg. In general, the comparison of the AP09 predictions to experiment is quite encouraging for all three configurations and also is superior to the AP05. Note the different trend of the body-tail data and body-canard data. The body tail has a slight uptrend with α due to a moderate aspect ratio (1.33) whereas the body canard has a decreasing trend with α due to a large aspect ratio (3.53). The higher aspect ratio wings stall and therefore lose lift curve slope, causing the decrease in roll damping capability. It is noteworthy that the roll damping of the canard-body-tail is much lower than the addition of the canard-body and body-tail cases added together. This lower value of C_{ℓ_p} for the complete configuration is due to the loss of roll damping effectiveness of the tails from the canard shed vortices. Note the canard shed vortex effects are reduced considerably at α = 25 deg since the canard shed vortices have mostly passed over the tails. On the other hand, at α = 30 deg, another complexity apparently has affected the roll damping, the asymmetric shedding of vortices. Note the large difference in roll damping moment on the canard-body-tail case at α = 30 deg between two different wind tunnel tests of the same model. Also note the sudden increase in C_{ℓ_p} for the body-tail case at α = 30 deg. The implication of this figure is that for subsonic speeds, the new nonlinear methodology of the AP09 is questionable above AOA 25 deg where asymmetric vortex shedding plays a role in the nonlinear aerodynamics.

The second canard-body-tail case is shown in Figure 66. The Figure 66 configuration has large wings and is quite similar in shape to a seasparrow missile. According to the AP09 C_{ℓ_p} predictions, the tail surface loses all roll damping effectiveness at AOA 0. This also agrees with the flight tests results[59] and clearly shows the AP09 predictions to be superior to the AP05.

In reviewing the results of the AP09 and AP05 when compared to the various configurations illustrated in Figures 59-66, it is clear the Figure 21 methodology for nonlinear roll damping captures correctly the physics involved in the increases or decreases in roll damping as AOA increases. It is also clear that the AP09 is clearly superior to the AP05, which has no nonlinear roll damping prediction capability. The AP09 also appears to be fairly robust in the roll damping predictions in that configurations with boattails, flares, 4 to 8 fins, one and two sets of lifting surfaces, Mach numbers 0.1 to 4.1 and AOA to 40 deg were considered with reasonable accuracy. The AP09 methodology of Figure 21 can also be refined as more data becomes available.

3.6 TANGENT SLOPE FOR C_{N_α} AND C_{M_α}

To illustrate the difference between the tangent and secant slope for C_{N_α} and C_{M_α}, the 10 cal and 15 cal Army-Navy-Finner configurations shown in Figures 12 and 52 respectively will be considered. Figure 67 shows the AP05 and AP09 results for C_{N_α}, C_{M_α} and X_{CP}/d. Also

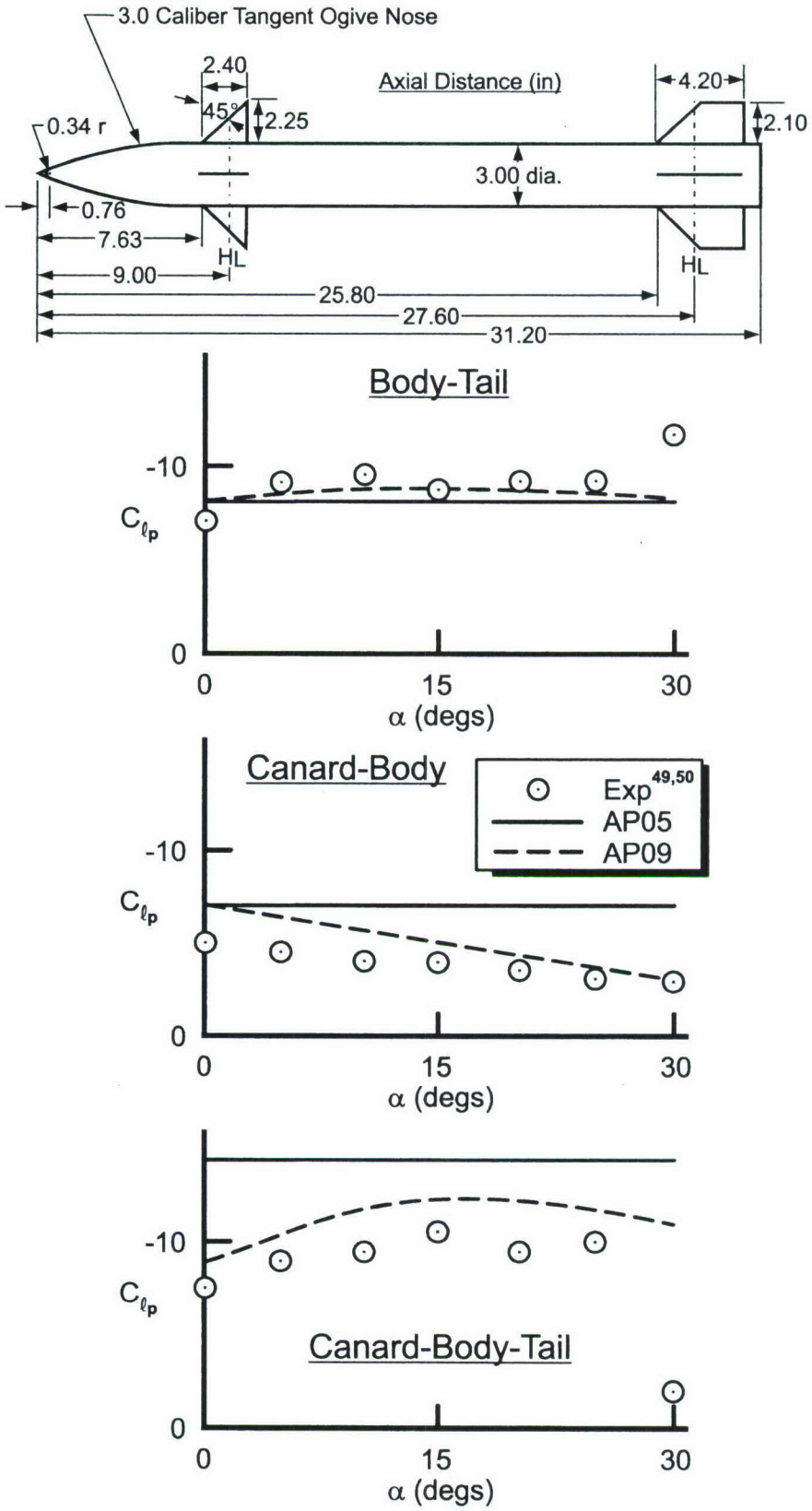

FIGURE 65. COMPARISONOF THEORYAND EXPERIMENT FOR ROLL DAMPING FOR CANARD CONTROL MISSILE CONFIGURATION (M_∞=0.1)

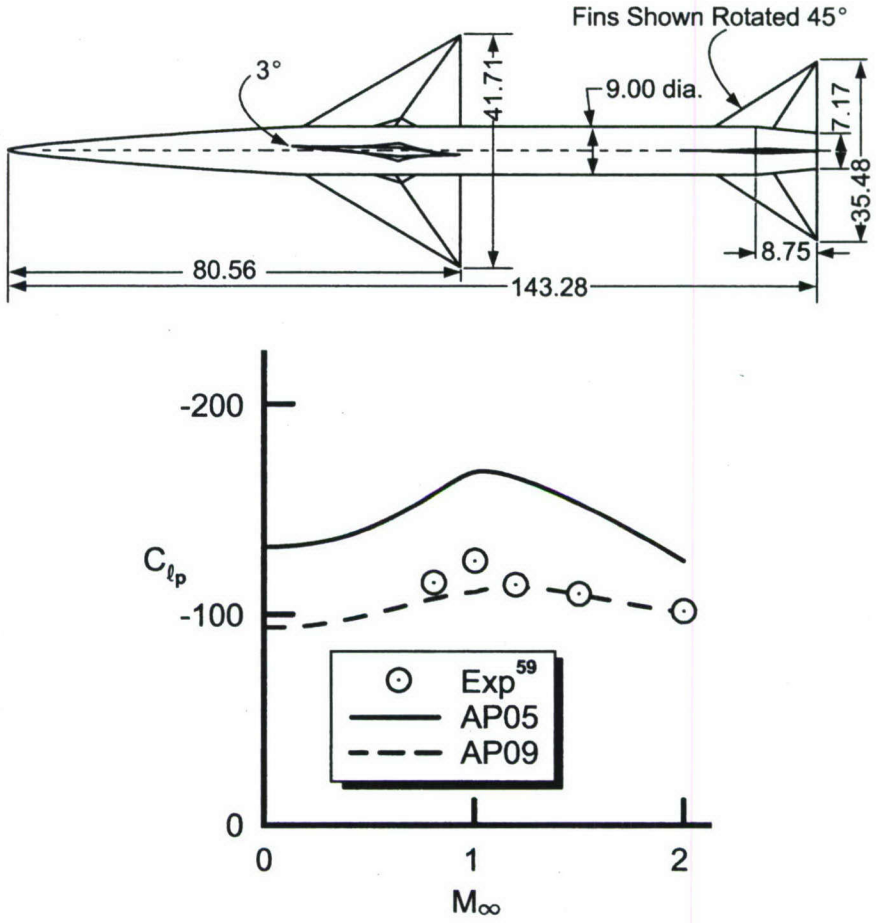

FIGURE 66. COMPARISON OF THEORYAND FLIGHT TESTS FOR ROLL DAMPING OF WING-BODY-TAIL CASE AT $\alpha \approx 0$

shown are the nonlinear experimental results from Reference 21 for C_{M_α}. No experimental results for C_{N_α} or X_{CP}/d were given. Note that for both the standard and extended versions of the ANF, there is a significant difference between the secant (AP05) and tangent slopes (AP09) for C_{N_α}. For α up to about 10 deg, the values of the secant slopes and tangent slopes are about the same. The AP09 then departs from the AP05 C_{N_α} due to the sharp increase in the C_N versus α curve around α of 10 deg. At a α of about 30 deg, the AP09 then starts to approach zero for C_{N_α} whereas the AP05 stays at a high level.

Similar behavior of secant and tangent slopes for C_{M_α} as for C_{N_α} is also seen in Figure 67. The 15 cal ANF in particular shows a large deviation for the AP05 and AP09 values of C_{M_α} with the AP09 values being closer to the experimental data. Note that the center of pressure values of the AP09 are generally less stable than the AP05 for both the 10 and 15 cal ANF when using the tangent versus secant slope.

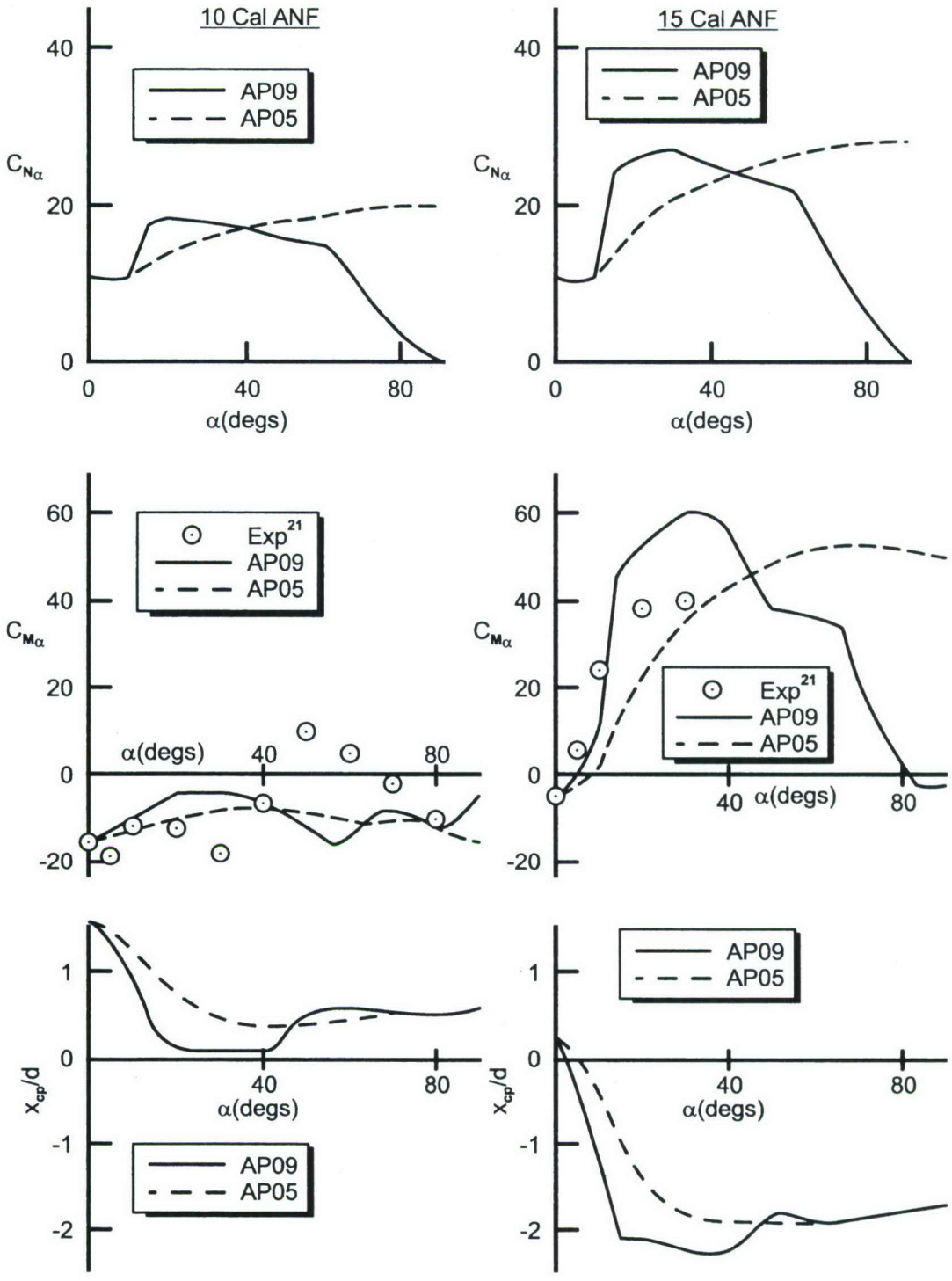

FIGURE 67. COMPARISON OF AP05, AP09, AND EXPERIMENT FOR $C_{N\alpha}$, $C_{M\alpha}$, X_{CP}/D FOR 10, 15 CAL ANF AT M=1.95(Φ=45°)

It should be pointed out that the AP05 and all previous versions of the APC used the secant slope for C_{M_α}, C_{N_α} and the force and moment for X_{CP}/d. All comparisons of theory and experiment were generally "apples to apples" comparisons where C_N, C_M and C_M/C_N were compared theory to experiment. The AP09 will use $C_{M_\alpha}/C_{N_\alpha}$ for center of pressure. As a result, one must be careful when comparing to previous results from wind tunnel tests, unless the results are for true tangent slopes of C_{M_α} and C_{N_α}. In other words, one could compare the AP09 center of pressure to the AP05 values and experiment and conclude the AP05 is more accurate. However, this conclusion may be based on an "oranges to apples" comparison. That is, X_{CP}/d from experiment is given based on $-C_M/C_N$ versus the true value of $-C_{M_\alpha}/C_{N_\alpha}$. To aid the user of the AP09, both true value of center of pressure and the value formerly computed by the AP05 ($-C_M/C_N$) will be printed out in the AP09 aerodynamics.

4.0 SUMMARY

To summarize, significant new improvements and technology has been added to the next version of the Aeroprediction Code (APC), the AP09. The major effect of the improvements is to improve the APC aerodynamic predictions for normal force, center of pressure, roll and pitch damping for configurations that have boattails. Configurations include mortars, low drag bombs, spin stabilized projectiles and missiles in that order. In addition, new methods to predict nonlinear roll and pitch damping were developed and integrated into the Aeroprediction Code.

Comparison of the new methods to experimental data showed significant improvement of the AP09 over the AP05 in roll and pitch damping, center of pressure and normal force prediction accuracy for configurations with boattails. Adding new nonlinear pitch and roll damping capability also significantly improved the AP09 prediction accuracy compared to experimental data for all weapon configurations.

The validation of the new nonlinear methodology for pitch and roll damping was hindered by the lack of generic data bases that varied fin size, shape, location, and freestream conditions. For pitch damping wind tunnel data, an additional concern of model to sting interference also existed. A truth model for roll and pitch damping consisting of nonlinear experimental results backed up by full Navier Stokes calculations would greatly enhance refinement of the new nonlinear dynamic derivative semiempirical models.

5.0 REFERENCES

1. Moore, F. G.; Hymer, T. G.; Downs, C.; and Moore, L., *The 2005 Version of the Aeroprediction Code: Part II – Users Guide*, API Report No. 2, Apr 2004.

2. Moore, F. G., "Approximate Methods for Weapon Aerodynamics," AIAA Progress in Astronautics and Aeronautics, Vol. 186, Aug 2000.

3. Moore, F. G., *Body Alone Aerodynamics of Guided and Unguided Projectiles at Subsonic, Transonic, and Supersonic Mach Numbers*, NWL TR-3796, Nov 1972.

4. Van Dyke, M. D.; "First and Second-Order Theory of Supersonic Flow Past Bodies of Revolution," Journal of Aeronautical Sciences, Vol. 18, No. 3, pp. 161-179, Mar 1951.

5. Whyte, R. H., *Effects of Boattail Angle on Aerodynamic Characteristics of 175mm M437 Projectile at Supersonic Mach Numbers*, U. S. Army Munitions Command TM 1646, Sep 1965.

6. Moore, F. G. and Hymer, T. G., "Semiempirical Prediction of Pitch Damping Moments for Configurations with Flares," JAS, Vol. 38, No. 2, pp. 150-158, Mar-Apr 2001.

7. Moore, F. G. and Hymer, T. G., *The 2002 Version of the Aeroprediction Code: Part I – Summary of New Theoretical Methodology*, NSWCDD/TR-01/108, Mar 2002.

8. Moore, F. G.; McInville, R. M.; and Robinson, D. L., "A Semiempirical Method for Predicting Multi-Fin Aerodynamics," AIAA 2000-0766, 38th Aerospace Science Meeting, Jan 2000.

9. Moore, F. G. and Hymer, T. G., "Improved Methodology for Axial Force at Angle of Attack." AIAA Paper 98-0579, Jan 1998 (also JSR, Vol. 35, No. 2, pp. 132-139, Mar-Apr 1998).

10. Rogers, R. M. and Butler, C. B., *Aerodynamic Characteristics of Several Bluff Body Configurations at Subsonic and Transonic Mach Numbers*, AFATL TR-72-25, Feb 1972 (Eglin Air Force Base, FL).

11. Wu, J. M. and Aoyoma, M., *Transonic Flow-Field Calculation Around Ogive Cylinders by Nonlinear-Linear Stretching Method*, U.S. Army Missile Command, TR No. RD-70-12, Apr 1970.

REFERENCES (Continued)

12. Spring, D. J.; *The Effect of Nose Shape and Afterbody Length on the Normal Force and Neutral Point Location of Axisymmetric Bodies at Mach Numbers from 0.8 to 4.50*, US Army Missile Command Report No. RF-TR-64-13, 1964.

13. Gwin, H. and Spring, D. J., *Stability Characteristics of a Family of Tangent Ogive-Cylinder Bodies at Mach Numbers 0.2 to 1.5*, US Army Missile Command Report No. RG-TR-61-1, 1961.

14. Washington, W. D. and Pettis, W. Jr., *Boattail Effects on Static Stability at Small Angles of Attack*, US Army Missile Command Report No. RD-TM-68-5, 1968.

15. MacAllister, L, C. and Krial, K. S., *Aerodynamic Properties and Stability Behavior of the 155mm Howitzer Shell M107*, BRL Report No. 2547, Oct 1975 (ARL, Aberdeen, MD).

16. Silton, S. I., *Navier-Stokes Computations for a Spinning Projectile from Subsonic to Supersonic Speeds*, ARL-TR-2850, Sep 2002.

17. Chadwick, W. R. and Sylvester, J. F., *Dynamic Stability of the 5"/54 Rocket Assisted Projectile*, US Naval Weapons Laboratory TR-No. 2059, Oct 1966 (NSWCDD, Dahlgren, VA 22448).

18. Ohlmeyer, E. J., *Dynamic Stability of the Improved 5"/54 Projectile*, NWL TR-2871, Dec 1974 (NSWCDD, Dahlgren, VA 22448).

19. Moore, F. G. and Hymer, T. G., *The 2005 Version of the Aeroprediction Code: Part I – Summary of New Theoretical Methodology*, API Report No. 1, Jan 2004.

20. Shantz, I. and Groves, R. T., *Dynamic and Static Stability Measurements of the Basic Finner at Supersonic Speeds*, NAVORD Report 4516, Jan 1960.

21. Uselton, B. L. and Uselton, J. C., *Test Mechanism for Measuring Pitch Damping Derivatives of Missile Configurations at High Angles of Attack*, AEDC-TR-75-43, May 1975 (NTIS AD-A009-865, US Dept. of Commerce, Springfield, VA 22151).

22. Uselton, B. L. and Jenke, L. M., "Experimental Missile Pitch and Roll Damping Characteristics at Large Angles of Attack," JSR, Vol. 14, No. 4, pp. 241-247, Apr 1977.

23. Gillis, C. L. and Chapman, R. Jr., *Summary of Pitch-Damping Derivatives of Complete Airplane and Missile Configurations as Measured in Flight at Transonic and Supersonic Speeds*, NACA RM L52K20, Jan 1963.

24. Pierens, D. A., *Pitch and Roll Damping Coefficients of the Australian 81mm Improved Mortar Projectile*, DSTO TR-0020, May 1994.

REFERENCES (Continued)

25. Anderson, C. F. and Carlton, W. E., *Static and Dynamic Stability Characteristics of the Fixed-Fin and Inflatable Stabilizer Retarder Configurations of the MK-82 Store at Transonic Speeds*, AEDC TR 75-149 and AFATL TR-75-141, Nov 1975.

26. Piper, W. D. and DeMeritte, F. J., *Summary of the NOL Investigations to Date of the Aerodynamic Characteristics of the Navy Low Drag Bomb*, NAVORD Report 5679, Feb 1960 (DTIC, Cameron Station, Alexandria, VA 22314).

27. Regan, F. J.; Holmes, J. E.; and Falusi, M. E., *Pitch Damping Tests of the M823 Research Store with Cruciform and Split-Skirt Stabilizers*, NOL TR 65-68, Oct 1966 (DTIC AD 644804, Cameron Station, Alexandria, VA 22314).

28. Billingsley, J. P. and Norman, W. S., *Relationship Between Local and Effective Aerodynamic Pitch Damping Derivatives as Measured by a Forced-Oscillation Balance for Preliminary Viking Configurations*, AEDC TR-72-25, May 1972 (NTIS, Springfield, VA 22151).

29. MacAllister, L. C., *The Aerodynamic Properties of a Simple Non-Rolling Finned Cone Cylinder Configuration Between Mach Numbers 1.0 and 2.5*, BRL Report No. 934, May 1955, (DTIC, 8725 John J. Kingman Road, Suite 0944, Ft. Belvoir, VA 22060-6218).

30. Davis, B. S., *Comparison of Aerodynamic Coefficients for the M483A1 and XM898 Projectiles Determined from Transonic Range Data*, BRL MR-3999, Sep 1992 (DTIC ADB168181).

31. Brown, G. T. and McCoy, R. L., *Free Flight Aerodynamic Characteristics of Three 120mm Mortar Projectiles: XM 934-HE, XM 930-Illuminating, XM 929-Smoke*, BRL MR-3884, Jan 1991 (DTIC ADB152531).

32. Robinson, M. L., *The Estimation of Pitch Damping Derivatives of Missile Configurations at Subsonic Speeds*, WRE TN HSA 144, Jan 1969 (DTIC AD857732).

33. Cyran, F. B. and Marquart, E. J., *Pitch- and Yaw-Damping Tests of the AFATL Aerodynamic Data Correlation Model at Mach Numbers 1.75 to 3.0*, AEDC-TSR-79-V34, Aug 1979 (DTIC ADB040452).

34. Uselton, J. C. and Uselton, B. L., *Wind Tunnel Investigation of the Static-Stability, Drag, Magnus and Damping Characteristics of a 105mm Projectile at M_∞ = 1.5 and 1.75*, AEDC-TR-71-203, Oct 1971 (DTIC AD888314).

REFERENCES (Continued)

35. Carroll, C. J. and Groves, R. T., *Pitch Damping of a 0.15 to -1 Scale Model of the Sidewinder 1C Missile at Mach Numbers of 1.53, 1.76, 2.28, 2.54, and 3.26*, NAVORD Report 6836, Mar 1960 (DTIC AD317948).

36. Chin, S. S., "Missile Configuration Design," McGraw Hill Book Company, Inc., New York, NY, 1961.

37. McInville, R. M.; Moore, F. G.; and Housh, C., *Nonlinear Structural Load Distribution Methodology for the Aeroprediction Code*, NSWCDD/TR-96/133, Sep 1996 (NSWC, Dahlgren Division, Dahlgren, VA 22448-5100).

38. Moore, F. G. and Swanson, R. G. Jr., *Aerodynamics of Tactical Weapons to Mach Number 3 and Angle of Attack 15° Part I – Theory and Application*, NSWC/DL TR-3584, Feb 1977.

39. Martin, J. C. and Jeffreys, I., *Span Load Distribution Resulting from Angle-of-Attack, Rolling, and Pitching for Tapered Sweptback Wings with Streamwise Tips*, NACA TN 2643, 1952.

40. Malvestuto, F. S. Jr.; Margolis, K.; and Ribner, H., *Theoretical Lift and Damping in Roll at Supersonic Speeds of Thin Sweptback Tapered Wings with Streamwise Tips, Subsonic Leading Edges, and Supersonic Trailing Edges*, NACA TR 9780, 1950,

41. Chadwick, W. R., *The Application of Non-Planar Lifting Surface Theory to the Calculation of External Store Loads*, Dec 1972.

42. Whyte, R. H., SPINNER – *A Computer Program for Predicting the Aerodynamic Coefficients of Spin Stabilized Projectiles*, General Electric Class 2 Reports, 1969.

43. Regan, F. J., *Roll Damping Measurements for the Basic Finner at Subsonic and Supersonic Speeds*, NAVORD Report 6652, Mar 1964.

44. Vlajurae, M., *Wind Tunnel Measurements of the Aerodynamic Characteristics of the 2.75 Wrap Around Fin Rocket using a Magnetic Suspension System*, Massachusetts Institute of Technology Aerophysics Laboratory TR 150, DSR No. 71083, Dec 1968 (DTIC AD No. 851832).

45. Owens, S.; Dohren, R.; and Malihke, G., *Test 101 (EMHSWT 1419), High Speed Wind Tunnel Test, Precision Guided Mortar Munition (PGMM)*, Alliant Tech Systems Test Report, ATK Missile Systems Company, Rocket Center, WV, Apr 2005.

REFERENCES (Continued)

46. Owens, S.; Dohren, R.; Sitts, J.; and Malejko, G., *Test Report (Test 101B – Part 2) for the Precision Guided Mortar Munition (PGMM)*, ATK Contractor Report prepared for U. S. Army TACOM-ARDEC, Picatinny Arsenal, New Jersey.

47. Jenke, L., *Experimental Roll-Damping, Magnus, and Static Stability Characteristics of Two Slender Missile Configurations at High Angles of Attack () to 90 Deg) and Mach Numbers 0.2 through 2.5*, AEDC-TR-76-58, Jul 1976 (DTIC AD A027027).

48. Wallace, A. R. and Shadow, T. O., *Magnus and Roll Damping Characteristics of the Fixed-Fin and Inflatable Stabilizer Retarder Configuration of the MK 82 Store at Transonic Speeds*, AEDC-TR-75-163, May 1975 (DTIC, Cameron Station, Alexandria, VA 22413, AD No. B008209).

49. Hardy, S. R., *Nonlinear Rolling Motion Analysis of a Canard Controlled Missile Configuration at Angles of Attack from 0 to 30° in Incompressible Flow*, NSWC TR-3808, May 1978 (NSWCDD, Dahlgren, VA 22448, Attn: Tech Library).

50. Hardy, S. R., *Subsonic Wind Tunnel Tests of a Canard-Control Missile in Pure Rolling Motion*, NSWC TR-3615, Jun 1977 (NSWCDD, Dahlgren, VA 22448, Attn: Tech Library).

51. Uselton, J. C. and Carmen, J. B., *Wind Tunnel Investigation of the Roll Characteristics of the Improved 2.75 Inch-Diameter Folding Fin Aircraft Rocket at Mach Numbers from 2.5 to 4.5*, AEDC TR-69-207, Nov 1969 (DTIC AD 861230).

52. Carmen, J. B.; Uselton, B. L.; and Burt, G. E., *Roll Damping, Static Stability, and Damping-in-Pitch Characteristics of Axisymmetric Bomblet Munition Models at Supersonic Mach Numbers*, AEDC-TR-71-88, Apr 1971 (DTIC AD 882636).

53. Shadow, T. O., *Transonic Roll-Damping and Magnus Characteristics of Three Bomblet Munition Models used in the Evaluation of Aerodynamic Dispersion Techniques*, AEDC-TR-71-33, Mar 1971 (DTIC AD No. 880981).

54. Daniels, P. and Hardy, S. R., *Theoretical and Experimental Methods in the Solution of Missile Nonlinear Roll Problems*, NSWC/DL-TR-3773, Jan 1978 (NSWCDD, Dahlgren, VA, Attn: Tech Library).

55. Oberkampf, W. L., "Theoretical Prediction of Roll Moments on Finned Bodies in Supersonic Flow," AIAA Paper 74-111, 12th Aerospace Sciences Meeting, Jan-Feb 1974, Washington, DC.

56. Oberkampt, W. L., *Prediction of Forces and Moments on Finned Missiles at High Angles of Attack in Transonic Flow*, AFATL-TR-80-107, Oct 1980, (DTIC ADA 103964).

REFERENCES (Continued)

57. Fuchs, H., "Prediction of Dynamic Derivatives," Paper No. 6, AGARD Conference Proceedings No. 451, Stability and control of Tactical Missile Systems, Ankara, Turkey, May 1988, AGARD CP-451.

58. Nicolaides, J. D. and Bolz, R. E., "On the Pure Rolling Motion of winged and/or Finned Missiles in Varying Supersonic Flight," JAS, pp. 160-168, Mar 1953.

59. Hopko, R. N., *A Flight Investigation of the Damping in Roll and rolling Effectiveness Including Aeroelastic Effects of Rocket-Propelled Missiles Having Cruciform, Triangular, Interdigitated Wings and Tails*, NACA RM L51D16, Sep 1951.

60. Prakash, S, and Khurana, D. D., A simple Estimation Procedure of Roll-Rate Derivatives for Finned Vehicles," JSR, Vol. 21, No. 3, pp. 318-320, May-Jun 1984.

61. Eastman, D. W., "Roll Damping of Cruciform Tailed Missiles," JSR Vol. 23, No. 1, pp. 119-120, Jan-Feb 1986.

62. Mikhail, A. G., *Roll Damping for Finned Projectiles Including: Wraparound, Offset and Arbitrary Number of Fins*, ARL-TR-846, Aug 1995 (U.S. Army Research Laboratory, Aberdeen Proving Ground, MD 21005-5066).

63. Hymer, T. G. and Rodriquez, V., *Compilation of 5"/54, Hi Frag, MK 64, and MK 48 Projectile Aerodynamics*, NSWCDD/TR-96/119, Mar 1996 (NSWCDD, Dahlgren, VA 22448).

64. McCoy, R. L., McDrag – *A Computer Program for Estimating the Drag Coefficients of Projectiles*, ARBRL-TR-02293, BRL, Aberdeen, MD, Feb 1981.

65. Pierens, D., *Aerodynamic Evaluation of Production Fuzes and Fins for the 81 MM Improves Mortar Projectile*, DSTO-TR-0142, AR-008-331, Mar 1995.

66. Malejke, G., *Static Aerodynamics for the 120 MM XM984 Extended Range DPICM Mortar Projectile at Subsonic Mach Numbers*, U. S. Army Armament Research Development and Engineering Center, TR ARAACCD-TR-00003, Jan 2001.

67. Malejko, G., *The Effect of Fuze Windshield Separation on Flight Performance of the 60-MM, HE, M494A Projectile with Fuze, RD, M935*, U. S. Army Armament Research, Development and Engineering Center, TR ARAED-TR-93009, Aug 1993 (also DTIC reference ADB175739).

68. Schermerhorn, V. L. and DeMeritte, F. J., *Wind Tunnel Tests of the Navy Low-Drag Bomb at Angles of Attack up to 70 Degrees*, NAVWEPS Report 7291, Mar 1961 (obtained from DTIC, Cameron Station, Alexandria, VA 22314, AD 884854).

REFERENCES (Continued)

69. Krishnamoorthy, L. V.; Kirk, D. R.; and Glass, R., *An Aerodynamic Data Base for the MK 82 General Purpose Low Drag Bomb*, Defense Science and Technology Organization DSTO-TR-0545, Jun 1997, P. O. Box 4331, Melbourne, Victoria 3001, Australia.

70. Miklos, W. J. and Ingram, C. W., *Wind Tunnel Tests of Three Candidate MK 82 Snakeye Bomb Replacement Configurations*, ARL-75-0174, Jun 1975 (NTIS, U. S. Department of Commerce, Washington, DC, AD-A014-735).

71. Hobbs. R. W., *Drag Coefficient Table for a MK-82 LDGP Unguided Bomb Developed from Grounded Base Techniques*, AEDC-TR-95-29, Feb 1996 (AFSEO/SKM, 205 West D Avenue, Suite 318, Eglin AFB, FL 32542-6865).

72. Miklos, W. J. and Ingram, C. W., *Wind Tunnel Tests of Three Candidate MK 82 Snakeye Bomb Replacement Configurations*, ARL-75-0174, Jun 1975 (NTIS, U. S. Department of Commerce, Washington, DC, AD-A014-735).

73. Sun, J. and Roman, J., *Flight Dynamics of MK 82 Inflatable Retarder Low Drag Bomb*, NSWC TR 3475, Jul 1976 (NSWCDD, Dahlgren, VA 22448).

74. Falkowski, E. W., *Transonic Aerodynamic Characteristics of a Full-Scale M117 Bomb with Three Fin Configurations*, U. S. Army Munitions Command, TR 3785, Oct 1968 (DTIC AD 841577).

75. Falkowski, E. W., *Subsonic Aerodynamic Characteristics of a 18 Percent Scale Model of The M117 750-lb Bomb with Folding Fins*, Picatinny Arsenal, TR 4096, Dec 1970 (DTIC AD 878305).

76. Marsden, P.; *Results of Wind Tunnel Tests on the M823 Research Store with fixed Monoplane Fins*, ARA Model Test Note M.25/1, Sep 1967. (Also AD 857732 from Defense Technical Information Center, 8725 John J. Kingman Rd., Suite 0944, Ft. Belvoir, VA 22060-6218)

77. Frierson, L., "Supersonic Aerodynamics of the 5-Inch Beamrider Guided Projectile," NSWC Dahlgren Aerodynamics Memo No. DG 44-75-67, Dahlgren, VA 22448, Oct 1975.

6.0 SYMBOLS AND DEFINITIONS

AOA	Angle of Attack
APC	Aeroprediction Code
AP72, AP74, AP77, AP81, AP93, AP95, AP98, AP02, AP05, AP09	Various versions of the APC and the year produced
SB, SBT	Slender Body, Slender-body Theory
A_{REF}	Reference area (maximum cross-sectional area of body, if a body is present, or planform area of wing, if wing alone)(ft^2)
A_W	Wing planform area (ft^2)
AR	Aspect ratio
b	Wing span (not including body)(ft)
C_A	Axial force coefficient
$C_{A_B}, C_{A_F}, C_{A_W}$	Base, skin-friction, and wave components, respectively, of axial force coefficient (C_{A_w} also used for axial force of wings)
C_{A_O}	Axial force coefficient at 0 deg AOA
$C_{A_{SF}}, C_{A_{SW}}$	Axial force coefficient of a single fin or wing, respectively
CG	Center of gravity location (calibers, ft or inches)
C_{ℓ_P}	Roll damping moment coefficient $(\gamma C_\ell / \gamma(pd/2V_\infty))$
C_M	Pitching moment coefficient (based on reference area and body diameter, if body present, or mean aerodynamic chord, if wing alone)

C_{M_B}, C_{M_T}	Pitching moment coefficient of body or tail alone, respectively
$C_{M_q} + C_{M_{\dot{\alpha}}}$	Pitch damping moment coefficient $[C_M(q)/(qd/2V_\infty) + C_M(\dot{\alpha})/(\dot{\alpha}d/2V_\infty)]$
C_{M_α}	Pitching moment coefficient derivative (per radian)
C_N	Normal force coefficient
C_{N_B}	Normal force coefficient of body alone
$\Delta C_{N_{B(W)}}, \Delta C_{N_{B(T)}}$	Additional normal-force coefficient on body in presence of wing or tail
$C_{N_{T(V)}}$	Negative canard shed vortex normal force coefficient on tail
C_{N_W}	Normal force coefficient of wing alone
$C_{N_{W(B)}}, C_{N_{T(B)}}$	Normal-force coefficient of wing or tail in presence of body
$C_{N_\alpha}, C_{N_\delta}$	Normal-force coefficient derivative (per radian) due to angle of attack or control deflection, respectively
C_P	Pressure coefficient $\left(\frac{P - P_\infty}{1/2\rho_\infty V_\infty^2}\right)$
C_{P_B}	Base pressure coefficient
c, c_r, c_t	Local chord, root and tip chord, respectively
d_B	Body base diameter (ft)
d_N	Diameter of truncated nose tip (ft)
d_{ref}	Reference body diameter (ft)
F_6, F_8	Empirical factors used to represent aerodynamics of 6 and 8 fins based on 4 fin aerodynamics
$K_{W(B)}$, $k_{W(B)}$	Ratio of normal-force coefficient of wing or tail in presence of body to that of wing or tail alone at $\delta = 0$ deg or $\alpha = 0$ deg, respectively
$\ell, \ell_n, \ell_a, \ell_B$	Total body, nose, afterbody or boattail length, respectively (ft or cal)

M	Pitching moment (ft – lbs)
M_N	Mach number normal to body = $M_\infty \sin \alpha$
M_L	Local Mach number
M_∞	Freestream Mach number
MFF	Multi-fin factor
NC	Number of canards
p, q	Roll and pitch rate respectively (rad/sec)
P_L, P_∞	Local and freestream pressure, respectively (lb/ft^2)
Q_L, Q_∞	Local or freestream dynamic pressure, respectively (lb/ft^2)
r_B, r_W	Local body radius and body radius at wing, respectively (ft)
r_r	Reference body radius (ft)
R_N	Reynolds number
T_L, T_∞	Local or freestream temperature, respectively (deg rankine)
V_∞, V_L	Freestream and local velocity, respectively (ft/sec)
w	Running load (lb/ft)
x,y,z	Coordinate system, x along body axis, y out right wing, z up
X_{CG}	Distance to center of gravity (ft)
X_{CP}	Center of pressure (in feet or calibers from some reference point that can be specified) in x direction
X_{CP}/d	Center of pressure (calibers from some reference point)
X_{LE}, X_{AFT}	Distance from nose tip to wing leading edge or afterbody, respectively (in feet or cal from reference point that can be specified)
y_c	Distance from body centerline to wing centroid of presented area
α	Angle of attack (deg)

γ	Ratio of specific heats of air
δ^*	Boundary layer displacement thickness (ft)
Φ	Roll position of missile fins (Φ = 0 deg corresponds to fins in the plus (+) orientation. Φ = 45 deg corresponds to fins rolled to the cross (×) orientation).
θ_b	Boattail angle (deg)

APPENDIX A
USER GUIDE EXAMPLE OF MORTAR AND BOMB CONFIGURATIONS

No inputs or outputs are significantly changed for the AP09 as compared to the AP05. As a result, the AP05 User Guide will continue to be used as the prime source for using the AP09. The AP05 User Guide has 37 examples and the intent here is to add a couple more examples for long boattail configurations to illustrate how to set up a configuration the code is not exactly suited for, yet get reasonable aerodynamics. The first example will be Example 38 so as to keep consistency with an extension of the AP05 Users Guide. All User Guide examples will be pre-loaded onto each AP09 computer disc for ease of training.

Two examples will be shown to illustrate how to use the AP09 to compute aerodynamics of a mortar and a low drag bomb. Both of these configurations require modifications of the configurations to allow them to fit into the nose-afterbody-bodytail/flare geometry requirement for the code. Since the AP05 users guide will be used for the AP09 and there are 37 examples in that reference, the first example here will be number 38. The first 37 examples shown in the Reference 1 are shown with the actual input screens with the inputs filled in. For the two examples shown here (38 and 39), the inputs will be given in a shortened way similar to the way all the examples are set up in the aeroprediction users course. To do this, Figure A-1 has been included which defines the nomenclature for a canard-body-tail configuration. Then the variables shown in Figure A-1 are correlated to the various geometry input screens of the AP09.

Definition of Terminology in Figure A-1 and Correlation to AP09 Geometry Input Screens

Nose Geometry Screen

- Cross sectional shape – Enter Type (default is circular)
- Circular radius at end of nose $\equiv r_r$ = reference radius = half the reference body diameter
- Nose Profile – Enter Type (Tangent ogive pointed is default) – we will choose tangent ogive blunt for case 38 so we can enter a nose cap or spherical cap radius = r_n; length of nose from tip to shoulder = ℓ_n

Afterbody Geometry Screen

- Standard is the default
- Longitudinal afterbody coordinate from nose tip = ℓ_a

Boattail Geometry Screen

- Longitudinal Boattail/Flare Coordinate from Nose Tip = ℓ_B
- Corresponding Boattail/Flare Characteristics half width = r_B

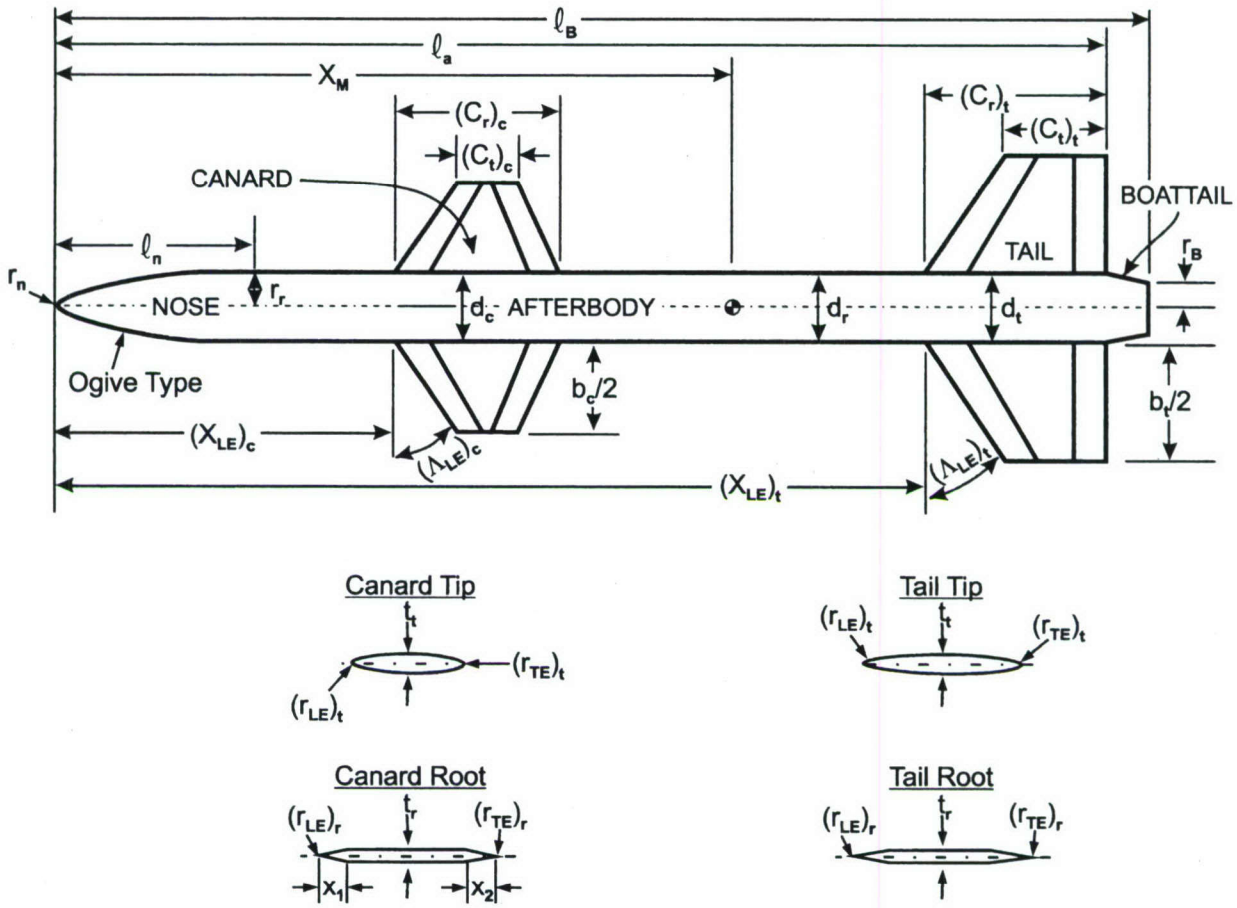

FIGURE A-1. GENERIC CANARD-BODY-TAIL GEOMETRY AND NOMENCLATURE USED IN AP09 CLASSES

Body Roughness Screen – Allows 5 boundary layer options with Typical Flight configuration as default

Canard/Wing Screen – Double wedge airfoil is default

- Leading edge sweep angle = Λ_{LE} (in deg)
- Semispan = $b_c/2$
- Root chord = $(C_r)_c$
- Tip chord = $(C_t)_c$
- Leading edge radius at root chord = $(r_{LE})_r$
- Trailing edge radius at root chord = $(r_{TE})_r$
- Root thickness = t_r
- Tip thickness = t_t
- Distance from leading edge to first discontinuity downstream at the root chord = X_1
- Distance from trailing edge to first discontinuity upstream at the root chord = X_2
- Number of fins – 2, 3, 4, 6, or 8
- Truncated LE, is the leading edge radius of the airfoil truncated, yes or no?

Tail Screen

Same parameter definitions as for canard/wing except enter the specific dimensions for the tail airfoil cross section

Main Geometry Screen

- Reference diameter or width of body = $d_r = 2r_r$
- Reference length for aerodynamic coefficients – user specified (default is d_r)
- Reference area for aerodynamic coefficients – user specified with default as $\pi d_r^2/4$
- Mean diameter or width of body at tail root chord = d_T
- Distance of tail leading edge from nose tip = x_T
- Mean diameter or width of body at canard/wing root chord = d_c
- Distance of canard/wing leading edge from nose tip = x_c
- Distance of moment reference from nose tip = x_m

Freestream conditions Screen

- α sweep
- M_∞ sweep
- δ sweep

} pick one

Example: α sweep

- Enter a initial and final angle of attack and an interval size
- Pick a constant lifting surface/flap deflection angle, default is 0
- Pick a roll angle (default is 0)
- Pick a Reynolds number or altitude
- Select up to 20 Mach numbers

Options Screen

- Select dynamic derivatives if desired
- Select spin stabilized if an unguided spin-stabilized projectile
- Select real or perfect gas ($M_\infty \geq 5.0$ for real gas); perfect gas is default
- Select pressure coefficients or structures option if desired, otherwise no loading or aerothermal information is default
- Aerodynamic smoother is on as default
- Drag bucket starts at a normal Mach number of, set to default
- Enter a title

The first case considered here, or Example 38, will be the 81 MM mortar configuration of Reference 24 which has an unlimited distribution statement. The geometry shown in Reference 24 is not detailed, so we cannot show detailed static aerodynamics. However, the geometry shown in Figure 64 (taken from Reference 24) can be scaled and approximated to obtain reasonable dynamic derivatives. The following geometry inputs are approximations based on the scaled drawing of Reference 24. Figure A-2 shows the scaled 81 MM drawing from Reference 24 and the AP09 representation of the configuration.

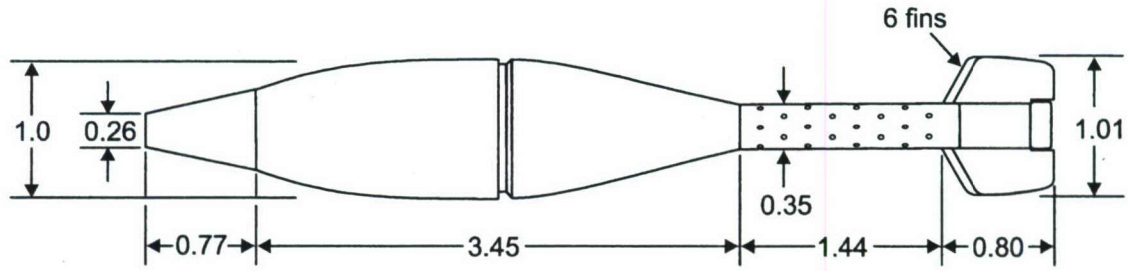

Scaled Drawing of 81MM Round (All Dimensions in Calibers, 1cal=80.45mm)

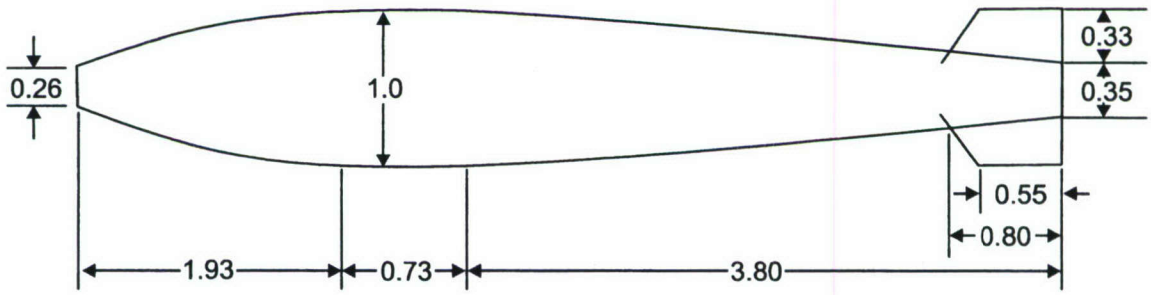

AP09 Representation of 81MM Mortar (In Calibers)

FIGURE A-2. 81MM AUSTRALIAN MORTAR ROUND AND APO9 REPRESENTATION

Example 38: 81 MM Mortar Configuration (see Figure A-2)

Nose: tangent ogive truncated

$r_r = 40.23$mm $\quad d_r = 80.45$
$r_n = 10.0 \quad d_T = 28.5$
$\ell_n = 155.0 \quad x_T = 456.0$
$\ell_a = 214.0 \quad x_M = 202.5$
$\ell_B = 520.0$ typical flight BL option
$r_B = 14.3$

Tails (6) – double Wedge Airfoil

$\Lambda_{LE} = 36.3$
$b/2 = 26.2$
$C_r = 64.0$
$C_t = 44.75$
$(r_{LE})_r = (r_{TE})_r = (r_{LE})_t = (r_{TE})_t = 0.0$
$X_1 = 32$
$X_2 = 32$
$t_r = t_t = 2.75$ mm

Freestream Condition

- α sweep 0 – 10 deg, 10 deg increments
- Roll position = 0 deg
- Control Deflection = 0 deg
- Altitude = h = 0
- M_∞ = 0.5, 0.8

Options Screen

- Select dynamic derivatives
- Input title
- Leave all other options as default

Note in the input geometry that ℓ_a was selected to go up to the end of the afterbody and ℓ_B includes the boattail plus the boom length. The output listing of Example 38 follows. Note in the output that the axial force coefficient is not expected to be accurate as we did not know the wing cross sectional shape from the Reference 24, only the approximate wing planform shape. On the other hand, normal force, center of pressure, pitching moments, roll and pitch damping should be reasonable approximations to data.

Also worthy of note in the Example 38 output is the fact that both Methods 2 (under $C_{M_q} + C_{M_\alpha}$) and 3 pitch damping predictions are listed in the output. Also note that under the total static aerodynamics, the AP05 value of X_{CP} ($-C_M/C_N$) is shown at the end of the lines of data. These are the only two changes from the AP05 output listing. Method 2 is currently plotted out for pitch damping. Hence, Method 3 pitch damping must be plotted offline.

1

CASE NO. 1
UG EXAMPLE 38- 81MM MORTAR APP

ANGLE OF ATTACK = 0.00 DEGS REFERENCE DIAMETER = 0.264 FT
DEFLECTION ANGLE = 0.00 DEGS

REFERENCE CONDITIONS

MOMENT REFERENCE = 2.52 CALIBERS FROM NOSE TIP
ALIMIT MACH NUMBER: TO BE COMPUTED
ALIMS MACH NUMBER = 1.80

NOTE: (CNAL,CMAL) ARE TANGENT SLOPES IN THE AP09 VS SECANT SLOPES IN AP05. THUS CNAL,CMAL AND XCP WILL DIFFER.

TAIL/WING GEOMETRY(DOUBLE WEDGE OR MODIFIED DOUBLE WEDGE AIRFOIL DESIGN)

SPAN= 0.172 FT.
ROOT CHORD=0.210 FT.
TIP CHORD=0.147 FT.
LEADING EDGE SWEEP=36.30 DEG.
FIRST LINE OF SINKS= 36.30 DEGS.
SECOND LINE OF SINKS= -0.02 DEGS.
TRAILING EDGE SWEEP= -0.02 DEGS.
FIRST CHORD SEGMENT=0.105 FT.
REAR CHORD SEGMENT=0.105 FT.
ROOT THICKNESS=0.0090 FT.
TIP THICKNESS=0.0090 FT.
LEADING EDGE RADIUS AT ROOT=0.0000 FT.
LEADING EDGE RADIUS AT TIP=0.0000 FT.
TRAILING EDGE BLUNTNESS=0.0000 FT.
DEFLECTION ANGLE= 0.00 DEGS.

BODY COORDINATES

X	R
0.0000	0.1246
0.2144	0.2058
0.4288	0.2763
0.6431	0.3366
0.8575	0.3871
1.0719	0.4280
1.2863	0.4597
1.5007	0.4821
1.7151	0.4955
1.9294	0.5000
2.6600	0.5000
6.4636	0.1778

1

SUMMARY OF AERODYNAMIC COEFFICIENTS FOR CASE NO. 1

UG EXAMPLE 38- 81MM MORTAR APP

ROLL = 0

BODY AXIAL FORCE CONTRIBUTIONS

MACH NO.	REYS. NO./MACH NO./FT.	SKIN FRICTION	BASE PRESSURE	PRESSURE	PROTRUSIONS	TOTAL
0.800	0.7101E+07	0.0527	0.0372	0.0127	0.0000	0.1026
0.500	0.7101E+07	0.0531	0.0312	0.0000	0.0000	0.0843

WING AXIAL FORCE CONTRIBUTIONS

MACH NO.	REYS. NO./MACH NO./FT.	SKIN FRICTION	BASE PRESSURE	PRESSURE	TOTAL
0.800	0.7101E+07	0.0069	0.0000	0.0000	0.0069
0.500	0.7101E+07	0.0055	0.0000	0.0000	0.0055

NORMAL FORCE CONTRIBUTIONS

MACH NO.	BODY ALONE	WING ALONE	CANARD ALONE	WING-BODY	BODY-WING	CANARD-BODY	BODY-CANARD	CANARD-WING	TOTAL
0.80	0.0000	0.0000	0.0000	0.0000	0.0000	0.0000	0.0000	0.0000	0.0000
0.50	0.0000	0.0000	0.0000	0.0000	0.0000	0.0000	0.0000	0.0000	0.0000

MOMENT CONTRIBUTIONS ABOUT C.G.

MACH NO.	BODY ALONE	WING-BODY	BODY-WING	CANARD-BODY	BODY-CANARD	CANARD-WING	TOTAL
0.800	0.0001	-0.0001	0.0000	0.0000	0.0000	0.0000	0.0000
0.500	0.0001	-0.0001	0.0000	0.0000	0.0000	0.0000	0.0000

TOTAL STATIC AERODYNAMICS(FORCE/ALPHA)

MACH NO.	CA	CN	CD	CL	CM	CNAL	CMAL	XCP/DREF	XCP/L	XCP(-CM/CN)
0.800	0.109	0.000	0.109	0.000	0.000	3.097	-2.363	0.763	0.116	0.464
0.500	0.090	0.000	0.090	0.000	0.000	2.722	-2.584	0.949	0.144	0.757

NOTE: THE ABOVE CM, CMAL, AND XCP/DREF ARE REFERENCED TO THE POINT AT 2.5171 CALIBERS FROM NOSE TIP

CONFIGURATION DYNAMIC DERIVATIVES

MACH NO.	CLP	CMQ+CMAD	CNPA1	CNPA5	METHOD 3 PITCH DAMPING
0.80	-0.224	-46.201	0.000	0.000	-121.448
0.50	-0.223	-46.719	0.000	0.000	-37.155

1

CASE NO. 2
UG EXAMPLE 38- 81MM MORTAR APP

ANGLE OF ATTACK = 10.00 DEGS REFERENCE DIAMETER = 0.264 FT
DEFLECTION ANGLE = 0.00 DEGS

REFERENCE CONDITIONS

MOMENT REFERENCE = 2.52 CALIBERS FROM NOSE TIP
ALIMIT MACH NUMBER = 2.00
ALIMS MACH NUMBER = 1.80

****************** BODY GEOMETRY SAME AS PREVIOUS CASE *****************

1

SUMMARY OF AERODYNAMIC COEFFICIENTS FOR CASE NO. 2

UG EXAMPLE 38- 81MM MORTAR APP

ROLL = 0

BODY AXIAL FORCE CONTRIBUTIONS

MACH NO.	REYS. NO./MACH NO./FT.	SKIN FRICTION	BASE PRESSURE	PRESSURE	PROTRUSIONS	TOTAL
0.800	0.7101E+07	0.0527	0.0629	-.0049	0.0000	0.1107
0.500	0.7101E+07	0.0531	0.0567	-.0069	0.0000	0.1029

WING AXIAL FORCE CONTRIBUTIONS

MACH NO.	REYS. NO./MACH NO./FT.	SKIN FRICTION	BASE PRESSURE	PRESSURE	TOTAL
0.800	0.7101E+07	0.0069	0.0000	0.0000	0.0069
0.500	0.7101E+07	0.0055	0.0000	0.0000	0.0055

NORMAL FORCE CONTRIBUTIONS

MACH NO.	BODY ALONE	WING ALONE	CANARD ALONE	WING-BODY	BODY-WING	CANARD-BODY	BODY-CANARD	CANARD-WING	TOTAL
0.80	0.2268	0.1836	0.0000	0.2586	0.1037	0.0000	0.0000	0.0000	0.5891
0.50	0.1912	0.1718	0.0000	0.2448	0.1005	0.0000	0.0000	0.0000	0.5365

MOMENT CONTRIBUTIONS ABOUT C.G.

MACH NO.	BODY ALONE	WING-BODY	BODY-WING	CANARD-BODY	BODY-CANARD	CANARD-WING	TOTAL

0.800	0.6738	-0.8808	-0.3531	0.0000	0.0000	0.0000	-0.5600
0.500	0.5973	-0.8367	-0.3434	0.0000	0.0000	0.0000	-0.5828

TOTAL STATIC AERODYNAMICS (FORCE/ALPHA)

MACH NO.	CA	CN	CD	CL	CM	CNAL	CMAL	XCP/DREF	XCP/L	XCP(-CM/CN)
0.800	0.118	0.589	0.218	0.560	-0.560	3.953	-4.351	1.101	0.167	0.951
0.500	0.108	0.537	0.200	0.510	-0.583	3.736	-4.586	1.227	0.186	1.086

NOTE: THE ABOVE CM, CMAL, AND XCP/DREF ARE REFERENCED TO THE POINT AT 2.5171 CALIBERS FROM NOSE TIP

CONFIGURATION DYNAMIC DERIVATIVES

MACH NO.	CLP	CMQ+CMAD	CNPA1	CNPA5	METHOD 3 PITCH DAMPING
0.80	-0.404	-64.717	0.000	0.000	-119.651
0.50	-0.360	-61.758	0.000	0.000	-35.692

The second example chosen (Example 39) is the MK 82 low drag bomb of Reference 21-24 and 26 with the configuration and AP09 representation shown in figure 35. Note once again in Figure 35 that the afterbody was modified so the configuration would fit into the nose-afterbody-boattail requirement of the AP09. The actual input parameters of the MK 82 GPLDB are as follows:

Example 39: Navy MK 82 GPLDB (see Figure 35)

- Nose-secant ogive pointed
- $r_r = 5.325$
- Radius of curvature = 200.0
- $\ell_n = 40.0$
- $\ell_a = 55.63$
- $\ell_B = 87.11$
- $r_B = 2.0$
- BL = smooth model with no B.L. trip
- $d_r = 10.65$
- $d_T = 4.26$
- $x_T = 78.35$
- $x_M = 38.76$

Tails (4)
$\Lambda_{LE} = 45.0$
$b/2 = 5.325$
$C_r = 10.12$
$C_t = 5.54$
$t_r = .506$
$t_t = .277$
$X_1 = X_2 = 4.0$
$(r_{LE})_r = (r_{TE})_r = (r_{LE})_t = (r_{TE})_t = 0$

Freestream Conditions

- α sweep –0 to 25 deg, 5 deg increments
- $M_\infty = 1.5, 1.3, 1.1, 0.8, 0.6$
- $\Phi = 0$ deg roll
- $R_e/ft = 2 \text{ X } 106$
  Options – All default except select dynamic derivative

The outputs of Example 39 are given in the following AP09 listing. Some of the MK 82 GPLDB AP09 results are plotted in Figures 36-38, 54, and 61. Note once again the only differences between the AP05 and AP09 output listing are the nonlinearity of the roll and pitch damping with AOA, the fact the AP09 has two values of pitch damping corresponding to Method 2 (listed under $C_{M_q} + C_{M_{\dot{\alpha}}}$) and Method 3, and the additional listing of the AP05 center of pressure at the end of the static aerodynamics line.

1

CASE NO. 1
EXAMPLE 39 MK 82 LOW DRAG BOMB

ANGLE OF ATTACK = 0.00 DEGS REFERENCE DIAMETER = 0.887 FT
DEFLECTION ANGLE = 0.00 DEGS

REFERENCE CONDITIONS

MOMENT REFERENCE = 3.64 CALIBERS FROM NOSE TIP
ALIMIT MACH NUMBER: TO BE COMPUTED
ALIMS MACH NUMBER = 2.50

NOTE: (CNAL,CMAL) ARE TANGENT SLOPES IN THE AP09 VS SECANT SLOPES IN AP05. THUS CNAL,CMAL AND XCP WILL DIFFER.

TAIL/WING GEOMETRY(DOUBLE WEDGE OR MODIFIED DOUBLE WEDGE AIRFOIL DESIGN)

SPAN= 0.888 FT.
ROOT CHORD=0.843 FT.
TIP CHORD=0.462 FT.
LEADING EDGE SWEEP=45.00 DEG.
FIRST LINE OF SINKS= 33.43 DEGS.
SECOND LINE OF SINKS= 25.64 DEGS.
TRAILING EDGE SWEEP= 7.97 DEGS.
FIRST CHORD SEGMENT=0.333 FT.
REAR CHORD SEGMENT=0.333 FT.
ROOT THICKNESS=0.0422 FT.
TIP THICKNESS=0.0231 FT.
LEADING EDGE RADIUS AT ROOT=0.0000 FT.
LEADING EDGE RADIUS AT TIP=0.0000 FT.
TRAILING EDGE BLUNTNESS=0.0000 FT.
DEFLECTION ANGLE= 0.00 DEGS.

BODY COORDINATES

X	R
0.0000	0.0000
0.4173	0.0942
0.8346	0.1785
1.2520	0.2530
1.6693	0.3178
2.0866	0.3731
2.5039	0.4189
2.9212	0.4553
3.3385	0.4823
3.7559	0.5000
5.2235	0.5000
8.1793	0.1878

1

SUMMARY OF AERODYNAMIC COEFFICIENTS FOR CASE NO. 1

EXAMPLE 39 MK 82 LOW DRAG BOMB

ROLL = 0

BODY AXIAL FORCE CONTRIBUTIONS

MACH NO.	REYS. NO./MACH NO./FT.	SKIN FRICTION	BASE PRESSURE	PRESSURE	PROTRUSIONS	TOTAL
1.500	0.1333E+07	0.0479	0.0458	0.1218	0.1330	0.3485
1.300	0.1538E+07	0.0492	0.0542	0.1307	0.1330	0.3671
1.100	0.1818E+07	0.0505	0.0546	0.1437	0.1330	0.3818
0.800	0.2500E+07	0.0521	0.0386	0.0100	0.1500	0.2507
0.600	0.3333E+07	0.0530	0.0342	0.0000	0.1150	0.2022

WING AXIAL FORCE CONTRIBUTIONS

MACH NO.	REYS. NO./MACH NO./FT.	SKIN FRICTION	BASE PRESSURE	PRESSURE	TOTAL
1.500	0.1333E+07	0.0042	0.0000	0.0222	0.0264
1.300	0.1538E+07	0.0042	0.0000	0.0273	0.0314
1.100	0.1818E+07	0.0042	0.0000	0.0346	0.0387
0.800	0.2500E+07	0.0042	0.0000	0.0000	0.0042
0.600	0.3333E+07	0.0042	0.0000	0.0000	0.0042

NORMAL FORCE CONTRIBUTIONS

MACH NO.	BODY ALONE	WING ALONE	CANARD ALONE	WING-BODY	BODY-WING	CANARD-BODY	BODY-CANARD	CANARD-WING	TOTAL
1.50	0.0000	0.0000	0.0000	0.0000	0.0000	0.0000	0.0000	0.0000	0.0001
1.30	0.0000	0.0000	0.0000	0.0000	0.0000	0.0000	0.0000	0.0000	0.0001
1.10	0.0000	0.0000	0.0000	0.0000	0.0000	0.0000	0.0000	0.0000	0.0001
0.80	0.0000	0.0000	0.0000	0.0000	0.0000	0.0000	0.0000	0.0000	0.0001
0.60	0.0000	0.0000	0.0000	0.0000	0.0000	0.0000	0.0000	0.0000	0.0001

MOMENT CONTRIBUTIONS ABOUT C.G.

MACH NO.	BODY ALONE	WING-BODY	BODY-WING	CANARD-BODY	BODY-CANARD	CANARD-WING	TOTAL
1.500	0.0001	-0.0002	-0.0001	0.0000	0.0000	0.0000	-0.0001
1.300	0.0001	-0.0002	-0.0001	0.0000	0.0000	0.0000	-0.0001
1.100	0.0001	-0.0002	-0.0001	0.0000	0.0000	0.0000	-0.0001
0.800	0.0001	-0.0001	0.0000	0.0000	0.0000	0.0000	-0.0001
0.600	0.0001	-0.0001	0.0000	0.0000	0.0000	0.0000	-0.0001

TOTAL STATIC AERODYNAMICS(FORCE/ALPHA)

MACH NO.	CA	CN	CD	CL	CM	CNAL	CMAL	XCP/DREF	XCP/L	XCP(-CM/CN)
1.500	0.375	0.000	0.375	0.000	0.000	4.217	-5.212	1.236	0.151	1.261
1.300	0.399	0.000	0.399	0.000	0.000	4.729	-7.844	1.659	0.203	1.701
1.100	0.421	0.000	0.421	0.000	0.000	4.721	-8.462	1.792	0.219	1.725
0.800	0.255	0.000	0.255	0.000	0.000	4.182	-6.444	1.541	0.188	1.421
0.600	0.206	0.000	0.206	0.000	0.000	3.643	-5.683	1.560	0.191	1.479

NOTE: THE ABOVE CM, CMAL, AND XCP/DREF ARE REFERENCED TO THE POINT AT 3.6394 CALIBERS FROM NOSE TIP

CONFIGURATION DYNAMIC DERIVATIVES

MACH NO.	CLP	CMQ+CMAD	CNPA1	CNPA5	METHOD 3 PITCH DAMPING
1.50	-0.909	-100.220	0.000	0.000	-132.913
1.30	-0.855	-121.343	0.000	0.000	-146.495
1.10	-0.742	-117.500	0.000	0.000	-143.418
0.80	-0.744	-96.644	0.000	0.000	-314.605
0.60	-0.739	-94.336	0.000	0.000	-92.088

1

CASE NO. 2
EXAMPLE 39 MK 82 LOW DRAG BOMB

ANGLE OF ATTACK = 5.00 DEGS REFERENCE DIAMETER = 0.887 FT
DEFLECTION ANGLE = 0.00 DEGS

REFERENCE CONDITIONS

MOMENT REFERENCE = 3.64 CALIBERS FROM NOSE TIP
ALIMIT MACH NUMBER = 2.00
ALIMS MACH NUMBER = 2.50

********** BODY GEOMETRY SAME AS PREVIOUS CASE **********

1

SUMMARY OF AERODYNAMIC COEFFICIENTS FOR CASE NO. 2

EXAMPLE 39 MK 82 LOW DRAG BOMB

ROLL = 0

BODY AXIAL FORCE CONTRIBUTIONS

MACH NO.	REYS. NO./MACH NO./FT.	SKIN FRICTION	BASE PRESSURE	PRESSURE	PROTRUSIONS	TOTAL
1.500	0.1333E+07	0.0479	0.0579	0.1316	0.1330	0.3704
1.300	0.1538E+07	0.0492	0.0699	0.1309	0.1330	0.3830
1.100	0.1818E+07	0.0505	0.0715	0.1363	0.1330	0.3912
0.800	0.2500E+07	0.0521	0.0516	0.0059	0.1500	0.2596
0.600	0.3333E+07	0.0530	0.0476	-.0012	0.1150	0.2145

WING AXIAL FORCE CONTRIBUTIONS

MACH NO.	REYS. NO./MACH NO./FT.	SKIN FRICTION	BASE PRESSURE	PRESSURE	TOTAL
1.500	0.1333E+07	0.0042	0.0000	0.0222	0.0264
1.300	0.1538E+07	0.0042	0.0000	0.0273	0.0314
1.100	0.1818E+07	0.0042	0.0000	0.0346	0.0387
0.800	0.2500E+07	0.0042	0.0000	0.0000	0.0042
0.600	0.3333E+07	0.0042	0.0000	0.0000	0.0042

NORMAL FORCE CONTRIBUTIONS

MACH NO.	BODY ALONE	WING ALONE	CANARD ALONE	WING-BODY	BODY-WING	CANARD-BODY	BODY-CANARD	CANARD-WING	TOTAL
1.50	0.0999	0.1819	0.0000	0.2101	0.0643	0.0000	0.0000	0.0000	0.3743
1.30	0.0946	0.1963	0.0000	0.2409	0.0866	0.0000	0.0000	0.0000	0.4221
1.10	0.1126	0.1878	0.0000	0.2320	0.0782	0.0000	0.0000	0.0000	0.4227
0.80	0.1190	0.1567	0.0000	0.1960	0.0499	0.0000	0.0000	0.0000	0.3649
0.60	0.0864	0.1462	0.0000	0.1865	0.0451	0.0000	0.0000	0.0000	0.3179

MOMENT CONTRIBUTIONS ABOUT C.G.

MACH NO.	BODY ALONE	WING-BODY	BODY-WING	CANARD-BODY	BODY-CANARD	CANARD-WING	TOTAL
1.500	0.7037	-0.8908	-0.2743	0.0000	0.0000	0.0000	-0.4613
1.300	0.6865	-1.0151	-0.3693	0.0000	0.0000	0.0000	-0.6979
1.100	0.5399	-0.9677	-0.3263	0.0000	0.0000	0.0000	-0.7541
0.800	0.4503	-0.8071	-0.2056	0.0000	0.0000	0.0000	-0.5624
0.600	0.4587	-0.7688	-0.1859	0.0000	0.0000	0.0000	-0.4960

TOTAL STATIC AERODYNAMICS(FORCE/ALPHA)

MACH NO.	CA	CN	CD	CL	CM	CNAL	CMAL	XCP/DREF	XCP/L	XCP(-CM/CN)
1.500	0.397	0.374	0.428	0.338	-0.461	4.377	-5.360	1.224	0.150	1.233
1.300	0.414	0.422	0.450	0.384	-0.698	4.902	-8.167	1.666	0.204	1.653
1.100	0.430	0.423	0.465	0.384	-0.754	5.090	-9.644	1.895	0.232	1.784
0.800	0.264	0.365	0.295	0.341	-0.562	4.451	-7.487	1.682	0.206	1.541
0.600	0.219	0.318	0.246	0.298	-0.496	4.022	-6.617	1.645	0.201	1.560

NOTE: THE ABOVE CM, CMAL, AND XCP/DREF ARE REFERENCED TO THE POINT AT 3.6394 CALIBERS FROM NOSE TIP

CONFIGURATION DYNAMIC DERIVATIVES

MACH NO.	CLP	CMQ+CMAD	CNPA1	CNPA5	METHOD 3 PITCH DAMPING
1.50	-0.976	-103.386	0.000	0.000	-135.256
1.30	-0.897	-127.145	0.000	0.000	-148.733
1.10	-0.949	-140.979	0.000	0.000	-145.272
0.80	-0.915	-114.673	0.000	0.000	-317.562
0.60	-0.815	-105.050	0.000	0.000	-92.737

1

CASE NO. 3
EXAMPLE 39 MK 82 LOW DRAG BOMB

ANGLE OF ATTACK = 10.00 DEGS REFERENCE DIAMETER = 0.887 FT
DEFLECTION ANGLE = 0.00 DEGS

REFERENCE CONDITIONS

MOMENT REFERENCE = 3.64 CALIBERS FROM NOSE TIP
ALIMIT MACH NUMBER = 2.00
ALIMS MACH NUMBER = 2.50

****************** BODY GEOMETRY SAME AS PREVIOUS CASE *****************

1

SUMMARY OF AERODYNAMIC COEFFICIENTS FOR CASE NO. 3

EXAMPLE 39 MK 82 LOW DRAG BOMB

ROLL = 0

BODY AXIAL FORCE CONTRIBUTIONS

MACH NO.	REYS. NO./MACH NO./FT.	SKIN FRICTION	BASE PRESSURE	PRESSURE	PROTRUSIONS	TOTAL
1.500	0.1333E+07	0.0479	0.0682	0.1418	0.1330	0.3908
1.300	0.1538E+07	0.0492	0.0835	0.1298	0.1330	0.3956
1.100	0.1818E+07	0.0505	0.0863	0.1227	0.1330	0.3924
0.800	0.2500E+07	0.0521	0.0632	-.0065	0.1500	0.2588
0.600	0.3333E+07	0.0530	0.0598	-.0074	0.1150	0.2204

WING AXIAL FORCE CONTRIBUTIONS

MACH NO.	REYS. NO./MACH NO./FT.	SKIN FRICTION	BASE PRESSURE	PRESSURE	TOTAL
1.500	0.1333E+07	0.0042	0.0000	0.0222	0.0264
1.300	0.1538E+07	0.0042	0.0000	0.0273	0.0314
1.100	0.1818E+07	0.0042	0.0000	0.0346	0.0387
0.800	0.2500E+07	0.0042	0.0000	0.0000	0.0042
0.600	0.3333E+07	0.0042	0.0000	0.0000	0.0042

NORMAL FORCE CONTRIBUTIONS

MACH NO.	BODY ALONE	WING ALONE	CANARD ALONE	WING-BODY	BODY-WING	CANARD-BODY	BODY-CANARD	CANARD-WING	TOTAL
1.50	0.2295	0.3670	0.0000	0.4105	0.1238	0.0000	0.0000	0.0000	0.7638
1.30	0.2053	0.3937	0.0000	0.4736	0.1679	0.0000	0.0000	0.0000	0.8468

1.10	0.2368	0.3918	0.0000	0.4838	0.1608	0.0000	0.0000	0.0000	0.8813
0.80	0.2552	0.3290	0.0000	0.4113	0.1103	0.0000	0.0000	0.0000	0.7768
0.60	0.2177	0.3007	0.0000	0.3834	0.1009	0.0000	0.0000	0.0000	0.7019

MOMENT CONTRIBUTIONS ABOUT C.G.

MACH NO.	BODY ALONE	WING-BODY	BODY-WING	CANARD-BODY	BODY-CANARD	CANARD-WING	TOTAL
1.500	1.3417	-1.7445	-0.5280	0.0000	0.0000	0.0000	-0.9307
1.300	1.3201	-2.0017	-0.7163	0.0000	0.0000	0.0000	-1.3979
1.100	1.0436	-2.0277	-0.6739	0.0000	0.0000	0.0000	-1.6580
0.800	0.8555	-1.7051	-0.4572	0.0000	0.0000	0.0000	-1.3068
0.600	0.8544	-1.5908	-0.4185	0.0000	0.0000	0.0000	-1.1549

TOTAL STATIC AERODYNAMICS(FORCE/ALPHA)

MACH NO.	CA	CN	CD	CL	CM	CNAL	CMAL	XCP/DREF	XCP/L	XCP(-CM/CN)
1.500	0.417	0.764	0.543	0.680	-0.931	4.725	-5.103	1.080	0.132	1.218
1.300	0.427	0.847	0.568	0.760	-1.398	5.033	-7.374	1.465	0.179	1.651
1.100	0.431	0.881	0.578	0.793	-1.658	5.480	-10.111	1.845	0.226	1.881
0.800	0.263	0.777	0.394	0.719	-1.307	5.071	-8.895	1.754	0.214	1.682
0.600	0.225	0.702	0.343	0.652	-1.155	4.752	-8.146	1.714	0.210	1.645

NOTE: THE ABOVE CM, CMAL, AND XCP/DREF ARE REFERENCED TO THE POINT AT 3.6394 CALIBERS FROM NOSE TIP

CONFIGURATION DYNAMIC DERIVATIVES

MACH NO.	CLP	CMQ+CMAD	CNPA1	CNPA5	METHOD 3 PITCH DAMPING
1.50	-0.940	-102.598	0.000	0.000	-141.986
1.30	-0.867	-125.926	0.000	0.000	-155.161
1.10	-0.980	-143.605	0.000	0.000	-150.597
0.80	-0.970	-123.128	0.000	0.000	-326.058
0.60	-0.856	-114.374	0.000	0.000	-94.602

1

CASE NO. 4
EXAMPLE 39 MK 82 LOW DRAG BOMB

ANGLE OF ATTACK = 15.00 DEGS REFERENCE DIAMETER = 0.887 FT
DEFLECTION ANGLE = 0.00 DEGS

REFERENCE CONDITIONS

MOMENT REFERENCE = 3.64 CALIBERS FROM NOSE TIP
ALIMIT MACH NUMBER = 2.00
ALIMS MACH NUMBER = 2.50

********** BODY GEOMETRY SAME AS PREVIOUS CASE **********

1

SUMMARY OF AERODYNAMIC COEFFICIENTS FOR CASE NO. 4

EXAMPLE 39 MK 82 LOW DRAG BOMB

ROLL = 0

BODY AXIAL FORCE CONTRIBUTIONS

MACH NO.	REYS. NO./MACH NO./FT.	SKIN FRICTION	BASE PRESSURE	PRESSURE	PROTRUSIONS	TOTAL
1.500	0.1333E+07	0.0479	0.0708	0.1576	0.1330	0.4093
1.300	0.1538E+07	0.0492	0.0866	0.1357	0.1330	0.4045
1.100	0.1818E+07	0.0505	0.0893	0.1134	0.1330	0.3862
0.800	0.2500E+07	0.0521	0.0651	-.0205	0.1500	0.2468
0.600	0.3333E+07	0.0530	0.0615	-.0153	0.1150	0.2142

WING AXIAL FORCE CONTRIBUTIONS

MACH NO.	REYS. NO./MACH NO./FT.	SKIN FRICTION	BASE PRESSURE	PRESSURE	TOTAL
1.500	0.1333E+07	0.0042	0.0000	0.0222	0.0264
1.300	0.1538E+07	0.0042	0.0000	0.0273	0.0314
1.100	0.1818E+07	0.0042	0.0000	0.0346	0.0387
0.800	0.2500E+07	0.0042	0.0000	0.0000	0.0042
0.600	0.3333E+07	0.0042	0.0000	0.0000	0.0042

NORMAL FORCE CONTRIBUTIONS

MACH NO.	BODY ALONE	WING ALONE	CANARD ALONE	WING-BODY	BODY-WING	CANARD-BODY	BODY-CANARD	CANARD-WING	TOTAL
1.50	0.4412	0.5465	0.0000	0.5912	0.1754	0.0000	0.0000	0.0000	1.2079
1.30	0.3835	0.5846	0.0000	0.6724	0.2409	0.0000	0.0000	0.0000	1.2968
1.10	0.4227	0.5947	0.0000	0.7166	0.2405	0.0000	0.0000	0.0000	1.3798
0.80	0.4448	0.5060	0.0000	0.6272	0.1781	0.0000	0.0000	0.0000	1.2501
0.60	0.3940	0.4600	0.0000	0.5865	0.1668	0.0000	0.0000	0.0000	1.1474

MOMENT CONTRIBUTIONS ABOUT C.G.

MACH NO.	BODY ALONE	WING-BODY	BODY-WING	CANARD-BODY	BODY-CANARD	CANARD-WING	TOTAL
1.500	1.9260	-2.5177	-0.7482	0.0000	0.0000	0.0000	-1.3399
1.300	1.9047	-2.8504	-1.0275	0.0000	0.0000	0.0000	-1.9732
1.100	1.5406	-3.0163	-1.0122	0.0000	0.0000	0.0000	-2.4880
0.800	1.2436	-2.6158	-0.7427	0.0000	0.0000	0.0000	-2.1148
0.600	1.2267	-2.4481	-0.6963	0.0000	0.0000	0.0000	-1.9177

TOTAL STATIC AERODYNAMICS(FORCE/ALPHA)

MACH NO.	CA	CN	CD	CL	CM	CNAL	CMAL	XCP/DREF	XCP/L	XCP(-CM/CN)
1.500	0.436	1.208	0.733	1.054	-1.340	6.750	-4.645	0.688	0.084	1.109
1.300	0.436	1.297	0.757	1.140	-1.973	5.657	-5.618	0.993	0.121	1.522
1.100	0.425	1.380	0.768	1.223	-2.488	5.838	-8.244	1.412	0.173	1.803
0.800	0.251	1.250	0.566	1.142	-2.115	5.618	-8.997	1.601	0.196	1.692
0.600	0.218	1.147	0.508	1.052	-1.918	5.337	-8.814	1.651	0.202	1.671

NOTE: THE ABOVE CM, CMAL, AND XCP/DREF ARE REFERENCED TO THE POINT AT 3.6394 CALIBERS FROM NOSE TIP

CONFIGURATION DYNAMIC DERIVATIVES

MACH NO.	CLP	CMQ+CMAD	CNPA1	CNPA5	METHOD 3 PITCH DAMPING
1.50	-0.863	-102.211	0.000	0.000	-152.242
1.30	-0.797	-122.849	0.000	0.000	-164.958
1.10	-0.872	-150.990	0.000	0.000	-158.713
0.80	-0.965	-131.039	0.000	0.000	-339.006
0.60	-0.878	-123.199	0.000	0.000	-97.445

1

CASE NO. 5
EXAMPLE 39 MK 82 LOW DRAG BOMB

ANGLE OF ATTACK = 20.00 DEGS REFERENCE DIAMETER = 0.887 FT
DEFLECTION ANGLE = 0.00 DEGS

REFERENCE CONDITIONS

MOMENT REFERENCE = 3.64 CALIBERS FROM NOSE TIP
ALIMIT MACH NUMBER = 2.00
ALIMS MACH NUMBER = 2.50

********** BODY GEOMETRY SAME AS PREVIOUS CASE **********

1

SUMMARY OF AERODYNAMIC COEFFICIENTS FOR CASE NO. 5

EXAMPLE 39 MK 82 LOW DRAG BOMB

ROLL = 0

BODY AXIAL FORCE CONTRIBUTIONS

MACH NO.	REYS. NO./MACH NO./FT.	SKIN FRICTION	BASE PRESSURE	PRESSURE	PROTRUSIONS	TOTAL
1.500	0.1333E+07	0.0479	0.0725	0.1720	0.1330	0.4254
1.300	0.1538E+07	0.0492	0.0886	0.1387	0.1330	0.4095
1.100	0.1818E+07	0.0505	0.0911	0.0987	0.1330	0.3733
0.800	0.2500E+07	0.0521	0.0663	-.0456	0.1500	0.2228
0.600	0.3333E+07	0.0530	0.0624	-.0386	0.1150	0.1919

WING AXIAL FORCE CONTRIBUTIONS

MACH NO.	REYS. NO./MACH NO./FT.	SKIN FRICTION	BASE PRESSURE	PRESSURE	TOTAL
1.500	0.1333E+07	0.0042	0.0000	0.0222	0.0264
1.300	0.1538E+07	0.0042	0.0000	0.0273	0.0314
1.100	0.1818E+07	0.0042	0.0000	0.0346	0.0387
0.800	0.2500E+07	0.0042	0.0000	0.0000	0.0042
0.600	0.3333E+07	0.0042	0.0000	0.0000	0.0042

NORMAL FORCE CONTRIBUTIONS

MACH NO.	BODY ALONE	WING ALONE	CANARD ALONE	WING-BODY	BODY-WING	CANARD-BODY	BODY-CANARD	CANARD-WING	TOTAL
1.50	1.0938	0.7135	0.0000	0.7457	0.2174	0.0000	0.0000	0.0000	2.0570
1.30	0.7550	0.7627	0.0000	0.8371	0.3032	0.0000	0.0000	0.0000	1.8953
1.10	0.6909	0.7832	0.0000	0.9045	0.3119	0.0000	0.0000	0.0000	1.9073
0.80	0.6898	0.6784	0.0000	0.8175	0.2501	0.0000	0.0000	0.0000	1.7573
0.60	0.6193	0.6202	0.0000	0.7723	0.2418	0.0000	0.0000	0.0000	1.6334

MOMENT CONTRIBUTIONS ABOUT C.G.

MACH NO.	BODY ALONE	WING-BODY	BODY-WING	CANARD-BODY	BODY-CANARD	CANARD-WING	TOTAL
1.500	2.3341	-3.1817	-0.9272	0.0000	0.0000	0.0000	-1.7749
1.300	2.4547	-3.5583	-1.2934	0.0000	0.0000	0.0000	-2.3969

1.100	2.0461	-3.8222	-1.3182	0.0000	0.0000	0.0000	-3.0942
0.800	1.6000	-3.4283	-1.0488	0.0000	0.0000	0.0000	-2.8771
0.600	1.5625	-3.2412	-1.0146	0.0000	0.0000	0.0000	-2.6932

TOTAL STATIC AERODYNAMICS(FORCE/ALPHA)

MACH NO.	CA	CN	CD	CL	CM	CNAL	CMAL	XCP/DREF	XCP/L	XCP(-CM/CN)
1.500	0.452	2.057	1.128	1.778	-1.775	11.391	-6.037	0.530	0.065	0.863
1.300	0.441	1.895	1.063	1.630	-2.397	9.999	-5.974	0.597	0.073	1.265
1.100	0.412	1.907	1.040	1.651	-3.094	7.325	-6.600	0.901	0.110	1.622
0.800	0.227	1.757	0.814	1.574	-2.877	6.108	-7.584	1.242	0.152	1.637
0.600	0.196	1.633	0.743	1.468	-2.693	5.606	-7.485	1.335	0.163	1.649

NOTE: THE ABOVE CM, CMAL, AND XCP/DREF ARE REFERENCED TO THE POINT AT 3.6394 CALIBERS FROM NOSE TIP

CONFIGURATION DYNAMIC DERIVATIVES

MACH NO.	CLP	CMQ+CMAD	CNPA1	CNPA5	METHOD 3 PITCH DAMPING
1.50	-0.823	-109.897	0.000	0.000	-164.715
1.30	-0.751	-121.945	0.000	0.000	-176.872
1.10	-0.738	-146.860	0.000	0.000	-168.582
0.80	-0.869	-135.771	0.000	0.000	-354.751
0.60	-0.866	-129.464	0.000	0.000	-100.901

1

CASE NO. 6
EXAMPLE 39 MK 82 LOW DRAG BOMB

ANGLE OF ATTACK = 25.00 DEGS REFERENCE DIAMETER = 0.887 FT
DEFLECTION ANGLE = 0.00 DEGS

REFERENCE CONDITIONS

MOMENT REFERENCE = 3.64 CALIBERS FROM NOSE TIP
ALIMIT MACH NUMBER = 2.00
ALIMS MACH NUMBER = 2.50

********** BODY GEOMETRY SAME AS PREVIOUS CASE **********

1

SUMMARY OF AERODYNAMIC COEFFICIENTS FOR CASE NO. 6

EXAMPLE 39 MK 82 LOW DRAG BOMB

ROLL = 0

BODY AXIAL FORCE CONTRIBUTIONS

MACH NO.	REYS. NO./MACH NO./FT.	SKIN FRICTION	BASE PRESSURE	PRESSURE	PROTRUSIONS	TOTAL
1.500	0.1333E+07	0.0479	0.0733	0.1844	0.1330	0.4386
1.300	0.1538E+07	0.0492	0.0895	0.1386	0.1330	0.4103
1.100	0.1818E+07	0.0505	0.0920	0.0794	0.1330	0.3548
0.800	0.2500E+07	0.0521	0.0666	-.0817	0.1500	0.1870
0.600	0.3333E+07	0.0530	0.0626	-.0793	0.1150	0.1513

WING AXIAL FORCE CONTRIBUTIONS

MACH NO.	REYS. NO./MACH NO./FT.	SKIN FRICTION	BASE PRESSURE	PRESSURE	TOTAL
1.500	0.1333E+07	0.0042	0.0000	0.0222	0.0264
1.300	0.1538E+07	0.0042	0.0000	0.0273	0.0314
1.100	0.1818E+07	0.0042	0.0000	0.0346	0.0387
0.800	0.2500E+07	0.0042	0.0000	0.0000	0.0042
0.600	0.3333E+07	0.0042	0.0000	0.0000	0.0042

NORMAL FORCE CONTRIBUTIONS

MACH NO.	BODY ALONE	WING ALONE	CANARD ALONE	WING-BODY	BODY-WING	CANARD-BODY	BODY-CANARD	CANARD-WING	TOTAL
1.50	1.9420	0.8632	0.0000	0.8930	0.2502	0.0000	0.0000	0.0000	3.0852
1.30	1.6412	0.9232	0.0000	0.9646	0.3536	0.0000	0.0000	0.0000	2.9595
1.10	1.3216	0.9473	0.0000	1.0466	0.3716	0.0000	0.0000	0.0000	2.7399
0.80	1.0118	0.8384	0.0000	0.9812	0.3230	0.0000	0.0000	0.0000	2.3161
0.60	0.9036	0.7765	0.0000	0.9081	0.3141	0.0000	0.0000	0.0000	2.1258

MOMENT CONTRIBUTIONS ABOUT C.G.

MACH NO.	BODY ALONE	WING-BODY	BODY-WING	CANARD-BODY	BODY-CANARD	CANARD-WING	TOTAL
1.500	2.4901	-3.8165	-1.0673	0.0000	0.0000	0.0000	-2.3938
1.300	2.6460	-4.1104	-1.5084	0.0000	0.0000	0.0000	-2.9728
1.100	2.3348	-4.4387	-1.5758	0.0000	0.0000	0.0000	-3.6798
0.800	2.0589	-4.1358	-1.3616	0.0000	0.0000	0.0000	-3.4384
0.600	1.9300	-3.8295	-1.3246	0.0000	0.0000	0.0000	-3.2241

TOTAL STATIC AERODYNAMICS(FORCE/ALPHA)

MACH NO.	CA	CN	CD	CL	CM	CNAL	CMAL	XCP/DREF	XCP/L	XCP(-CM/CN)
1.500	0.465	3.085	1.725	2.600	-2.394	12.389	-7.706	0.622	0.076	0.776
1.300	0.442	2.959	1.651	2.496	-2.973	12.647	-6.823	0.539	0.066	1.004
1.100	0.394	2.740	1.515	2.317	-3.680	11.846	-6.379	0.538	0.066	1.343
0.800	0.191	2.316	1.152	2.018	-3.438	7.380	-5.513	0.747	0.091	1.485
0.600	0.156	2.126	1.039	1.861	-3.224	5.933	-4.771	0.804	0.098	1.517

NOTE: THE ABOVE CM, CMAL, AND XCP/DREF ARE REFERENCED TO THE POINT AT 3.6394 CALIBERS FROM NOSE TIP

CONFIGURATION DYNAMIC DERIVATIVES

MACH NO.	CLP	CMQ+CMAD	CNPA1	CNPA5	METHOD 3 PITCH DAMPING
1.50	-0.849	-117.985	0.000	0.000	-177.799
1.30	-0.766	-128.674	0.000	0.000	-189.370
1.10	-0.653	-157.058	0.000	0.000	-178.935
0.80	-0.761	-139.577	0.000	0.000	-371.269
0.60	-0.805	-131.108	0.000	0.000	-104.527

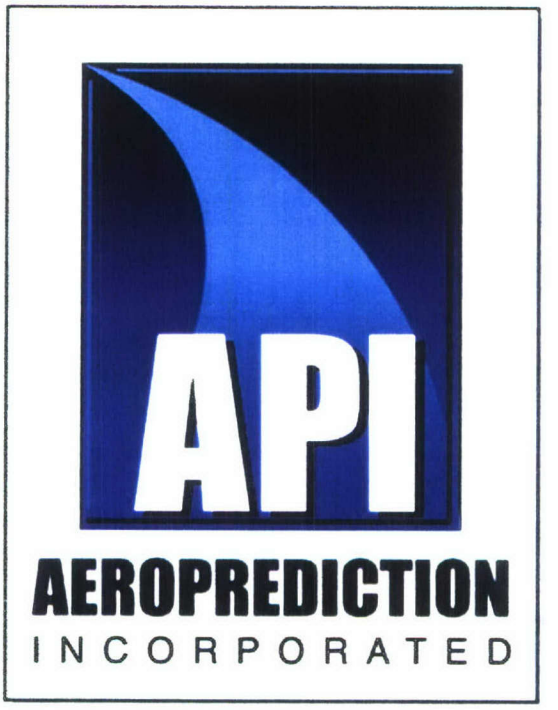
API
AEROPREDICTION
INCORPORATED